RL-TR-92-104
Final Technical Report
May 1992

OPTICAL SIGNAL DISTRIBUTION SCHEMES FOR MILLIMETER PHASED ARRAY RADAR

University of Minnesota

Ali Ghiasi and Anand Gopinath

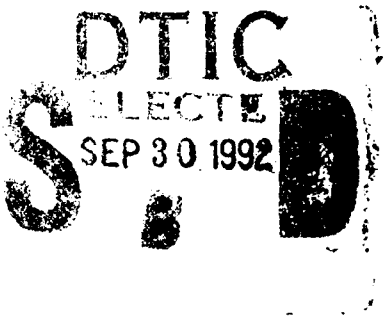

APPROVED FOR PUBLIC RELEASE; DISTRIBUTION UNLIMITED.

Rome Laboratory
Air Force Systems Command
Griffiss Air Force Base, NY 13441-5700

This report has been reviewed by the Rome Laboratory Public Affairs Office (PA) and is releasable to the National Technical Information Service (NTIS). At NTIS it will be releasable to the general public, including foreign nations.

RL-TR-92-104 has been reviewed and is approved for publication.

APPROVED: Andrew Davis

ANDREW DAVIS
Project Engineer

FOR THE COMMANDER: Harold Roth

HAROLD ROTH
Director
Electromagnetics & Reliability Directorate

If your address has changed or if you wish to be removed from the Rome Laboratory mailing list, or if the addressee is no longer employed by your organization, please notify RL(ERO) Hanscom AFB MA 01731-5000. This will assist us in maintaining a current mailing list.

Do not return copies of this report unless contractual obligations or notices on a specific document require that it be returned.

REPORT DOCUMENTATION PAGE

Form Approved
OMB No. 0704-0188

1. AGENCY USE ONLY (Leave Blank)	2. REPORT DATE	3. REPORT TYPE AND DATES COVERED
	May 1992	Final

4. TITLE AND SUBTITLE
OPTICAL SIGNAL DISTRIBUTION SCHEMES FOR MILLIMETER PHASED ARRAY RADAR

5. FUNDING NUMBERS
C - F19628-88-K-0007
PE - 61102F
PR - 2306
TA - J2
WU - 64

6. AUTHOR(S)
Ali Ghiasi, Anand Gopinath

7. PERFORMING ORGANIZATION NAME(S) AND ADDRESS(ES)
University of Minnesota
Department of Electrical Engineering
123 Church Street., S.E.
Minneapolis MN 55455

8. PERFORMING ORGANIZATION REPORT NUMBER

9. SPONSORING/MONITORING AGENCY NAME(S) AND ADDRESS(ES)
Rome Laboratory (ERO)
Hanscom AFB MA 01731-5000

10. SPONSORING/MONITORING AGENCY REPORT NUMBER
RL-TR-92-104

11. SUPPLEMENTARY NOTES
Rome Laboratory Project Engineer: Andrew Davis/ERO(617) 377-3598

12a. DISTRIBUTION/AVAILABILITY STATEMENT
Approved for public release; distribution unlimited.

12b. DISTRIBUTION CODE

13. ABSTRACT (Maximum 200 words)

The goal is the modulation of lasers above the -3dB modulation bandwidth. The approach is to coat one laser facet with an anti-reflection coating and form an external cavity. The external cavity laser was built and characterized theoretically. An impedance-matching microstrip was designed and measured. An 8 GHz oscillator was built using a 0.3 micron MESFET. It was found that the optical feedback increases the light modulation depth by 25 dB on the first harmonic and 34dB on the second harmonic in external cavity laser diodes. The model, which has proven accurate thus far, indicates that diode parasitics make it preferable to use the second harmonic generated by a 30 GHz cavity, rather chan the first harmonic from a 60 GHz cavity.

14. SUBJECT TERMS	15. NUMBER OF PAGES
Phased Arrays	148
	16. PRICE CODE

17. SECURITY CLASSIFICATION OF REPORT	18. SECURITY CLASSIFICATION OF THIS PAGE	19. SECURITY CLASSIFICATION OF ABSTRACT	20. LIMITATION OF ABSTR
UNCLASSIFIED	UNCLASSIFIED	UNCLASSIFIED	U/L

ABSTRACT

Optical signal distribution schemes for phase and frequency control of the pha sed array modules require the optical signal from a semiconductor laser diode be modulated at the radar frequency.or at its subharmonic. The problem of direct modulating the laser diode at these high frequencies was investigated and the results are reported here.

The high-speed modulation characteristics of semiconductor laser diode are studied and techniques to enhance the maximum speed are investigated. The three limiting factors for efficient high-speed modulation of semiconductor laser diodes examined here are parasitics, the matching circuit, and the photon relaxation oscillation frequency.

Parasitics are reduced by employing microwave packaging techniques which reduce the bond inductance and prevents additional package capacitance. A "Through-Load-Reflect" (TRL) calibration technique is implemented and thereafter, the laser chip Scattering-parameters are de-embedded. The parasitics effects on the modulation characteristics of the semiconductor laser diode are determined from the de-embedded Scattering-parameters of the laser diode chip.

A lowloss microstrip matching circuit with 90% bandwidth, for connecting to a laser diode of nominal impedance of 2 ohms to a 50 ohm system, is developed. The technique utilizes a microstrip Chebychev transformer without very wide line widths to obtain the match at a center frequency of 10.5 GHz with bandwidth of 9 GHz, insertion loss of less than 1.5 dB, and reflection coefficient of better than -10 dB.

A rate equation theory is developed for a semiconductor laser diode coupled to an external cavity under strong optical feedback. The theoretical and experimental results show that a semiconductor laser diode may be modulated at frequencies larger than its relaxation oscillation frequency. The laser diode under investigation had AR (anti-reflection) coating on one facet and a relaxation oscillation frequency of about 5 GHz,

was placed in external cavities with fundamental resonances at 5 and 10 GHz. The external cavity enhances the rf modulation response at the frequencies corresponding to the external cavity resonance. The level of signal enhancement at the fundamental frequency is 20 to 25 dB, and at the second harmonic frequency is 30 to 38 dB. Large signal results show that the level of signal enhancement at the fundamental frequency remains high even at a modulation depth in the range of 10% to 20%. Furthermore, large signal results indicate, that it is not necessary to drive a laser at very large modulation depths to achieve significant harmonic enhancement. The region of modulation enhancement, with the external cavity, is about 10% bandwidth. Theoretically, a 24 GHz laser modulation is investigated, where the output amplitude is even higher than the low frequency level. The external cavity laser is shown to be a viable option for laser light modulation at millimeterwave frequencies.

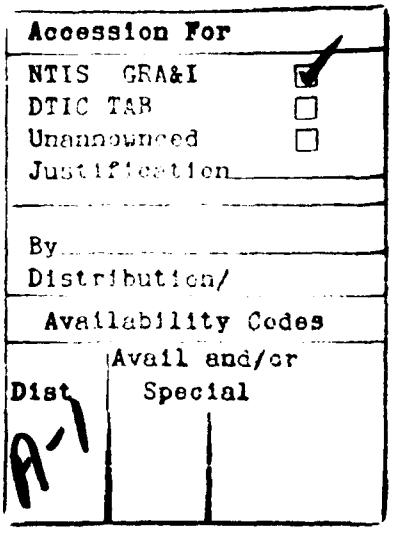

CONTENTS

LIST OF FIGURES

Chapter I

INTRODUCTION

Laser diodes are attractive for signal distribution in a variety of microwave and millimeterwave applications, such as antenna remoting, phased array antenna, and high-speed communication links. Phased array systems for military and civilian radars and satellite communication systems, with large numbers of elements have become feasible with the advent of GaAs monolithic microwave integrated circuit (MMIC) [1, 2]. The phased array antenna is attractive because it can scan a limited angular region very fast electronically. However, it is necessary that the phase of each transmitter element be locked to a master oscillator, and this requires synchronization signal distribution either at the radar frequency or its subharmonic frequencies [3, 4, 5]. At millimeterwave frequencies, signal distribution with waveguides is bulky and is not practical with a large number of elements [6].

Optical signal distribution using optical fibers in this context is attractive for several reasons: both digital and analog signals may be transmitted on the same fibers. The size and weight are small and there is immunity from electromagnetic interference. Optical signal distribution, using optical fibers, requires that the light be modulated either at the radar frequency or at some subharmonic frequency. In the case of a 60 GHz radar, the detected light modulation should be at 60 GHz; but since there are no optical modulators at this frequency and direct modulation of lasers not feasible subharmonic optical injection locking has been proposed [4]. A schematic diagram showing the fundamental and subharmonic (3rd harmonic) optical injection locking is shown in Figs. 1.1 and 1.2 respectively. A drawback of subharmonic locking is that the harmonic power generated by the laser is usually small unless the laser is driven at

very high modulation depths. It has been reported [7] that when the laser is driven at a modulation depth of about 90%, self-pulsation is present in the output and this is not acceptable. An alternative technique is to enhance the intrinsic modulation characteristics of the semiconductor laser diode, where fundamental and harmonics are enhanced without the need for excessively large modulation depth.

The intrinsic modulation response of the semiconductor laser diode is governed by the interactions between the carrier and photon populations. For a laser biased at an operating point above the threshold, the laser will retain its carrier and photon population after reaching thermal equilibrium. However, when the rf modulation is superimposed on the dc current for frequencies beyond the intrinsic relaxation oscillation frequency (f_r), the photon population does not follow and respond to the variations in the rf drive. This reduces the light modulation depth and effectively attenuates the modulation signal. This type of modulation is referred to as intensity modulation and is similar to amplitude modulation (AM) as in the commercial radio broadcast. Several papers, notably those of Lau [8], Tucker [9], and Su [10] have discussed in considerable details the 3 dB modulation bandwidth of semiconductor laser diode and have shown that this is slightly larger than the relaxation oscillator frequency (f_r). These authors have characterized the laser as a second order low pass network which has resonant peaks at f_r.

Currently, multiple quantum wells lasers have demonstrated the highest laser relaxation oscillation frequency f_r to date, which is about 30 GHz [11]. However, reliable modulation has only been demonstrated to 10 GHz in a short cavity Double Channel Buried Heterostructure (DCBH) laser [12]. The short cavity lasers have reduced photon lifetime and consequently, the relaxation oscillation frequency increases. The drawback associated with these short cavity lasers is that the threshold current density continues to rise to a point, beyond which long term reliability is compromised. This ultimately sets a limit on how short a laser may be and its' maximum cutoff frequency. From the life test of Buried Heterostructure (BH) lasers on SI substrate it has been shown that

minimum cavity length should be at least 150 μm [8]. Alternatively, when the semiconductor laser diode is coupled to an external cavity, the light modulation is enhanced at the frequencies associated with roundtrip time of the external cavity.[12-19]. It has been reported that the external cavity increases the optical intensity and the modulation depth of both fundamental (3.456 GHz) and its' harmonics by approximately 20 dB [20]. Furthermore, a monolithically integrated external cavity laser has demonstrated a 20 GHz signal output at nearly the same amplitude level of its' low frequency level [21]. A readily available buried hetero-structure (BH) laser diode, with only several gigahertz relaxation oscillation frequency, when placed in an external cavity may therefore allow millimeterwave light modulation generation.

For efficient light modulation at millimeterwave frequencies, it is necessary to reduce the laser chip parasitics and devise a proper matching circuit. The laser chip parasitics arise from the bond-wire inductance, distributed capacitance, and both shunt and series resistances, which form a low Q (quality factor) series resonance circuit. When the modulation frequency is larger than the parasitics series resonance frequency, then increasingly, the modulation drive appearing across the diode junction reduces with the frequency. At a frequency well above the series resonance, the diode capacitance appears as a short circuit and the bond wire inductance as an open circuit. Therefore improving the laser intrinsic resonance frequency f_r is of little help. Furthermore, for efficient modulation, a matching network is required to match the generator impedance of usually 50 Ω to the laser impedance of 1 to 9 Ω. Often to prevent circuit mismatch, a series resistance is added: in the case of a 2 Ω laser, the series resistance is 48 Ω, and the power delivered to the laser is then only 4% of input drive, which is a phenomenal loss of power.

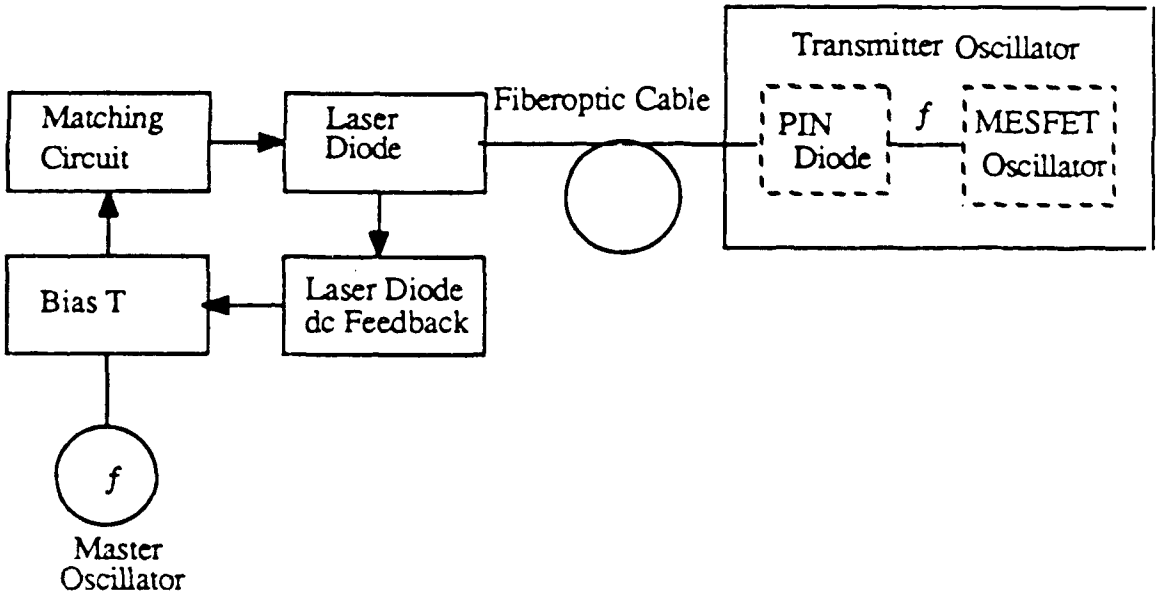

Fig. 1.1 A direct injection locking scheme

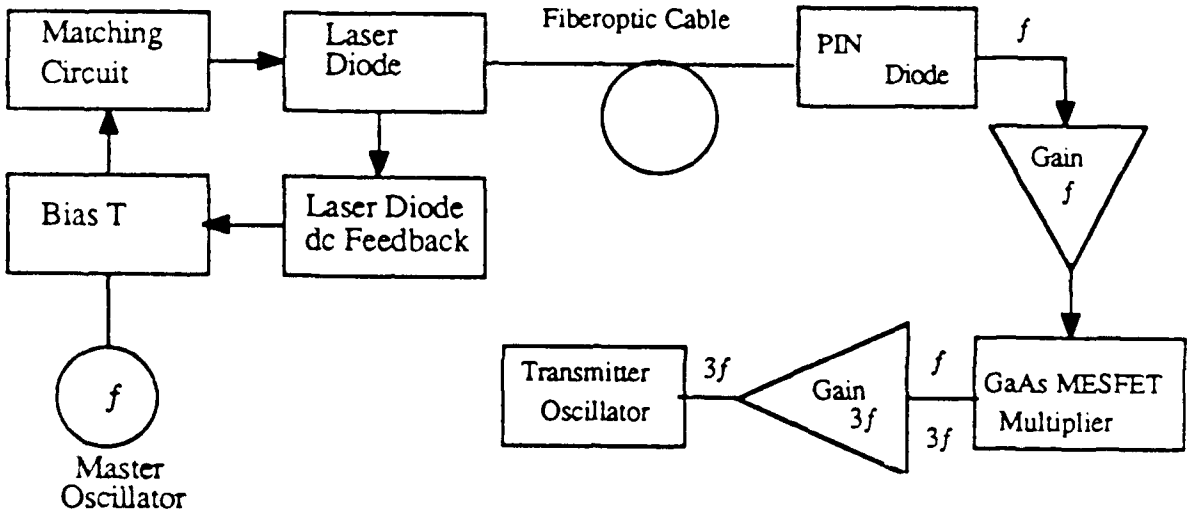

Fig. 1.2 Subharmonic injection locking scheme.

The goal of this thesis is to overcome some of the problems encountered in the high frequency modulation of semiconductor lasers. These limitations are namely the parasitics, the matching, and the relaxation oscillation frequency f_r. The techniques employed here have ultimately increased the laser modulation frequency response. Also, the possibility of efficient millimeterwave light modulation with currently available lasers is discussed.

In Chapter 2, various elements of high-speed lightwave systems are reviewed: high-speed semiconductor laser diodes, photoconductors, and photodiodes. Chapter 3 presents a de-embedding technique to extract laser diode chip Scattering-parameters, and a mixed lumped and distributed element equivalent circuit of the laser diode (Ortel SL 1000) is extracted. The equivalent circuit shows degradation of the laser modulation response because of the parasitics. In Chapter 4, a lowloss microstrip matching circuit with large bandwidth for connecting to a laser diode of nominal impedance of 2 Ω to 50 Ω system is described. The technique utilizes mixed distributed and lumped elements without the need for very wide microstrip lines. Theoretical and experimental results of the modulation characteristics of the semiconductor laser diode coupled to an external cavity under strong optical feedback are presented in Chapter 5. Finally, Chapter 6 provides a summary of this work and makes suggestions for future improvements.

Chapter II

ELEMENTS OF HIGH-SPEED LIGHTWAVE SYSTEM

High-speed lightwave links are currently replacing some of the conventional microwave links and assuming a greater role in the communication technology than ever before. This is due to the development of high-speed semiconductor laser diodes, photodetectors, and the availability of low loss optical fibers.

The first wide spread use of lightwave communication was in the telecommunication industry where it has been used for digital communication. In these applications, devices are required with the ability to only switch on or off. Therefore, LEDs or laser diodes with very rudimentary modulation characteristics are used. However, transmission of high quality analog and digital signals must meet stringent linearity and noise requirements. This has become possible with the recent improvement of semiconductor laser diodes. High-speed lasers are now available with modulation bandwidth well into the Ku-band (12.4-18 GHz).

Some of the applications considered for high-speed lightwave systems are antenna remoting where the receiver and the transmitter may be several kilometers apart, satellite communication, and phased array radar. Analog fiber-optic links are also becoming popular in the CATV industry for transmission of FM video and AMVSB[1] with its' demanding noise and linearity requirements.

---

1 AM Vestigial-Sideband Modulation is similar to Single-Sideband modulation but, without the need for a sharp cutoff filter at the carrier frequency and with improved low frequency response. AMVSB is widely used in commercial television broadcasting.

2.1. Semiconductor Laser Diode

Modern semiconductor injection laser diodes have a double - heterojunction (DH) structure with a buried stripe geometry [22] ; ie , a planar structure, where the current is confined to a 1 to 1.5 um wide stripe. To fabricate these lasers, the active n-GaAs layer is sandwiched by a p-Ga_{1-y} Al_yAs and n-$Ga_{1-x}Al_x$As layer which exhibits a higher bandgap, as shown in Fig. 2.1, and is grown on a n-GaAs substrate.

The light modulation from laser diodes are often required to transmit information as far as possible in a fiber without a need for a repeater. The information bandwidth is primarily limited by the S/N ratio and by the pulse broadening because of chromatic dispersion in the fiber [23]. However, if the optical source has a narrower spectral width, chromatic dispersion improves and this gives rise to the need for single longitudinal mode light sources. Two distinct double-heterostructures (DH) for lasers are: gain-guide and indexed-guide. Gain guided lasers have very wide spectral width and therefore are not suitable for high-speed lightwave systems. The diodes investigated here are buried double-heterostructure index-guided (BHDH) lasers. In these lasers, the refractive index of the regrown area acts as a transverse waveguide and confines the optical power just as the lateral heterojunction confines the carriers. A well designed BHDH laser usually lases in single longitudinal mode but, a gain guided laser may have transverse and multiple longitudinal side modes.

When the laser diode is forward biased, electrons and holes are injected into the active layer of (GaAs) due to the lower band gap of the active layer. Since GaAs is a direct band gap semiconductor, electrons and holes injected into this region recombine radiatively with high quantum efficiency. The electrons and holes are prevented from diffusing out into the p region by the potential barrier due to the difference ΔEg between the energy gaps of GaAs and the sandwiching layers. GaAlAs laser diodes, utilizing a buried DH structure have been fabricated with threshold currents as low as 1 mA; more typically lasers have a threshold of 10 mA or more [24]. This double confinement of injected carriers, as well as the optical

mode energy is the primary factor for the emergence of the low threshold semiconductor lasers [25-27]. The cleaved facets of semiconductor lasers forms a Fabry-Perot cavity and provides the positive feedback for the onset of laser oscillation.

2.1.1. P-N Junction

At the heart of semiconductor laser diodes is the P-N junction [24]. For an unbiased device, the valance and conduction band are separated by the band-gap energy, E_g. Under heavy injection of carriers, the separation between energy levels exceeds the band-gap energy and photons of energy $h\nu=E_g$ are emitted during radiative recombination process. When the biased current increases further, a condition known as population inversion is achieved, in which the rate of photon emission exceeds that of absorption. The P-N junction then amplifies the electromagnetic radiation and the active layer exhibits optical gain so that it's wavelength satisfies the equation:

$$\lambda \approx \frac{1.24}{E_g} \qquad (2\text{-}1)$$

where E_g is the bandgap energy, ie E_g= 1.43 ev for GaAs at room temperature. Initially, when the laser current is below the threshold, spontaneous emission processes occurs and photons are emitted randomly with no phase relationship among them. Above threshold, for a particular mode, the round-trip gain for the electromagnetic wave exceeds the bulk and mirror losses. The laser then begins to emit photons that render coherent light. At this point the device is lasing and stimulated emission has taken over. Fig. 2.2 shows spontaneous and stimulated processes.

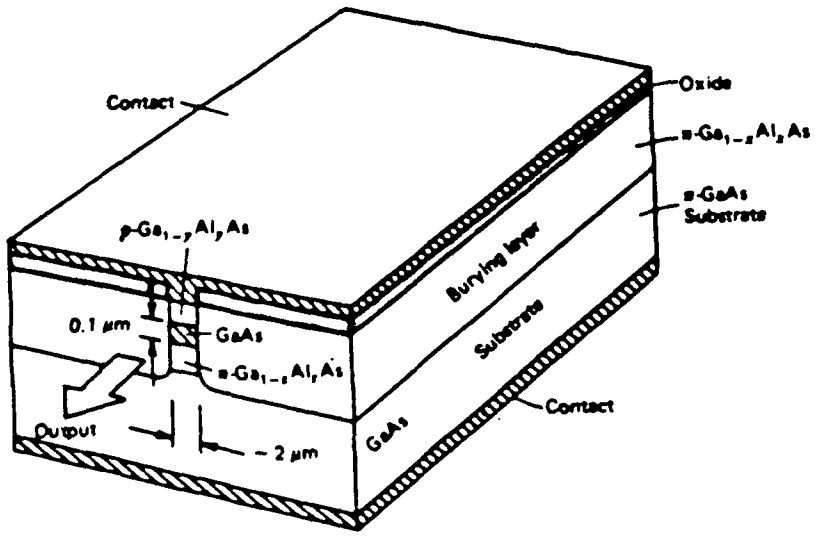

Fig. 2.1 Schematic of a buried heterojunction AlGaAs Laser [24].

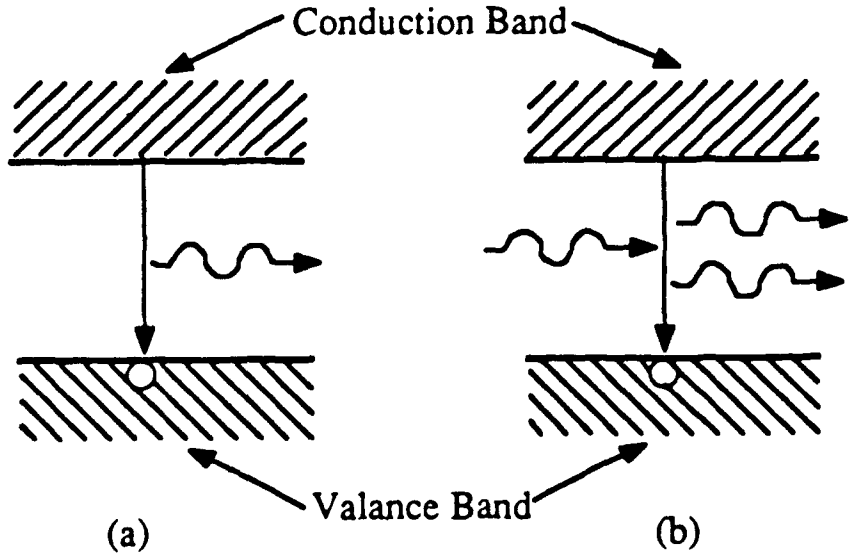

Fig. 2.2 Schematic illustration of (a) Spontaneous and (b) stimulated emission processes in the laser.

2.1.2. Semiconductor Laser Modulation and Dynamic Behavior

Dynamic behavior of semiconductor laser diodes is of great importance in the high-speed lightwave links. In these types of applications, semiconductor laser diodes are biased well above the threshold and are then sinusoidally modulated. Three dynamical types of behaviors of interest in the direct modulation of semiconductor laser diodes will be discussed in the following sections.

2.1.2a. Modulation Bandwidth Limit

The rate equation describes the dynamic behavior of semiconductor laser diodes. The modulation bandwidth is defined as the frequency, at which the laser response to the current modulation drops by 3 dB compared to its dc values. Two phenomena limit the modulation bandwidth of a laser diode: relaxation oscillation frequency, f_r, and the device's parasitics. In the low GHz frequency range where parasitics are not dominant, the relaxation oscillation frequency, f_r , determines the modulation bandwidth. The relaxation oscillation frequency is a phenomenon arising from interplay between the oscillation field in the resonator and population inversion. An increase in the field intensity causes a reduction in the inversion due to the increased rate of stimulated transitions [24]. This reduces the gain, which in turn tends to decrease the field intensity. The actual 3 dB bandwidth is slightly higher than the photon inherent resonance f_r [28]. However, at higher frequency, the device and package parasitics may limit the cutoff frequency [9].

Modulation response of the laser is derived from the small signal analysis of the rate equations [24] and the relaxation oscillation frequency f_r is given by

$$f_r = \frac{1}{2\pi}\sqrt{\frac{AP_0}{\tau_p}} \qquad (2\text{-}2)$$

where A is the optical gain coefficient, P_0 is the steady state active region photon density, and τ_p is the photon life time given by

$$\tau_p = \frac{1}{v_g}(a_{int} + a_m) \tag{2-3}$$

where v_g is the group velocity, a_{int} is the distributed losses, L is the cavity length, R_1 and R_2 are mirror reflectivities, and a_m is the mirror losses given by

$$a_m = \frac{1}{2L}\mathrm{Ln}\left(\frac{1}{R_1 R_2}\right). \tag{2-4}$$

The above equations suggest three obvious techniques to increase the relaxation frequency f_r: increasing the optical gain coefficient, increasing the photon density, or decreasing the photon life time. The gain coefficient A may be increased roughly by a factor of 5 when the laser is cooled from room temperature to 77 degree Kelvin [29]. Biasing the laser at higher currents would increase the photon density in the active region, which simultaneously increases the output power density. Catastrophic mirror damage occurs at a power density of about 1 MW/cm^2 for a laser with mirror reflectivity of 0.3 [8]. This sets the maximum permissible photon density, and hence the maximum modulation frequency. The photon density may be increased to as high as 10 MW/cm^2 by techniques such as the window buried laser [9].

The third way to increase the modulation bandwidth is to reduce photon life time by decreasing the laser cavity length. Such a laser has to be driven at higher current densities, and thermal effect, due to excessive heating will limit the highest attainable modulation bandwidth.

Another factor which limits the laser modulation response is the input parasitics of the diode. Fig. 2.3 shows the effects of parasitics on the modulation response of a buried heterostructure laser with $I_{th} \approx 30$ mA for three bias currents [9]. The input impedance of a laser diode may be

modeled as an equivalent RLC circuit, Fig. 2.4. The diode has a nominal impedance of 2 to 10 Ω when forward biased beyond threshold [8]. As the modulation frequency extends into the upper microwave frequency, parasitics become the dominant factor limiting the laser bandwidth [8, 9].

2.1.2b. Single Longitudinal Mode Operation

Single longitudinal operation may be obtained in an index-guided laser, i.e. a laser whose dielectric waveguide supports only one longitudinal mode. When the injection current is well above the threshold, side modes are present but with reduced amplitude, as shown in Fig. 2.5. One scheme of reducing the adjacent modes is to decrease the cavity length, thereby forcing the side mode space outside the optical gain envelope, Fig. 2.6. Generally, after the laser reaches its steady state region and if it is emitting in single-mode, the laser will retain its single mode spectrum even at a modulation depth of up to 90 percent, regardless of the modulation frequency [7].

As the modulation frequency increases the sidebands broaden, although the relative amplitudes of the mode do not change. The spectrum broadening arises from fluctuations in the refractive index of the cavity as a result of fluctuations in the carrier density. The reason for this is that the fluctuation in the carrier density increases with increasing modulation frequency and consequently the line broadening effect is more visible at higher frequencies [31].

These types of lasers have been found to possess mode hoping as a function of temperature and output power. In general, stable single mode operations of lasers even under transients or high frequency modulation, is only possible with those lasers with a built-in frequency selective elements, such as the distributed feedback laser (DFB) [28], [32], external cavity [16], or cleaved-coupled cavity (C^3) [33].

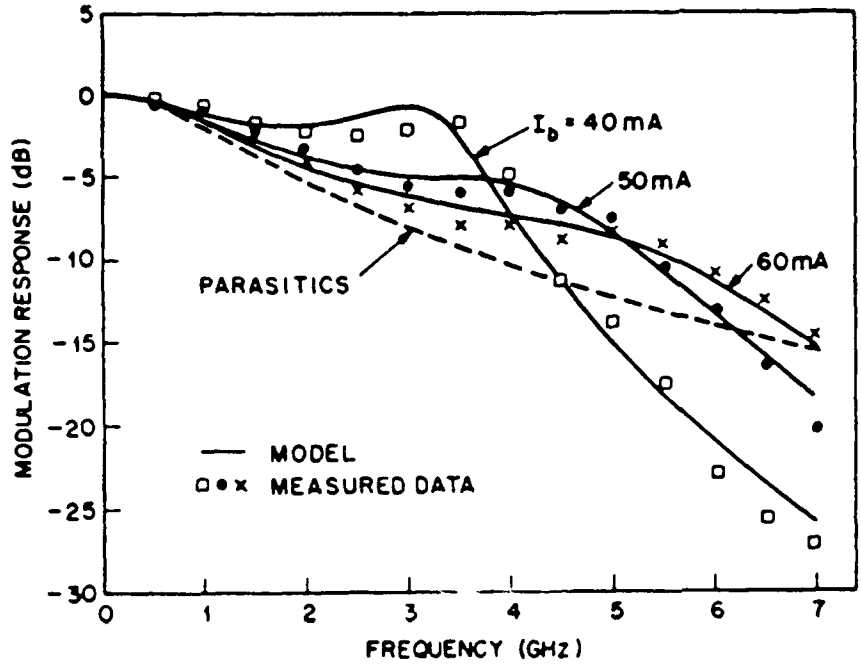

Fig. 2.3 Effects of parasitics on the modulation response of laser diode [9].

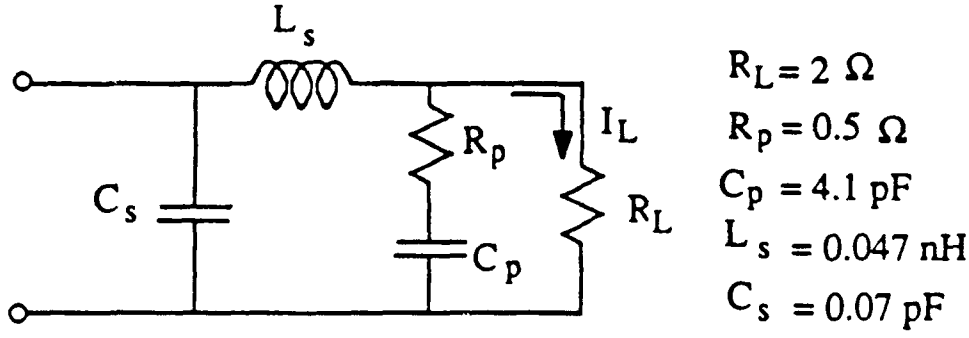

Fig. 2.4 The equivalent circuit of Ortel SL 1000 laser diode.

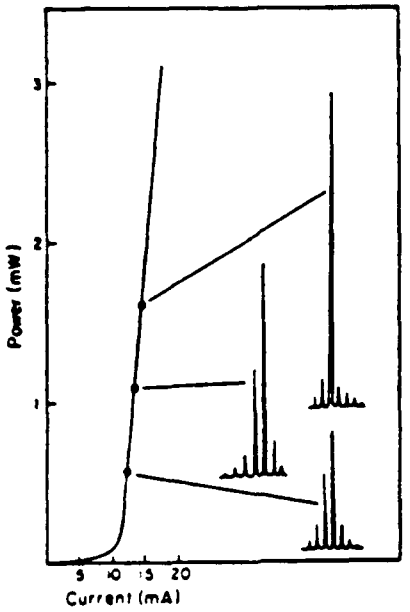

Fig. 2.5 CW light verses current and spectral characteristics of a GaAs laser whose cavity length is 250 μm [7].

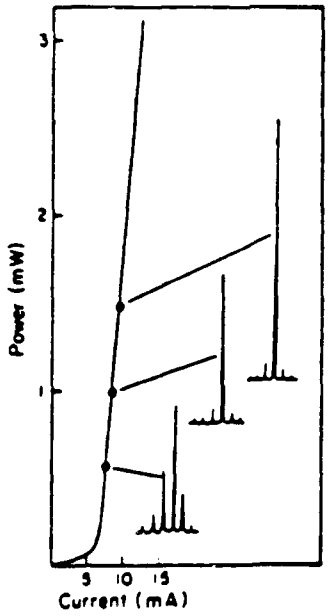

Fig. 2.6 CW light verses current spectral characteristics of GaAs laser identical to that shown in Fig. 2.5 except the cavity length is 120 um [7].

2.1.2c. Laser Noise

Laser noise is of great concern in high frequency fiber-optics signal transmission. At the receiver, the optical power is quite high because the transmission distance is limited by the fiber bandwidth and not by the attenuation [34], therefore the laser noise dominates the receiver noise. Laser noise can be put into two categories: intensity and phase fluctuations. The origin of these fluctuations lies in the inherent laser instability and the light fluctuation from a distant reflector.

The intrinsic fluctuation behavior of the semiconductor laser diode was theoretically described for the first time by MacCumber[35]. It is due to the quantum statistical nature of carrier recombination and photon generation and is unavoidable. The low frequency intensity fluctuation increases with the increase in the photon density until it reaches a maximum at threshold. Above this threshold, where strong pumping occurs, stabilization is effective and the intensity fluctuations decrease rapidly with increasing population density. The intrinsic fluctuations can promote excess noise or even self-sustained oscillation in the semiconductor lasers along with nonlinear output characteristics [36]. Excess noise or the oscillation appears more frequently in semiconductor lasers with gain guiding than indexed guiding lasers [36, 37].

The intensity noise spectrum shows a peak near the relaxation oscillation frequency f_r, as the consequence of the intrinsic laser resonance [35, 38]. Feedback from a distant reflector also causes periodic noise enhancement at a high frequency near the relaxation oscillation frequency [39] which is of great concern in high frequency microwave fiber-optic systems. This resonant peak may be flatten if the distant reflector is placed at the round-trip time shorter than the inverse of the relaxation oscillation frequency, f_r, of the solitary laser [34]. The experiments that were carried out by [34] for different structure and material parameters, show that the lasers oscillating in a single longitudinal mode have almost identical noise level at the same normalized injection current. It was also found that laser

noise increases as the number of oscillating longitudinal modes increases. This is the primary reason why the gain-guided lasers are not a good choice for wideband analog communication systems.

Originally, it was thought that $1/f$ noise is not a problem for high frequency applications, however the low frequency noise can beat with the modulated signal and create enhanced noise sidebands around the modulation signal [40]. The beat noise spectrum is proportional to the modulation signal and therefore, $1/f$ noise limits the S/N ratio at high frequency up to a maximum limit which cannot be exceeded even if the modulated signal amplitude is increased. $1/f$ type of low frequency noise is believed to be related to mode hopping.

Some applications require stable microwave phase information, such as phased array radar and therefore phase fluctuations are of great importance. Generally, phase fluctuation can be categorized as : long term phase shift, short term phase noise, and phase variation due to the physical disturbance of the transmission media [41]. Long term fluctuations are related to drift in the operating point or gradual change in the properties of materials. Short term phase noise on the modulated signal originates from the quadrature part of the additive intensity noise in the laser output [41].

Phase fluctuation in the laser modulated light can be the result of physical movement or Raleigh backscattering from the end of the fiber [39]. As the result, the reflected light of random phase causes intensity and frequency fluctuation in the laser output. The output spectra show a periodic peak with fundamental frequency equal to the round-trip frequency of the reflected light [42]. Later it was shown by Agrawal [39] that side peaks appear at each of the fiber-laser longitudinal mode spacing. The mechanism responsible is believed to be that of the phase noise which is signified through the amplified side peaks in the spectral line [43]. Index-guided lasers are far more sensitive to the reflected light because of its longer coherent length, typically of several meters, compared to a few 100 μm for gain guided lasers [36].

These unwanted reflections into the laser may be minimized by AR (Antireflection) coating, index matching fluid, optical isolator, or by proper positioning of the external reflector so that the noise peak is broadened.

2.1.3. Summary

Semiconductor laser diodes which are the high intensity sources for the high-speed lightwave systems have been discussed. The types of laser structures discussed were gain-guided and index-guided. Index-guided lasers usually have narrower linewidth and lower RIN (relative intensity noise), but are more sensitive to phase fluctuations when compared to the gain guided lasers.

The dynamical parameters of semiconductor laser diode that are of concerned were also discussed. They included the modulation bandwidth, single mode operation, and the electrical intensity and phase noise in the semiconductor laser diode.

2.2. High-Speed Optical Detectors

Optical detectors and semiconductor laser diodes are the two most important elements of a high-speed fiber-optic distribution network. Photodetectors may be classified as those based on the concept of optically generated carriers, i.e.photoconductors, or depleted junction devices, such as PIN, Schottky barrier, or avalanche photodiodes.

The important parameters of photodetectors are: responsivity, low capacitance for high-speed applications, low noise, and low dark current. The efficiency of photodetectors is expressed in term of responsivity, in the units of mA/mW of incident light. This quantity is the measure of the photocurrent generated per unit of incident optical power.

The speed of the photodetector should be sufficiently fast to accommodate the highest modulation frequency. The intrinsic noise in the photoconductor is composed of thermal and shot noise. Shot noise arises from the random fluctuation in the photocurrent when crossing a p-n junction, and thermal noise is the consequence of random thermal motion of the charge carriers [44]. Dark current originates from the leakage current and it ultimately reduces the sensitivity of the receiver, and also contributes to the shot noise.

In hybrid optical receivers, the choice of material for the optical detector is fairly clear. Silicon and germanium based detectors are ideal for emitting wavelengths near 0.7-0.9 um and 1.2-1.6 um respectively, since they have sensitivities greater by an order of magnitude larger than their III-V based counterparts. However, with the further trend in monolithic integration of microwave and optoelectronic devices on GaAs and InP substrates, there is currently great interest in the development of AlGaAs detectors for near infrared wavelengths, 0.7-0.9 um, and InGaAsP/InP and InGaAs compound for 1.2-1.6 um for long-wavelength systems.

There are many types of photodetectors, but only four structures are viable for optical communication. In the following sections these optical detectors, namely, photoconductors, PIN photodiode, Schottky photodiode, and avalanche photodiode, are discussed.

2.2.1. Photoconductors

In photoconductors, the electrical conductivity increases when illuminated by photons of light with energy greater than the material bandgap energy. Incident light beam generates free electron-hole pairs in the active region of the device. Under external field, the photo-generated carriers will drift toward the electrode until they are collected or recombine in the bulk semiconductor. For most materials, electrons have higher drift velocity than holes, resulting in faster electronic transit time. In such cases

when the minority carrier are electrons, the photoconductor's response is limited by electron transit time between the electrode which electron must travel. In photoconductors, under the incident light the conductivity increases and thus creates an internal gain mechanism. The internal gain coefficient for a photoconductor is the function of the ratio between the minority carrier lifetime to the transit time. However, the same mechanism is responsible for electron tailing effect which limits the maximum speed [45].

Gain as high as 1000 has been observed for silicon photoconductors compared to a gain of 50 to 100 for GaAs devices, but with practically the same gain bandwidth products. AlGaAs modulation doped photoconductor detectors [45] demonstrated a gain of 11 and 2 at 10 KHz and 1.5 GHz respectively. The sensitivity of photoconductors is limited by the dark current and by the external quantum efficiency. Photoconductive detectors suffer from reflection losses at the electrodes. Alternatively, a backside or sideways illuminated photoconductor may improve the electrode reflection losses, but causes fabrication difficulty [45].

Direct photoconduction in semiconductors has long been used for optical control of microwave and millimeterwave devices [5]. Photoconductive induced effects on several III-V compound semiconductor devices, such as GaAs MESFET, InP MESFET, AlGaAs/GaAs HEMT, and GaAs PBT have been investigated [46]. A uniformly doped GaAs MESFET had a typical optical gain in the range of 5-10 for photoconductive regime compared to a gain of 50-70 when operated in the photovoltic regime [47].

2.2.2. Photodiode based on p-n Junction, PIN, Schottky, APD

The most commonly, used photodetectors in fiber-optic systems are the PIN photodiode and avalanche photodiode (APD). More recently Schottky photodiodes have demonstrated millimeterwave speeds [48]. Detectors based on p-n junction are often reverse biased to fully deplete the junction from the carriers, and in turn reduce the depletion capacitance for

faster response time. When photodiodes are operated in the photoconductive mode instead of the photovoltaic mode, the dark current increases.

The choice of material for the construction of photodiodes depend on the wavelength of interest. Silicon photodiodes respond from visible light up to 1 μm wavelength, germanium photodiodes respond in the 1-1.6 μm range. GaAs response covers the range of 0.7-0.9 μm, where InGaAsP responds to light with wavelengths in the 1-1.6 μm. In general, semiconductor material with lower bandgap have higher dark current and are more sensitive to temperature.

PIN photodiode structure, Fig. 2.7, consists of a p and n region separated by a very lightly n doped intrinsic I-region. Unilluminated, the only current flowing is the dark current. However, when the incident photon on the I-layer have energy greater than or equal to the bandgap energy of semiconductor material, electron-hole pairs in this region sweep to the n and p side of diode, respectively, hence generating photocurrent. Due to the intrinsic layer, PIN devices have internal gain of unity, thus; for the same gain bandwidth product PIN photodiodes inherently have higher speed than photoconductors.

Photons absorbed in the top and bottom p and n layer also produce free carriers, which diffuse back into the I-region before they recombine. Since the diffusion time constant is quite long (on the order of nanoseconds), thus is a serious limitation in terms of maximum speed. Also limiting the speed is the capacitance associated with the depletion region. Finally, a less serious limitation on the speed is due to the finite drift time associated to the photogenerated carriers in the I-region. In a well designed photodiode, the drift time is less than 5 ps, and hence would not pose a significant problem except at very high frequencies (> 100 GHz) [49].

From the above discussion it is clear that the design of a high performance PIN photodiode must: a) have reduced doping in the I layer; b) have reduced shunt capacitance; and c) avoid optical absorption in the P and N sandwiching layers. The first condition can be accomplished in the processing, but will lower the depletion potential and consequently reduce

the leakage current while the device is operating with saturation drift velocity. The second condition may be achieved by reducing the active area of the device and careful packaging. The third condition may be accomplished effectively by using a heterostructure [49]. in which the top p layer is composed of GaAlAs while the I-layer is composed of GaAs and is sufficiently thick to absorb nearly all the incident light. The GaAlAs is of higher bandgap and is therefore transparent to incident radiation which would be absorbed in the I-layer.

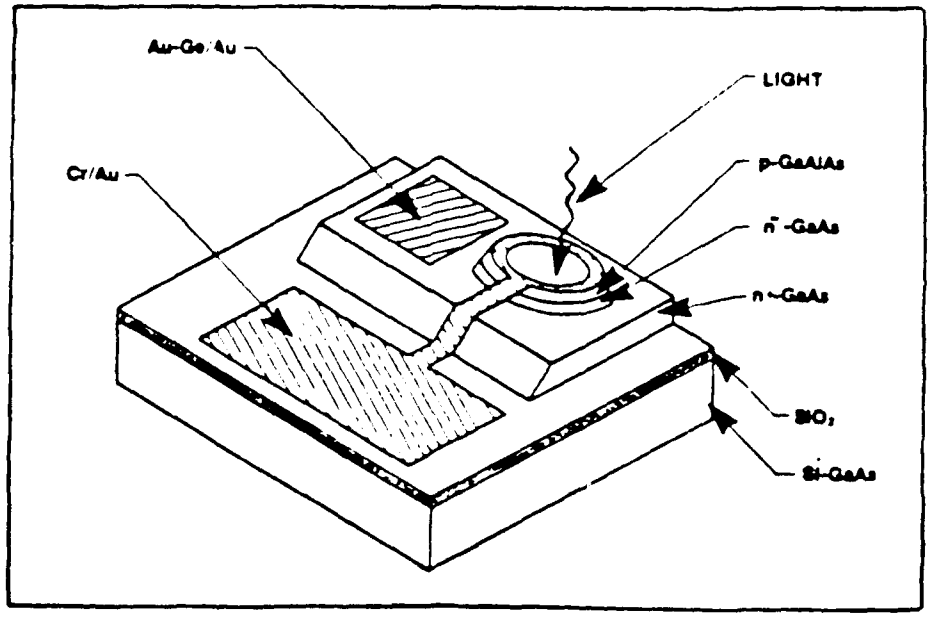

Fig. 2.7 Schematic representation of a GaAs PIN photodiode [49].

A heterostructure GaAlAs/GaAs PIN photodiode on a semi-insulating GaAs substrate has a 3 dB bandwidth of 15 GHz at 0.84 um with responsivity of 0.45 mA/mW, which corresponds to an external quantum efficiency of 65% [49]. InGaAs PIN photodiodes have shown impressive 3 dB bandwidth of 67 GHz [50].

A Schottky barrier photodiode works on the same principle as a PIN photodiode, but optical absorption takes place in the depletion region of the metal-semiconductor Schottky junction instead of the intrinsic layer of the p-n junction. The responsivity of these devices are lower due to the presence of a metallic layer on the surface of the photodiode. The fastest photodiode reported to date is a 100 GHz bandwidth, planar doped GaAs Schottky photodiode [48].

An avalanche photodiode works on the same principle as PIN photodiode, where the reverse bias p-n junction is depleted of carriers and upon illumination, electron-holes pairs are generated. In contrast to PIN devices, APD diodes are biased at a breakdown voltage, where the high electric field strength (on the order of 10^5 V/cm) at the junction accelerates the photo-generated electron and holes. These can collide with a bonded electron with sufficient energy to cause ionization, thereby creating an extra electron hole pair. This carrier multiplication mechanism is known as impact ionization [51]. The additional carriers, in turn, can gain enough energy from the field to cause further impact ionization until an avalanche of carriers is produced. Thus, one single incident photon can create M electron-hole pairs, and hence the responsivity of avalanche detector is increased by the multiplication factor M.

The collision of carriers in the avalanche process slow down the carrier speeds and hence adds another limiting factor on the bandwidth of APD compared to the PIN. A detailed analysis of APD [44] shows that for high values of M, the relationship between M and gain bandwidth product remains constant.

All photodiodes based on the p-n junction suffer from the shot noise and dark current similar to the photoconductor. However, in APD, the primarily source of noise is avalanche noise, which is due to the statistical nature of the ionization process. APD with gain bandwidth products of 40 GHz has been reported, which makes them useful as receivers with bandwidth of up to 5 GHz [52].

2.2.3. Summary

Four commonly used photodetectors suitable for high-speed fiber-optic links namely photoconductors, PIN photodiodes, APD photodiodes, and Schottky Photodiodes, were discussed. The PIN photodiode is the most frequently used detector, it has the best linear response, higher responsivity than Schottky photodiode, fast response, and lower noise than APD photodiode and photoconductor.

APD photodiodes are useful in the low GHz application but, Their large bias voltage is a drawback. Photoconductors are not commonly used for optical communication, but photoconduction effects in the microwave devices have been used for optical control of microwave systems. The Schottky barrier photodiode has demonstrated the largest bandwidth, 100 GHz, but with substantially lower responsivity than PIN structure.

The photodetectors based on III-V compounds are by an order of magnitude inferior to Si or Ge based. However, due to the trend in monolithically integrated optoelectronics systems, photoconductors based on III-V compounds are preferred over Si or Ge since they are readily integrateable.

Chapter III

DE-EMBEDDING S-PARAMETERS OF LASER DIODE

A problem encountered when measuring Scattering-parameters (S-parameters) of a Device Under Test (DUT) is that the reference planes for the measurements are at the terminals of the package thus, the embedded S-parameters are measured. In the case of a laser diode, de-embedding gives the S-parameters of the device, which may then be used to design matching circuits or determine the effect of parasitics on the modulation characteristics of the laser. De-embedding has been used for calibrating the automatic network analyzer [53]. In these systems de-embedding compensates for imperfections, which limits the measurement accuracy at microwave frequencies, such as finite directivity, coupling error, residual VSWR. All of these and other similar imperfections limit the accuracy of the measurements performed by the network analyzer. To improve the accuracy and keep costs low, network analyzers are calibrated to remove the effects of these imperfections rather than making perfect components. Some of the common techniques to calibrate the automatic network analyzer are for example: Load-Open-Short-Through [54], Through-Short-Delay [55], and use of three offset shorts [56]. Another technique, although not as popular because of its computational requirements, is the un-termination technique [57].

The above techniques are well suited for packaged devices with connectors. However, for measurement of laser chip creating calibration or measurement standards such as short or open is not practical. One technique that circumvents these drawbacks is "Through-Reflect-Line" (TRL). This scheme requires only one length of precision transmission line which is easily fabricated on ceramics. Recently HP introduced their 8510B network analyzer which incorporates this technique based on a

paper written by G. Engen [58]. A drawback of the 8510B calibration is that the error correcting coefficients for the system and the package are coupled therefore, it requires that the user recalibrate the analyzer each time.

The TRL calibration developed here is resident on the IBM PC for our 8510A which does not have the HP TRL system. This locally configured system has a distinct advantage in that the system error coefficients are not lumped with the package error coefficients. The user recalibrates the 8510A each time with the calibration standards to the coaxial connector ports, which accounts for the instrument error. Since the microstrip fixtures do not change from day to day once the fixture error parameters are extracted using the TRL procedure, it is not necessary to recalibrate the fixture. This saves time, and avoids the required bond connection in the fixture each time for "through" and "line" measurements and eventually reducing the fixture life.

3.1. TRL Calibration Procedure

The advantage of the TRL Calibration is that it has eliminated the need for calibration standards. In contrast, the "Through-Short-Delay" (TSD), requires a short circuit of known reflection coefficient. The two requirements for TRL method are that a length of line be inserted between the left and right half of the fixture and the two halves at the interface junction have similar characteristics. The custom fixture designed and built here has a split-half design which can easily accommodate the extra line length. The second requirement is that each half have a similar reflection coefficient at the microstrip end, and is thus simply satisfied as long as the microstrip widths are the same, and the substrates are similarly mounted. These requirements are easily met in the fabrication. The functional block diagram of the TRL calibration is shown in the Fig. 3.1.

The scattering parameters of the three cascaded two-ports are obtained from the Through, Reflect, and Line connection as indicated by

the dashed line in Fig. 3.1. Where the emergent waves b_1, b_2, at the terminals 1 and 2 are related to the incident wave a_1, a_2, by the scattering matrix given

$$b_1 = S_{11}a_1 + S_{12}a_2 \tag{3.1}$$

$$b_2 = S_{21}a_1 + S_{22}a_2 \tag{3.2}$$

where S_{ij} is the scattering coefficient. Dividing equations (3.1) and (3.2) by a_1 and a_2 respectively gives

$$\frac{b_1}{a_1} = S_{11} + S_{12}\frac{a_2}{a_1} \tag{3.3}$$

$$\frac{b_2}{a_2} = S_{21}\frac{a_1}{a_2} + S_{22} \tag{3.4}$$

eliminating $\frac{a_1}{a_2}$ between equations (3.3) and (3.4) gives:

$$\frac{S_{12}S_{21}}{w_1 - S_{11}} = w_2 - S_{22} \tag{3.5}$$

where $w_1 = \frac{b_1}{a_1}$ and $w_2 = \frac{b_2}{a_2}$ and expanding this results in

$$w_2S_{11} + w_1S_{12} - \Delta = w_1w_2 \tag{3.6}$$

where $$\Delta = S_{11}S_{22} - S_{12}S_{21} \; . \tag{3.7}$$

In the next section it will be shown how the TRL scheme solves for the embedding box A and B.

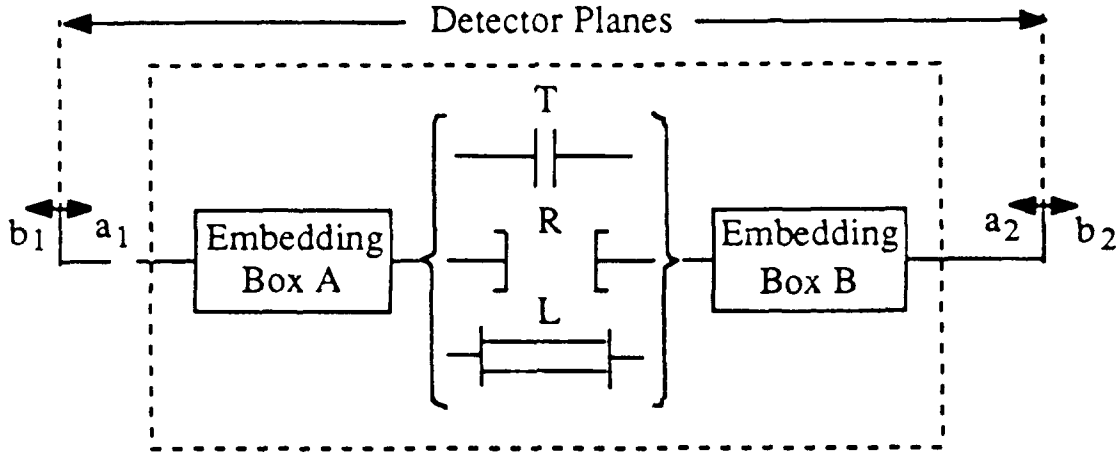

Fig. 3.1 The functional block diagram of the TRL Procedure.

3.1.1. The TRL Solution

Suppose S_{11}, S_{12}, S_{21}, and S_{22} are the S-parameters for three cascaded two ports which result from Through, Reflect, and Line measurements. The goal is to determine the scattering parameters of the individual error boxes.

Lets first solve equations (3.1) and (3.2) for a_1 and b_1 as the function of a_2 and b_2, this gives

$$\begin{pmatrix} b_1 \\ a_1 \end{pmatrix} = \frac{1}{S_{21}} \begin{pmatrix} -\Delta & S_{22} \\ S_{11} & 1 \end{pmatrix} \begin{pmatrix} a_2 \\ b_2 \end{pmatrix} = R \begin{pmatrix} a_2 \\ b_2 \end{pmatrix} \tag{3.8}$$

where R is known as the wave cascading matrix. The important property of R matrix is that the product of two-ports in cascade is merely the product of the individual R matrices.

Let the cascaded two port error matrices A, B be denoted by R_a and R_b respectively, while R_t represents their cascade "Thru" two-ports as

$$R_t = R_a R_b \tag{3.9}$$

while R_d represents the cascaded matrices A and B with a length of line inserted in the middle, given as

$$R_d = R_a R_l R_b \ . \tag{3.10}$$

R_l is the two port transfer parameter for the extra line length

$$R_L = \begin{pmatrix} e^{-\gamma l} & 0 \\ 0 & e^{+\gamma l} \end{pmatrix} \tag{3.11}$$

where γ is the propagation constant and l is the effective line length. Solving equation (3.9) for R_b gives

$$R_b = R_a^{-1} R_t \tag{3.12}$$

using equation (3.12) to eliminate R_b from equation (3.10) gives

$$R_d = R_a R_l R_a^{-1} R_t \tag{3.13}$$

rewriting the above equation as

$$TR_a = R_a R_l \tag{3.14}$$

where

$$T = R_d R_t^{-1} \ . \tag{3.15}$$

Expansion of equation (3.14), where the matrix elements R_a and T are represented by their corresponding row and column elements r_{ij} and t_{ij} respectively, gives:

$$t_{11}r_{11} + t_{12}r_{21} = r_{11}e^{-\gamma l} \tag{3.16}$$

$$t_{21}r_{11} + t_{22}r_{21} = r_{21}e^{-\gamma l} \tag{3.17}$$

$$t_{11}r_{12} + t_{12}r_{22} = r_{12}e^{+\gamma l} \tag{3.18}$$

$$t_{21}r_{12} + t_{22}r_{22} = r_{22}e^{+\gamma l} \ . \tag{3.19}$$

Next, taking the ratio of the equations (3.16) to (3.17) and (3.18) to (3.19) respectively gives:

$$t_{21}\left(\frac{r_{11}}{r_{21}}\right)^2 + (t_{22} - t_{11})\left(\frac{r_{11}}{r_{21}}\right) - t_{12} = 0 \tag{3.20}$$

$$t_{21}\left(\frac{r_{12}}{r_{22}}\right)^2 + (t_{22} - t_{11})\left(\frac{r_{12}}{r_{22}}\right) - t_{12} = 0 \tag{3.21}$$

the ratio of (r_{11}/r_{21}) and (r_{12}/r_{22}) are given by the solution of the quadratic equations (3.20) and (3.21), where the coefficients are the elements of the T-matrix. The problem of which root represents which ratio will be deferred for now and let's assume that (r_{11}/r_{21}) and (r_{12}/r_{22}) are known. Then, taking the ratio of equation (3.19) to (3.17) gives:

$$e^{2\gamma l} = \frac{t_{21}(r_{12}/r_{22}) + t_{22}}{t_{12}(r_{21}/r_{11}) + t_{11}} \tag{3.22}$$

At this point three roots have been solved (r_{11}/r_{21}), (r_{12}/r_{22}), and $e^{2\gamma l}$. Ordinarily, a system of equations such as (3.16) to (3.19) may be solved to yield four roots. One possibility, after examining the roots of equations (3.20) and (3.21) is that a singular root exist. This in turn, is only possible if for the error box A, $S_{12}S_{21}=0$, obviously not true for a practical system. Therefore, there must be two distinct roots the signs which of will be determined with the aide of equation (3.22). Hence, for a passive lossy length of line $|e^{2\gamma l}|<1$.

Solving equations (3.20) and (3.21) for (r_{11}/r_{21}), (r_{12}/r_{21}) in term of t_{ij}, then subsisting in (3.22) gives:

$$e^{2\gamma l} = \frac{t_{11} + t_{22} \pm R}{t_{11} + t_{22} \pm R} \tag{3.23}$$

where

$$R = \pm\sqrt{(t_{11} - t_{22})^2 + 4t_{12}t_{21}} \tag{3.24}$$

and the choice of the sign can easily be made using the condition $|e^{2\gamma l}|<1$ for a passive transmission line. Often $|e^{2\gamma l}|$ is very close to unity and sometimes the measurement accuracy may mask the difference. Therefore, in this procedure $|e^{2\gamma l}|$ was compared to the other root instead of comparing it to the unity.

After examination of equation (3.14), noting that the determinant of a product is equal to the product of determinants, one has

$$\det[T]\det[R_a] = \det[R_a]\det[R_L] \tag{3.25}$$

simplifying gives

$$t_{11}t_{22} - t_{12}t_{21} = 1 \tag{3.26}$$

and thus there are only three independent parameters in the T matrix. Since the three independent roots for the system of equation (3.16) to (3.19) have are already been obtained, no further information may be obtained from this system of equations.

By means of equations (3.20) to (3.22) it is possible to solve for (r_{11}/r_{21}), (r_{12}/r_{22}), and $e^{2\gamma l}$ in terms of ratios among the elements of the T matrix. The complete R_t matrix, which is A in cascade with B, needs to be determined, while only S_{11}, S_{22}, and $S_{12}S_{21}$ have been obtained. Examining equation (3.8) shows that R_t may be determined except for a constant multiplier which is $1/S_{21}$. The same also holds for R_d. Fortunately, a procedure may be developed from the ratios of the elements of the T matrix which gives the required information to solve for the individual embedding boxes [58].

The reflection coefficient w_1, which is at the fictitious connector plane for two port error box A, may be related to the reflection coefficient of the load Γ_l, by

$$w_1 = S_{11} + \frac{S_{12}S_{21}\Gamma_l}{1 - \Gamma_L S_{22}}$$

$$= \frac{S_{11} - \Gamma_1 S_{11} S_{22} - \Gamma_1 S_{12} S_{21}}{1 - \Gamma_1 S_{22}} \quad . \tag{3.27}$$

Rewriting the above expression in cascade form, one has

$$w_1 = \frac{a\Gamma_1 + b}{c\Gamma_1 + 1} \tag{3.28}$$

where the coefficients a, b, and c are given by

$$a = r_{11}/r_{22} \tag{3.29}$$

$$b = r_{12}/r_{22} \tag{3.30}$$

$$c = r_{21}/r_{22} \quad . \tag{3.31}$$

Comparing these with the solutions of quadratic equations (3.20) and (3.21) indicates that b and a/c have already been determined. Solving (3.28) gives

$$a = \frac{w_1 - b}{\Gamma_1(1 - w_1 c/a)} \tag{3.32}$$

if Γ_L is known and different from zero, a may be determined. For the TSD or TOD (Through-Open-Delay) one may stop here and solve for the remaining parameters. However, since open and short circuit are not well characterized, it is preferred not to rely on such measurement. For the "TRL" procedure, it is not required that Γ_L be known but, it must be similar for both halves. Γ_L has yet to be solved for. Returning to equation (3.20) and expanding it.gives

$$r_{22}\rho_{22} \begin{pmatrix} a & c \\ b & 1 \end{pmatrix} \begin{pmatrix} \alpha & \gamma \\ \beta & 1 \end{pmatrix} = g \begin{pmatrix} d & f \\ e & 1 \end{pmatrix} \tag{3.33}$$

where a, b, c, r_{22} and d, e, f, and α, γ, β, ρ_{22} correspond, respectively to matrix elements of R_a, R_b, and R_t. premultiplying by R_a^{-1} results in

$$\rho_{22} \begin{pmatrix} \alpha & \gamma \\ \beta & 1 \end{pmatrix} = \frac{1}{r_{22}(a-bc)} \begin{pmatrix} d-fb & -cd+af \\ e-b & -ce+a \end{pmatrix} \tag{3.34}$$

and solving for the element of R_b matrix in term of R_a and R_t one has

$$\rho_{22} = \frac{-ce + a}{r_{22}(a - bc)} \tag{3.35}$$

$$\gamma = \frac{f - d\ c/a}{1 - e\ c/a} \tag{3.36}$$

$$\beta/\alpha = \frac{e - b}{d - bf} \tag{3.37}$$

$$a\alpha = \frac{d - bf}{1 - e\ c/a} \tag{3.38}$$

where a and c/a are already known and d, e, f, and g are obtained from the ratio among R_t elements. Using equations (3.36) to (3.38) γ, β/α, $a\alpha$ may be solved, but a and α is yet remained to be solved for.

Returning back to the equation (3.28), one may write a similar expression for the embedding box B as

$$\alpha = \frac{w_2 + \gamma}{\Gamma_1(1 + w_2\ b/a)} \tag{3.39}$$

eliminating Γ_1 from equations (3.27) and (3.39), on gets

$$a\alpha = \frac{(w_1 - b)(1 + w_2\ \beta/\alpha)}{(w_2 + \gamma)(1 - w_1\ c/a)} \tag{3.40}$$

and combing with equation (3.40) and eliminating α, gives a value for

$$a = \pm \sqrt{\frac{(w_1 - b)(1 + W_2\ \beta/\alpha)(d - bf)}{(w_2 + \gamma)(1 - w_1\ c/a)(1 - e\ c/a)}} \tag{3.31}$$

$$\text{and} \quad \alpha = \frac{d - bf}{a(1 - e\ c/a)} \ . \tag{3.42}$$

Apart from the choice of sign for a, the requirement that Γ_l be known is eliminated and all of the error parameters are solved. The choice of the sign is easily made, depending whether the reflection coefficient of the load, Γ_l, has a negative or positive phase angle. To check for a valid solution, the value of a may be substituted back into the equation (3.32) and examine the credibility of Γ_l solution.

In the program that is listed in the appendix A, the choice of the sign is based on the reflection "R" standard. In general the sign are + for reflection standard > 50 Ω and - for <50 Ω respectively. However, to improve the accuracy it is preferred to have a threshold level and therefore reflection standard must be >>50 Ω or <<50 Ω. The TRL routine described here requires the user to enter the sign of reflection standard Γ_l, and threshold magnitude is set to |0.64|.

3.1.2. LRL a Variation of TRL

LRL stands for "Line-Reflect-Line" and is very similar to TRL procedure except, a non zero length of through line is used. This scheme's advantage is that the two length of lines and the wire bonds are symmetrical. Where in TRL, there is one bonding for "T" connection and two for "L" connection. This asymmetry may contribute to the discontinuities which is not corrected for. Therefore, it is preferable when the bond wire length cannot be made very short to use LRL even though it requires additional standards and bonding.

The LRL routine will be derived here by modifying the TRL procedure rather than starting from the beginning. Let's rewrite equation (3.10) with two lengths of line, namely R_{l_1}, R_{l_2}, one has

$$R_{d1} = R_a R_{l_1} R_b \tag{3.43}$$

$$R_{d2} = R_a R_{l_2} R_b \tag{3.44}$$

where R_{l_1} and R_{l_2} are the two port cascade matrix for the two line length l_1 and l_2 respectively. Solving equation (3.43) for R_b it gives

$$R_b = R_{l_1}^{-1} R_a^{-1} R_{d_1} \tag{3.45}$$

and substituting equation (3.43) in the equation (3.44) gives

$$R_{d_2} = R_a R_{l_2} R_{l_1}^{-1} R_a^{-1} R_{d_1} \tag{3.46}$$

rewriting equation (3.46) as

$$R_{d2} R_{d1}^{-1} R_a = R_a R_{L2} R_{L1}^{-1} \tag{3.47}$$

and let's define T as

$$T = R_a R_{l_2} R_{l_1}^{-1} . \tag{3.48}$$

Substituting equation (3.48) in (3.49) and writing in term of T results in

$$T R_a = R_a R_{l_2} R_{l_1}^{-1} \tag{3.49}$$

this expression is similar to equation (3.14) except R_L with $R_{l_2} R_{l_1}^{-1}$. Using equation (3.11) and multiplying R_{l_2} by inverse of R_{l_1} one has

$$R_{l_2} R_{l_1}^{-1} = \begin{pmatrix} e^{-\gamma(l_1 - l_2)} & 0 \\ 0 & e^{+\gamma(l_1 - l_2)} \end{pmatrix} . \tag{3.50}$$

Equations (3.49) and (3.50) are similar to (3.11) and (3.14) therefore, one may readily use a TRL program as an LRL procedure by just replacing the line length "l" by "l_1-l_2". In the next section, a de-embedding procedure will be discussed that uses the extracted error coefficients to de-embed the device under test (DUT).

3.2. A De-embedding Procedure

In the previous sections two schemes that extract S-parameter of the left and right halves of embedding boxes were described, namely TRL and LRL. The final task is to use these two-port correcting error coefficients of the package to de-embedd the S-parameter of DUT.

An explicit solution to the scattering parameters of the device under test has been presented [59]. The solution is as follows

$$N_1 = (1 + r_{11}G)(1 + r_{22}H) - r_{11}r_{22}EF \tag{3.51}$$

$$E = (T_{m2} - r_{03})/(r_{01}r_{23}) \tag{3.52}$$

$$F = (T_{m1} - r_{30})/(r_{10}r_{32}) \tag{3.53}$$

$$G = (\rho_{m1} - r_{00})/(r_{01}r_{10}) \tag{3.54}$$

$$H = (\rho_{m2} - r_{33})/(r_{23}r_{32}) \tag{3.55}$$

where ρ_{m1}, T_{m1}, ρ_{m2}, and T_{m2} correspond to the measured S-parameter of the DUT when embedded in the package as illustrated in the functional block diagram Fig. 3.2.

Additional simplification may be done by noting that for a reciprocal network

$$r_{01}r_{23} = r_{10}r_{32} = r_{01}r_{10} = r_{23}r_{32} \tag{3.56}$$

and neglecting the leakage, i.e. letting

$$r_{00} = r_{33} = 0 \ . \tag{3.57}$$

The solution of the DUT scattering parameter is then given by

$$S_{11} = \{G(1 + r_{22}H) - r_{22}EF\}/N_1 \tag{3.58}$$

$$S_{12} = E/N_1 \tag{3.59}$$

$$S_{21} = F/N_1 \tag{3.60}$$

$$S_{11} = \{H(1 + r_{11}G) - r_{11}EF\}/N_1 \ . \tag{3.61}$$

At this point, all of the required expressions have been derived to de-embed. The program de-embed, listed in the Appendix B, carries out this procedure. In the next section, performance of these procedures will be examined.

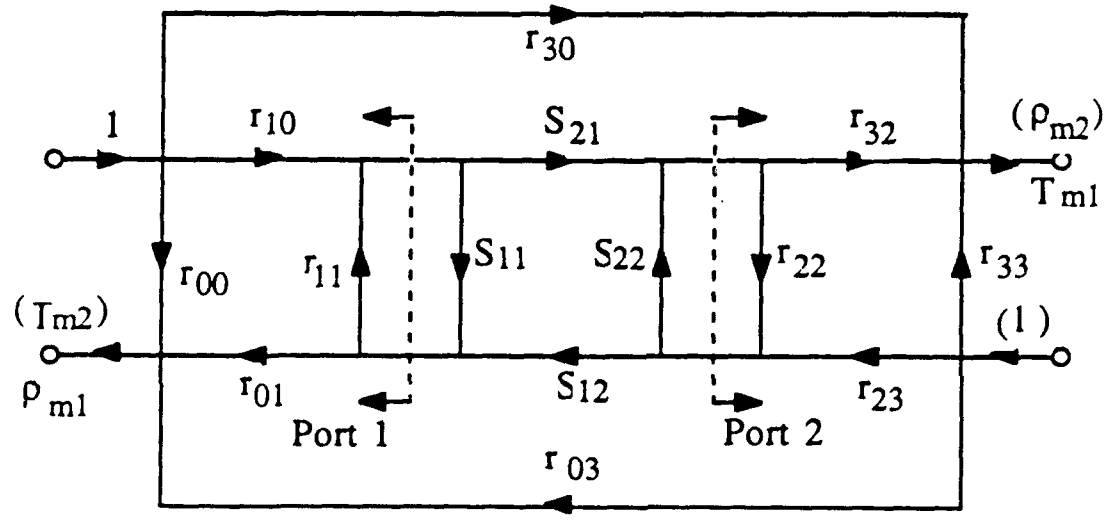

Fig. 3.2 Signal flow graph for measurements on a two port network.

3.3. Overall Performance of the De-embedding Program

A microstrip fixture with 10 mill Alumina substrate and K-connector as the luncher was built. The fixture is a split half design with each side holding a 0.5" long microstrip line. The extra length of line was easily inserted, and mesh bonded for reduced inductance. After calibrating the 8510 to the connector ports with the 3.5 mm standards, the fixture was then measured for through "T", Reflect (open) "R", and line "L". These

files were then stored in the PC. The program TRL reads these files and computes the right and left two port error boxes. To extract the S-parameter of the device under test, the program de-embedd read the left and right error coefficients and the two port measurement of the device to generate the de-embedded device characteristics (DUT).

One method to test the routine is to use the through "T" data also as the measurement data therefore, when de-embedded an identity matrix must result. This is a very severe test and usually runs into round-off error but, it is only used to illustrate that the routine perform well if not better. The results show $|S_{11}|$ and $|S_{22}| < -15$ dB, $|S_{21}| < -1$ dB, and phase of $S_{21} < \pm 2.5^{o}$. These are illustrated respectively in Figs. 3.3, 3.4, 3.5. The TRL de-embedding was performed with a single extra line length of 125 mil long. As the frequency nears the extra line length $\lambda/2$ frequency (~ 19 GHz) then, substantial error occurs in de-embedding. For broader de-embedding, i.e, from MHz to frequencies near and beyond the $\lambda/2$ frequency of the extra line length, multiple line length should be used to cover different frequency range. Also, contributing source of error in these measurements is the removal and subsequent attachment of the luncher after each bonding.

This procedure was used for variety of tasks such as de-embedding the S-parameters of Laser diodes, matching circuits, MESFET, and HBT. In the next section the de-embedded S-parameters of laser diodes and subsequent modeling are discussed.

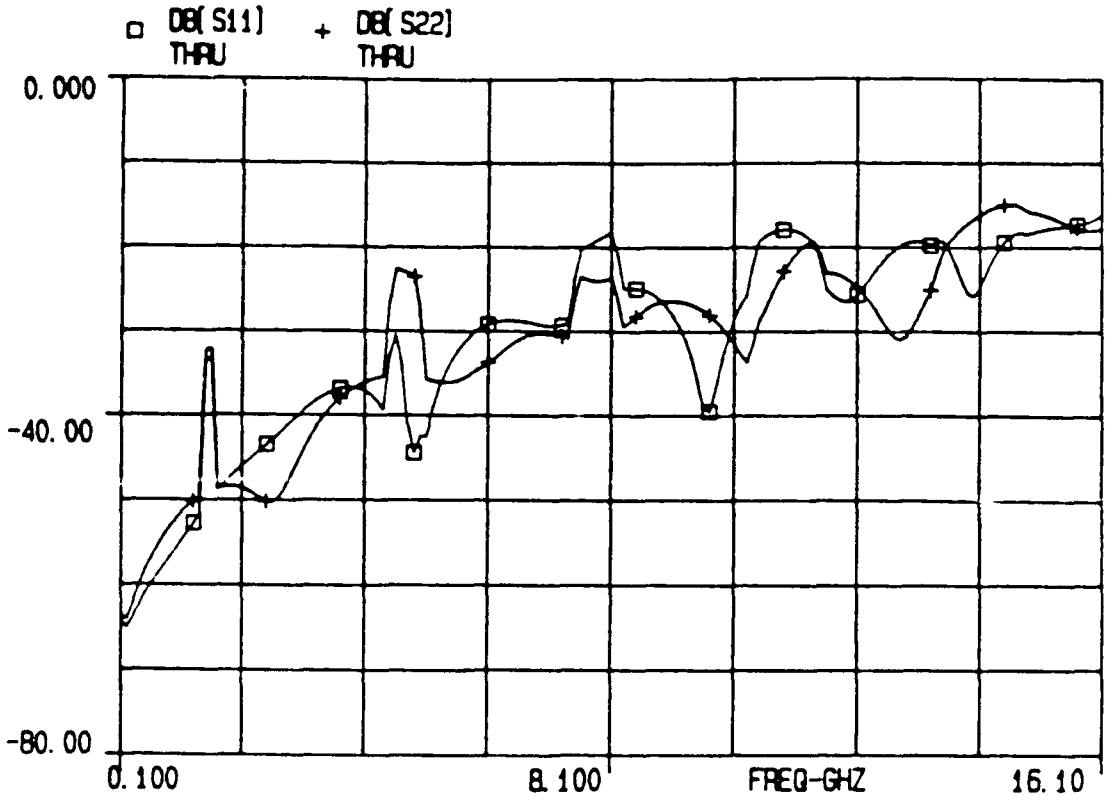

Fig. 3.3 Magnitude of the S_{11} & S_{22} when through line was de-embedded.

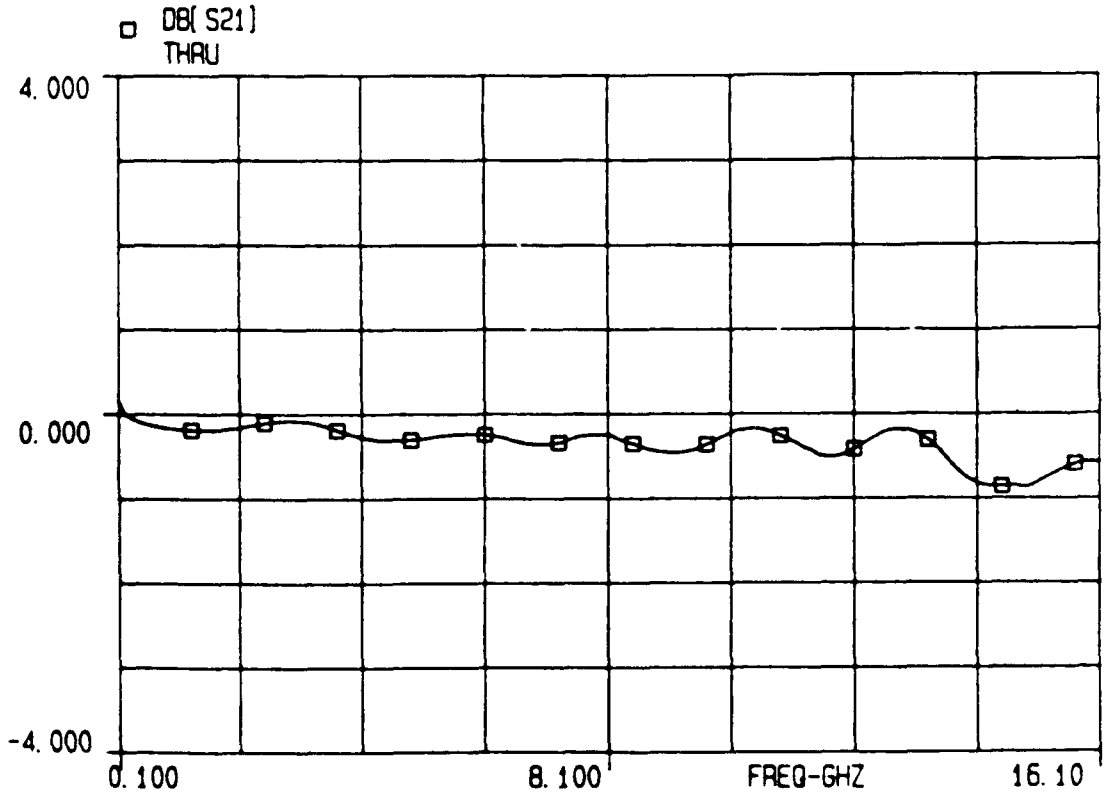

Fig. 3.4 Magnitude of the S_{21} when through line was de-embedded.

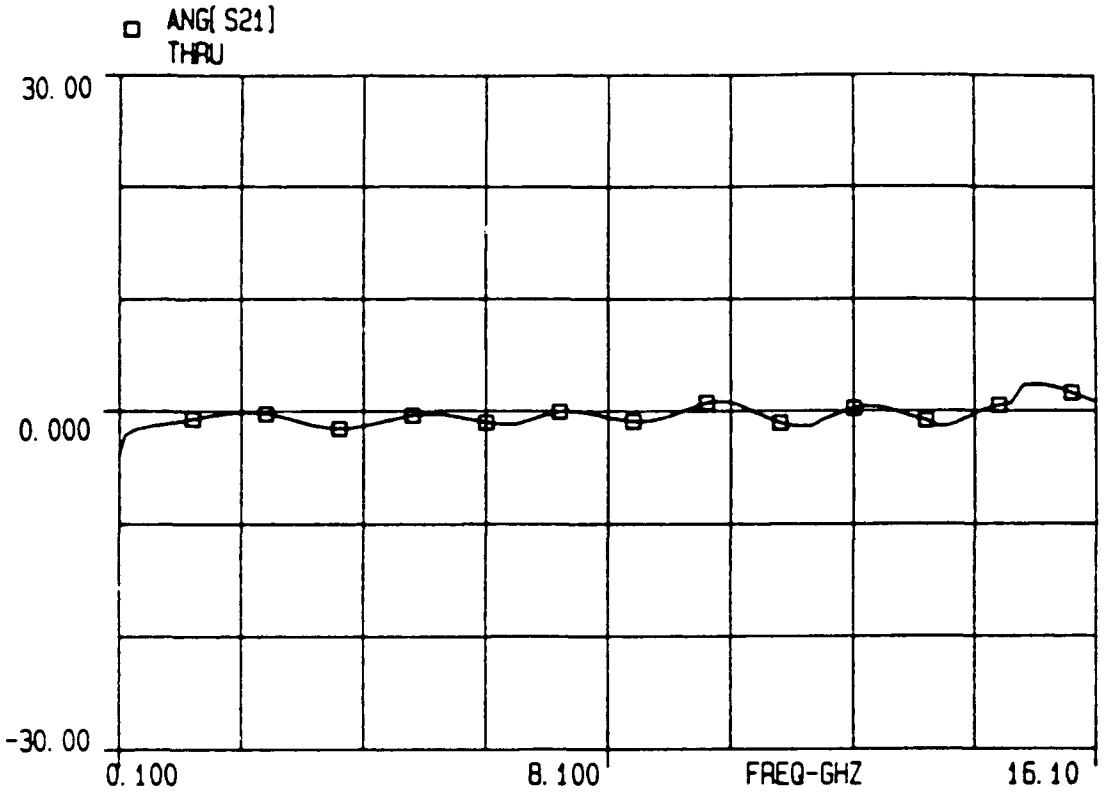

Fig. 3.5 Phase of the S_{21} when through line was de-embedded.

3.4. De-embedding and Modeling Laser Diode S-parameters

The S-parameter extraction and the de-embedding procedures, developed in the previous sections, are employed to de-embed the S-parameter of the Ortel SL1000 laser diodes. The de-embedding and parameter extraction in conjunction with a CAD program is useful in several ways, such as design of a matching circuit, to determine the effects of parasitics, and how to extend the laser modulation frequency.

The high-speed lasers studied in this dissertation were mounted on an open heat sink submount. To test the laser, two special packages were designed. One had a 50 Ω microstrip line on a 10 mil Alumina substrate and the other had a 50 Ω to about 15 Ω Chebychev taper transformer approximated by 10 microstrip sections each being 50 mils long. Fig. 3.6 shows the schematic diagram of the Chebychev taper transformer. A back

to back fixture containing two lunchers and two half-inch long microstrip lines were de-embedded using the TRL procedure and the left and right embedding scattering boxes are extracted. The left or right two-port embedding boxes are similar in characteristics to the actual laser package, which contains a luncher and a length of microstrip line. The 50 Ω and the transformer package responses are respectively shown in the Figs. 3.7 and 3.8. In these figures, the modeled characteristics correspond to the response of the microstrip circuit excluding the launcher response. The measured response shows a dip and a peak respectively in the forward transmission and in the return loss. This is only a computational error in the TRL de-embedding procedure, since the extra line length was about 125 mils which corresponds to a $\lambda/2$ of about 19 GHz and the measured response degrades at these frequencies. The 50 Ω package has a broader and improved response over the transformer package, but when the package is to hold a laser diode with a nominal impedance of a few ohms, the transformer package is preferred unless the device parasitics are too large. The transformer package response has a low frequency cutoff, arising from the microstrip taper length. The high frequency cutoff is due to the approximation made in fabricating the microstrip taper line, which is replaces the Chebychev taper by 10 line sections each 50 mils long.

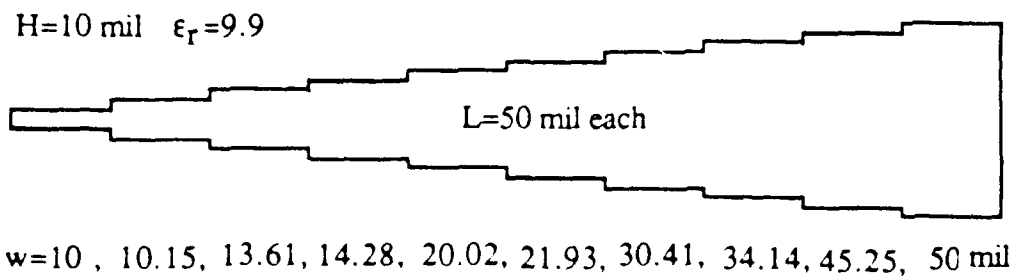

Fig. 3.6 Schematic diagram of the transformer package.

Three laser diodes were tested: a) in the original manufacture's laser submount inserted in the 50 Ω microstrip package, b) in the modified submount with reduced parasitics and inserted in the 50 Ω microstrip package, and c) in the modified submount inserted in the Chebychev transformer package (50 Ω ≈ 15 Ω) and bonded to the 15 Ω side. The return loss for the three package configuration are respectively shown in the Figs. 3.9, 3.10, and 3.11. The return losses, shown in these figures, were measured with the same SMA luncher instead of a K-luncher which is more difficult to attach three times with nearly the same response. As these figures indicate, the original manufacture's submount has the worst return loss. The modified submount, when attached to the 50 Ω line, has the best maximally flat and low reflection over the band. However, the transformer package has a better return loss at a low range of frequencies, but excessively long bond wire in conjunction with the device's capacitance creates a resonance at about 4 GHz and the response degrades beyond this frequency.

A laser diode is a two-port Electro-Optical device with no access to the internal electrical port, therefore it is only possible to make electrical reflection measurements. Using the TRL procedure described in the previous section, the characteristics of the individual fixture have been extracted and the return loss for each high-speed Ortel laser diode has been measured. Next, using the de-embedding procedure, the one-port S-parameter of each laser submount may be determined. The one-port S-parameter of the laser submount contains valuable information,which may be used to design a matching circuit. However, to characterize the parasitics' role on the modulation characteristics of the laser, a two-port S-parameter is required. The solution to this problem is to de-embed the one-port S-parameter and then from the physical geometry of the laser and the package parasitics, an equivalent circuit is devised. The equivalent lumped and distributed circuit model is implemented in the Touchston [60], CAD program and optimization is performed to match the extracted S-parameters. The equivalent circuit is then defined as a two-port network,

where the reflected and the transmitted rf signal to the laser may readily be determined.

The first step is to use the TRL calibration to de-embed the one-port scattering parameters of the laser submount for each package. The lasers mounted in the three packages described above in Fig. 3.12 show the measured return and insertion loss, optimized returned and insertion loss, and Fig. 3.13 similarly shows the phase response for the same quantities. Figs. 3.14 and 3.15 show the magnitude and phase response for another laser in the modified package with tremendous improvements, where as Figs. 3.16 and 3.17 respectively show the response of the laser in the transformer package. The transformer package has a better power coupling than packages with no matching, but its' upper 3 dB cutoff frequency range is not as high as the modified package. The extracted equivalent circuit models for the three cases are shown respectively in Figs. 3.18, 3.19, and 3.20.

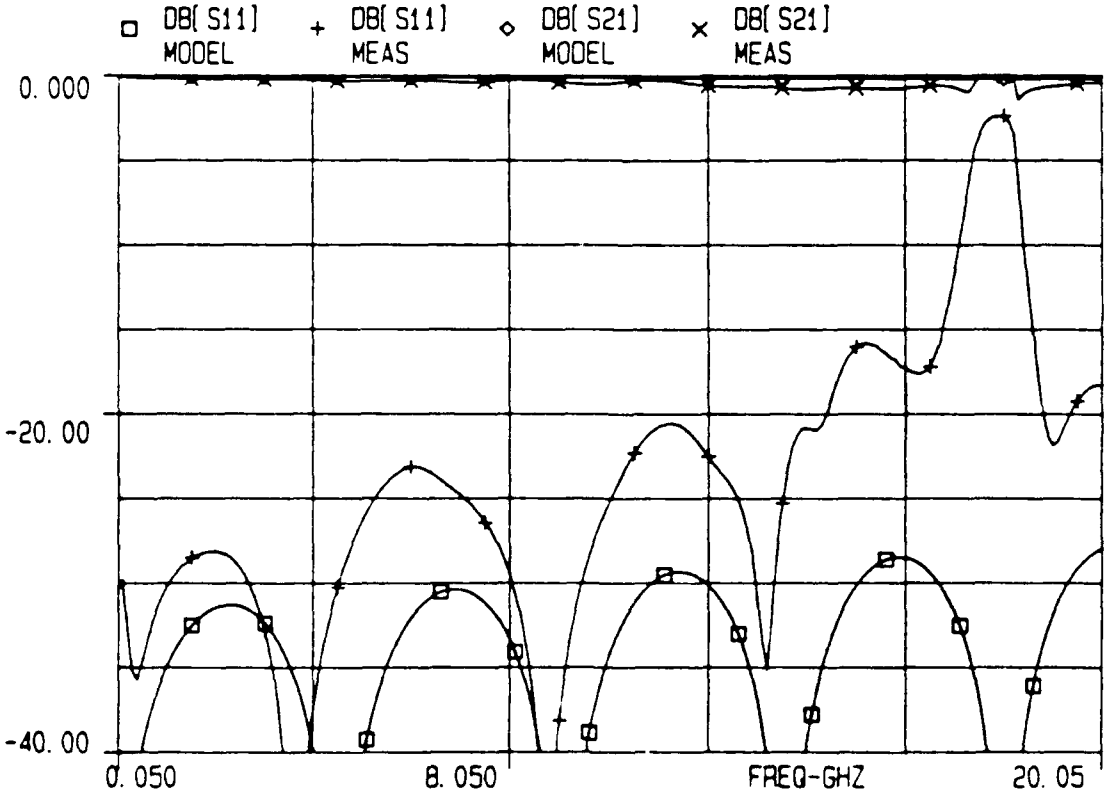

Fig. 3.7 Characteristics of the 50 Ω package.

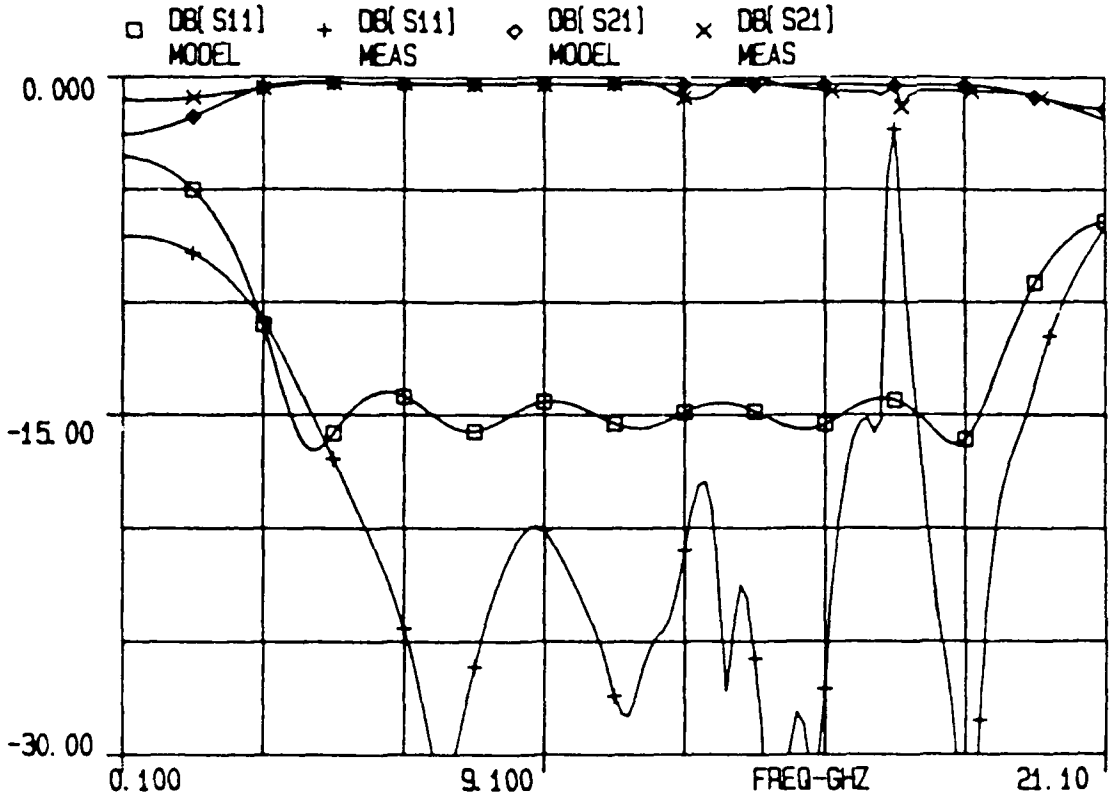

Fig. 3.8 Characteristics of the transformer package.

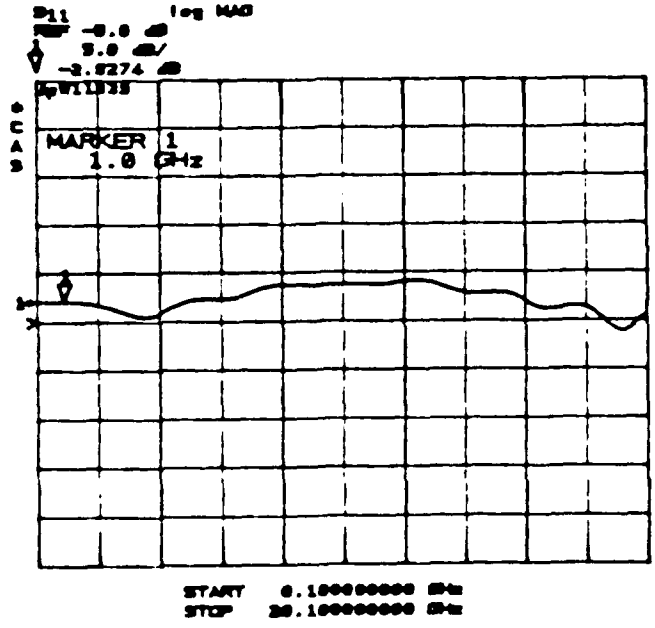

Fig. 3.9 Return loss of manufacture submount in the 50 Ω package.

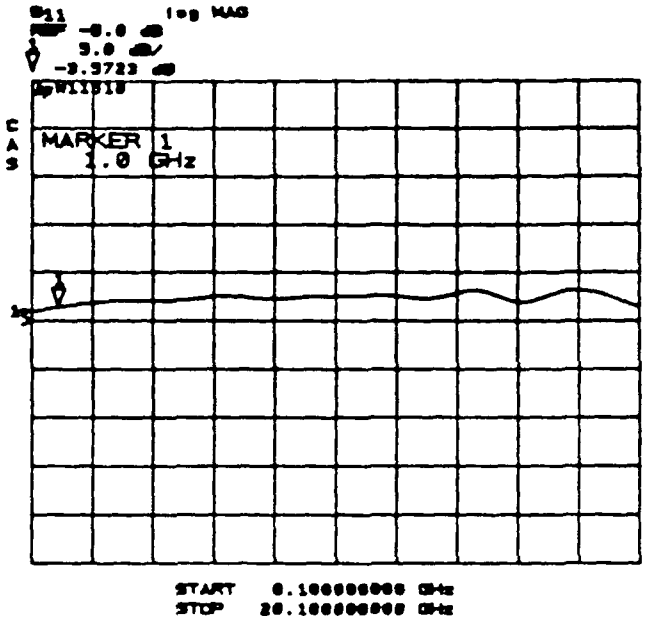

Fig. 3.10 Return loss of modified submount in the 50 Ω package.

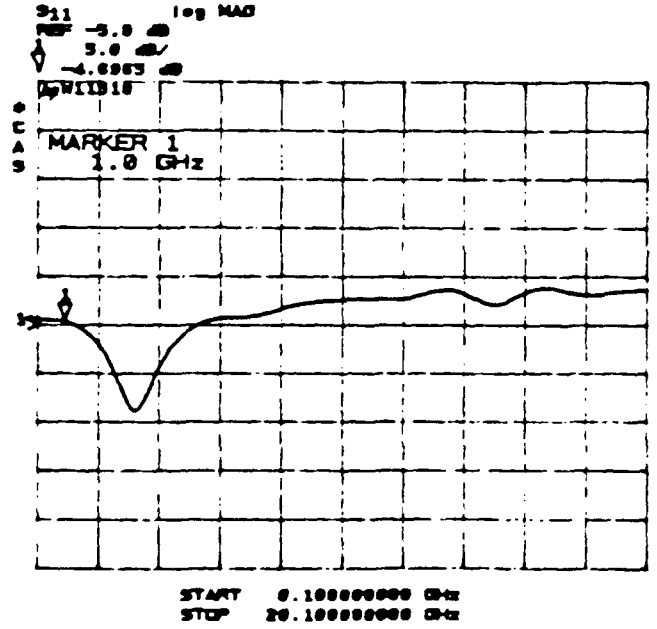

Fig. 3.11 Return loss of modified submount in the transformer package.

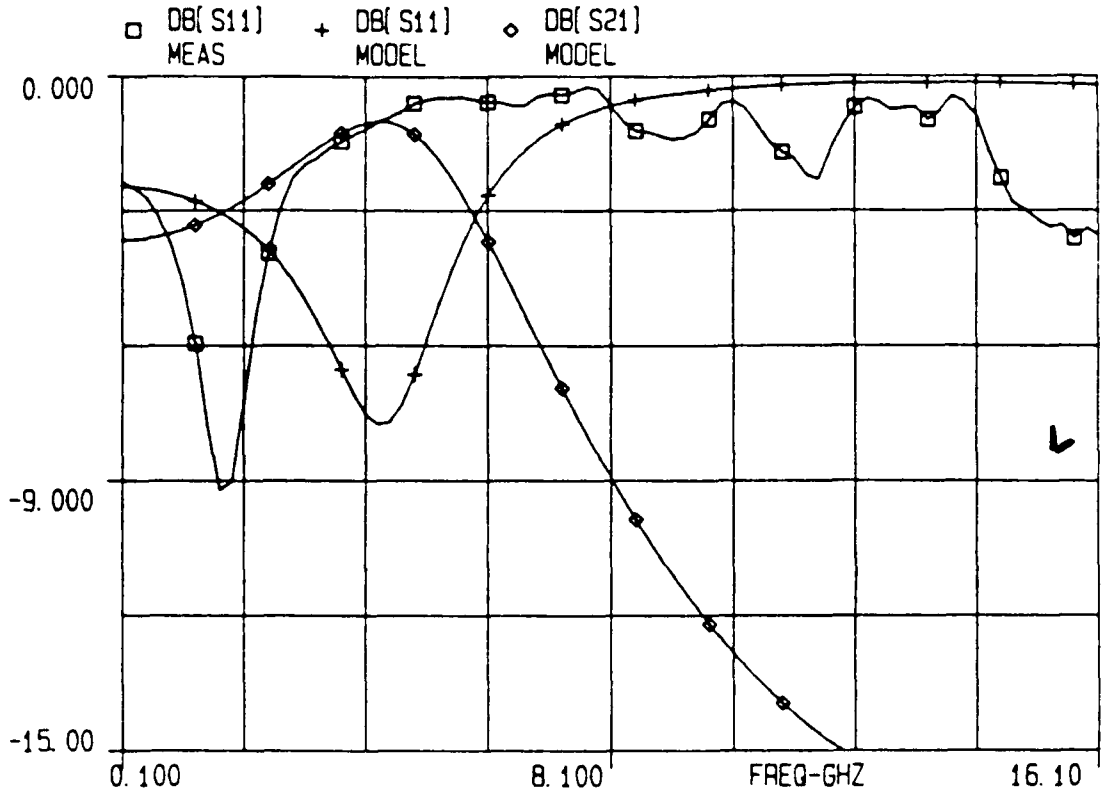

Fig. 3.12 Magnitude response of the laser with manufacture submount.

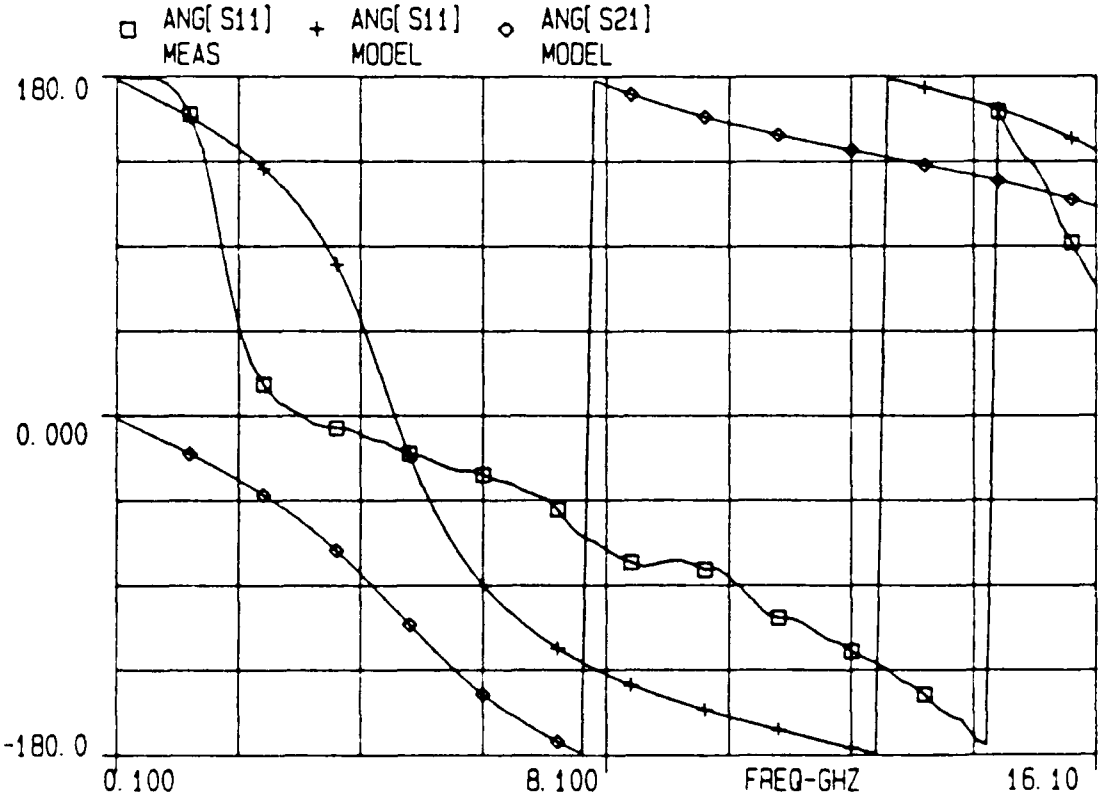

Fig. 3.13 Phase response of the laser with manufacture submount.

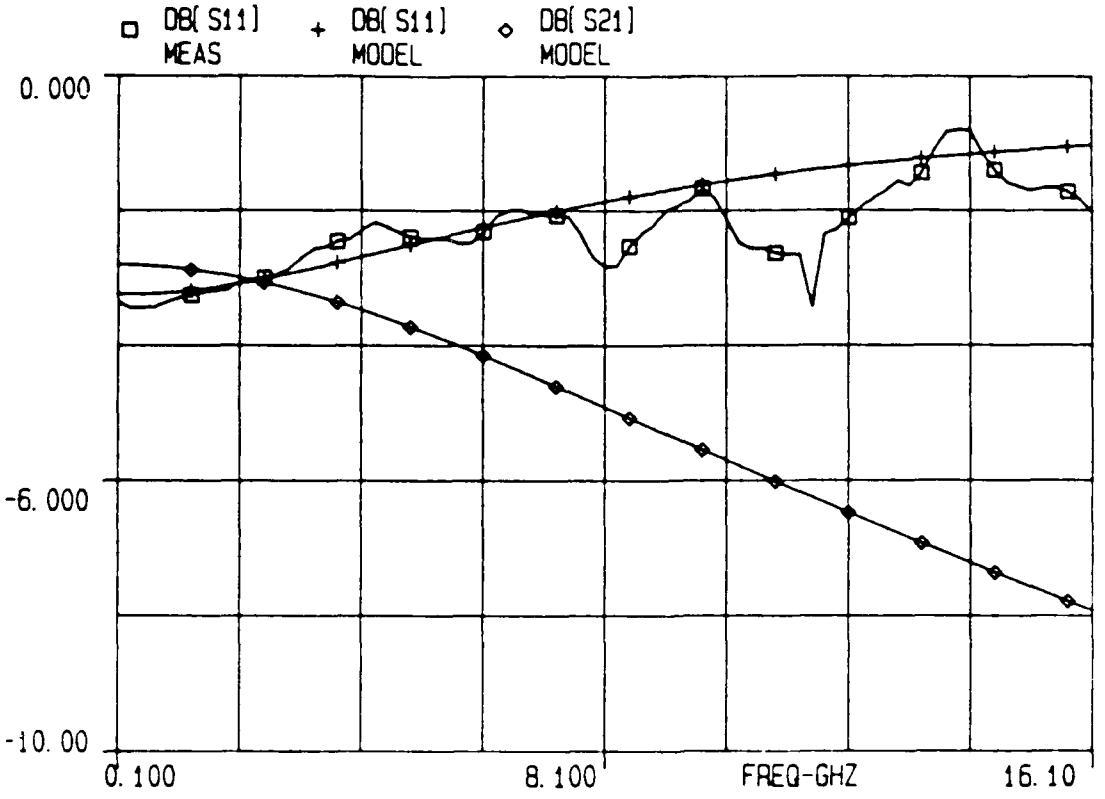

Fig. 3.14 Magnitude response of the modified laser submount.

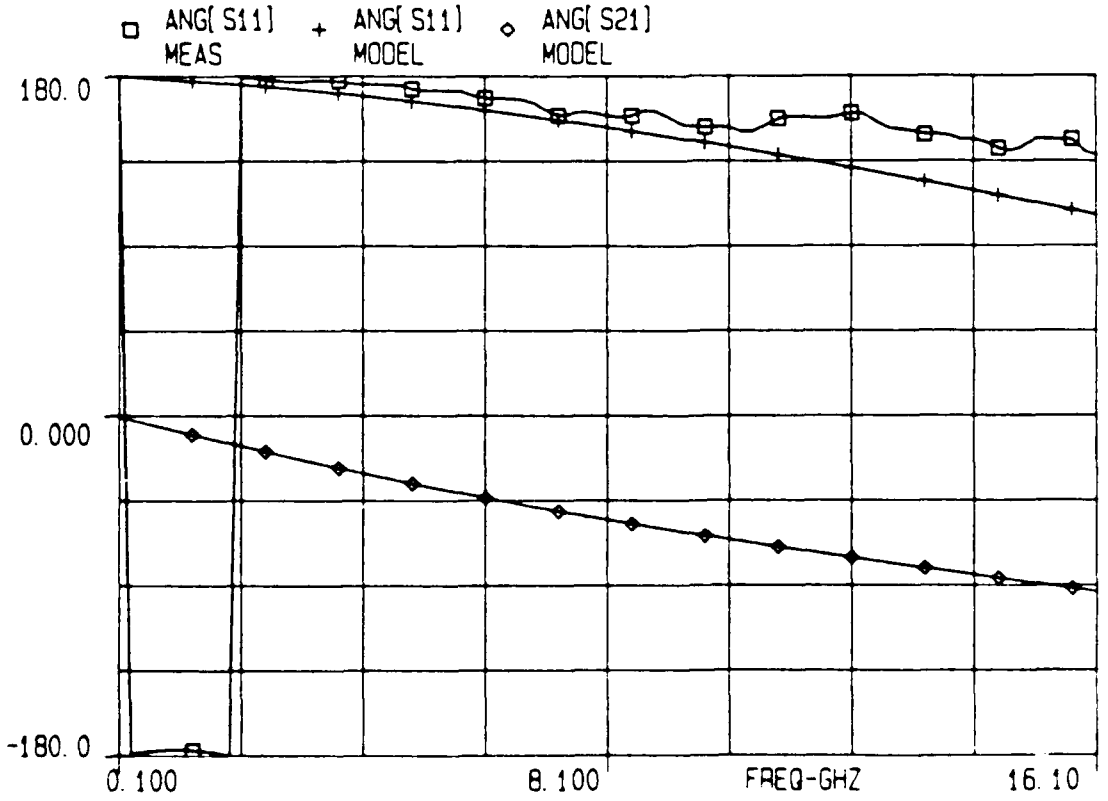

Fig. 3.15 Phase response of the modified laser submount.

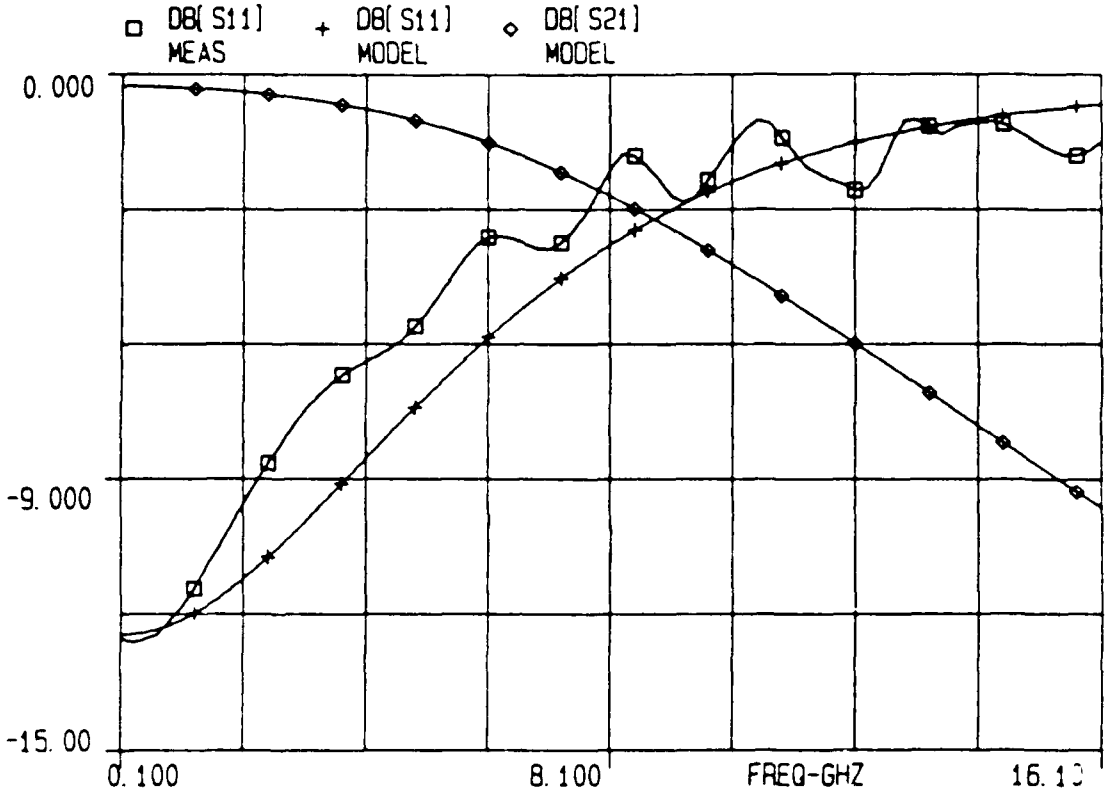

Fig. 3.16 Magnitude response of the modified laser submount, taper.

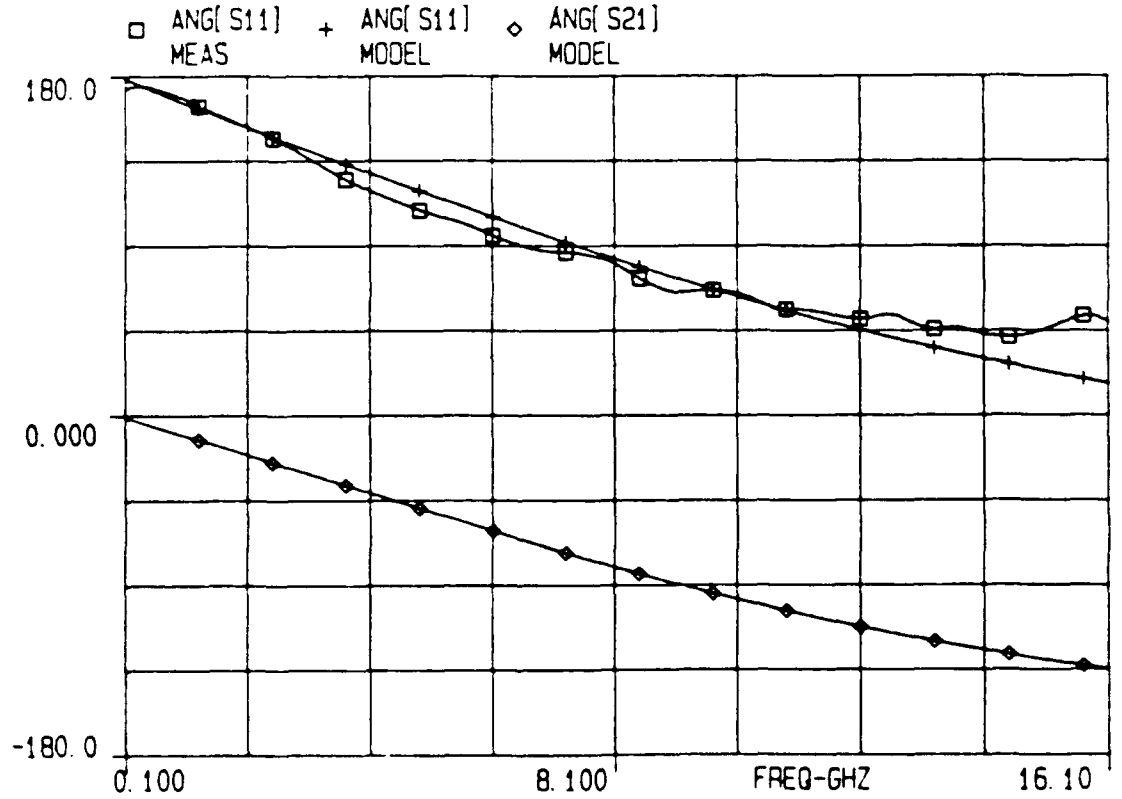

Fig. 3.17 Phase response of the modified laser submount, taper

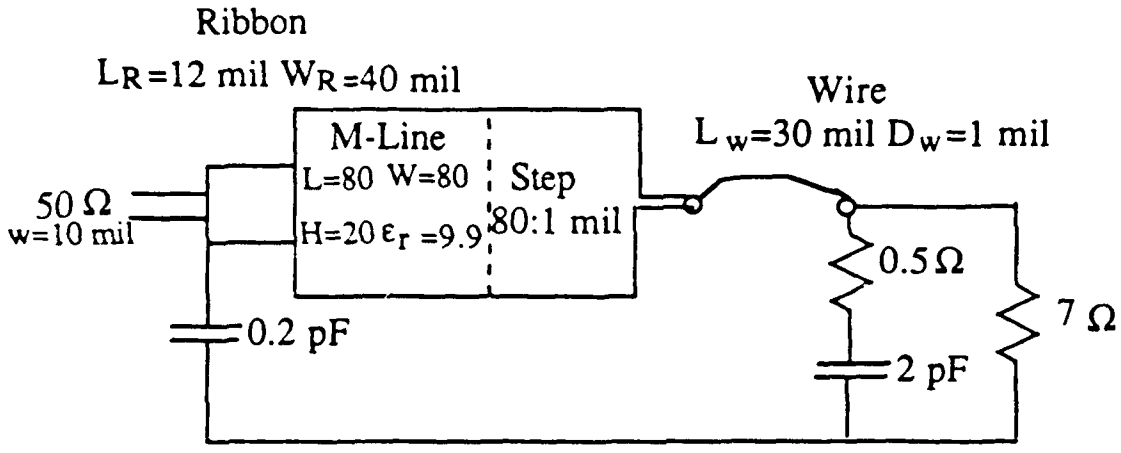

Fig. 3.18 Equivalent circuit of the laser in the manufacture package.

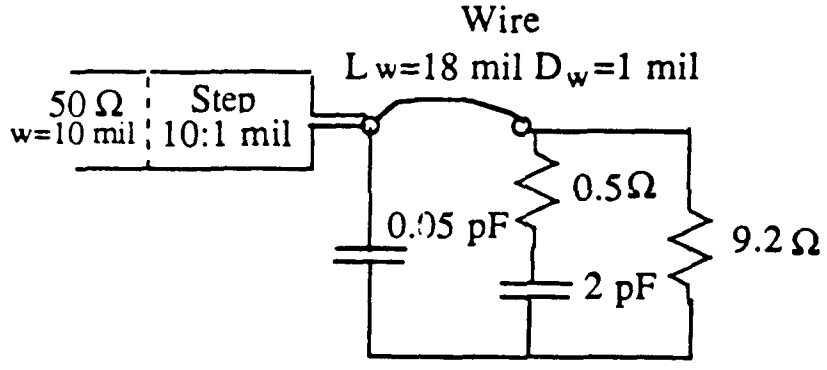

Fig. 3.19 Equivalent circuit of the laser in the modified package.

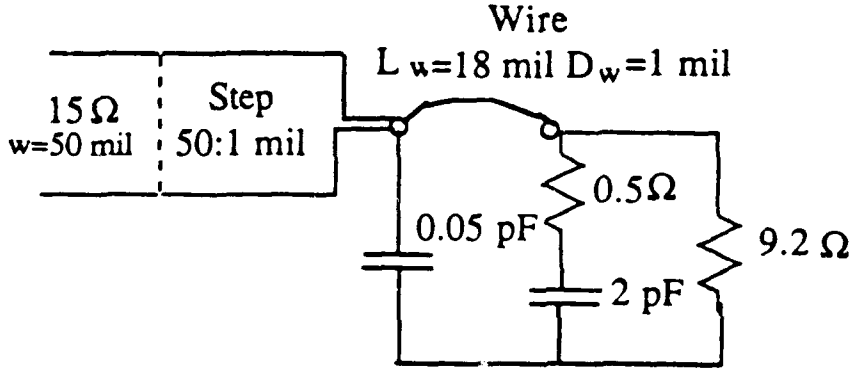

Fig. 3.20 Equivalent circuit of the laser in the transformer package.

3.4.1. Summary

A procedure using the TRL error extracting is developed. Through the use of this procedure, various fixtures and laser diode chip submounts were de-embedded. In the case of an Electro-Optical device such as a laser diode, the measured and de-embedded electrical S-parameter is one-port. However, to determine the effect of the parasitics on the high-speed modulation behavior of a semiconductor laser diode, a two-port scattering parameters are required. In a laser diode, there is no physical access to the second port, therefore to determine the two-port S-parameters, an indirect method must be implemented. The solution undertaken here was to implement the de-embedded one-port S-parameter and some of laser diode chip submount physical characteristics on a CAD program and then extract the two-port S-parameters.

The laser diodes tested have a typical input resistance of about 7 to 10 Ω. All of these lasers were attached on a submount and bonded with a 1 to 2 mm length of wire to a tab. The laser submount was fastened in our custom package and the bond wire was then cut from the tab and rebonded to the transmission line directly and avoiding additional series inductances. As it is seen from results in this section, the lasers response improves significantly compared to the original package. Even in the modified package the length of bond wire is still about 18 mils long, which corresponds to an inductance of about 0.3 nH. This in turn creates a series resonance which makes the laser impossible to match in the frequency range beyond a few gigahertz. The returned loss of the transformer package, when a laser is attached to it, degrades for frequencies larger than 4 GHz because of the series inductance. Results on the matching circuit and coupling improvement are further investigated in Chapter 4. Comparing the three packaging configurations tested here, the best power coupling achieved is with the transformer package, widest frequency range with the 50 Ω modified submount, and the worst response for the 50 Ω original manufacture submount.

Chapter IV

WIDEBAND IMPEADANCE MATCHING FOR LASER DIODE

High-Speed optical modulation of laser diodes is currently of interest in optically controlled phased array radar [1] and in high speed optical communication systems. As the modulation frequency extends into the upper microwave and millimeterwave frequencies, the need arises for an efficient wideband matching circuit for the laser diode. Currently, the technique used to match the laser diode to a 50 Ω system is to introduce a series resistance to bring up the total termination impedance to 50 Ω. In the case of the Ortel SL1000, the laser is usually modeled by a 2 Ω resistance [8] and thus, the required series resistance is 48 Ω. The power delivered to the laser diode is only 4% of the input drive, which is a large loss of power.

A new wideband matching circuit with mixed distributed and lumped elements is presented. This wideband matching circuit transforms a capacitive load with a nominal impedance of 2 Ω to 50 Ω source impedance. The matching is accomplished without the need for wide microstrip lines, but with the combination of a short length of transmission line and two shunt capacitors each placed at one end of the line. The combination of the shunt capacitors, length of line, bond wire, and the device transforms the impedance from 2 Ω to about 15 Ω. A multisection quarter wavelength transformer may then readily transform the impedance to 50 Ω.

This matching technique is illustrated here for a laser diode with a nominal impedance of 2 Ω. This matching circuit has a center frequency of 10.5 GHz and a bandwidth of 9 GHz, which is a fractional bandwidth of 86%.

4.1. Broadband Matching Criteria

Matching circuits may be composed of either lumped or distributed elements. Distributed circuit elements are large at low microwave frequencies and therefore lumped elements are used for frequencies up to 3 to 5 GHz. Above these frequencies distributed elements are suitable, therefore in this thesis a distributed matching circuit with lumped elements is discussed. Narrow band (~10% bandwidth) match of these laser diodes may readily be obtained either by stubs or by a combination of stub and transformer [61]. An improved scheme is to use a ladder network and then use a Kuroda transformation to approximate the lumped elements with transmission lines [62]. The advantage of this scheme is that it will also match a reactive load where a quarter wavelength transformer matches only resistive loads.

For a wider bandwidth, Butterworth and Chebychev polynomials are the common choice of the approximation functions to realize multisection or taper matching transformers [63, 64]. Usually these transformers are cascaded with a resonant circuit which cancels the reactance of the load. To realize a Chebychev or Butterworth quarter wavelength transformer on microstrip, the characteristic impedances of the sections at the outer ends of the transformer have to be close to the impedance of load and source. In our particular case, matching the laser diode with a nominal impedance of 2 ohm requires very low impedances in the sections close to the laser diode. A three step Chebychev transformer that matches 50 Ω to 2 ohm has the following quarter wave impedances: 26, 10, and 3.8 Ω for a fractional bandwidth of 100% [63]. The last two impedances are unacceptable in a microstrip structure, as they require the line widths to be very wide: for example a 3.8 Ω line has w/h ≈25.5 on Alumina substrate (ε_r= 9.9) and transverse modes may be excited [65]. The technique used here circumvents the need for these very wide lines.

4.2. Resonant Circuit

The input impedance of the laser diode (Ortel SL1000) when driven by a generator may be modeled as an equivalent RLC circuit [8], as shown in Fig. 4.1. The laser diode has a nominal impedance of 2 ohm when forward biased beyond threshold. The series inductance L_s is primarily due to the bond wire, component C_p is due to the diffusion capacitance of the diode, and C_s is the parasitic capacitance of the structure and its package having a typical value of less than 0.1 pF. The response of this equivalent circuit is in the form of a second order low-pass filter with a reactive input impedance. A shunt capacitor, C_L, is added in parallel with C_s so that the equivalent circuit is resonant at midband At resonance, the input impedance is real and hence the device is easier to match.

Letting the capacitor C_T denote the parallel combination of the capacitor C_s and the additional lumped matching capacitor C_L, the input admittance of this circuit may easily be written as

$$Y_{in} = \frac{1+(R_L+R_p)j\omega_0 C_p}{R_L-\omega_0^2 L_s C_p(R_L+R_p)+j\omega_0(L_s+R_L R_p C_p)} + j\omega_0 C_T \quad (4.1)$$

Rearranging the above equation the input impedance is

$$Z_{in} = \frac{R_L-\omega_0^2 L_s C_p(R_L+R_p)+j\omega_0(L_s+R_L R_p C_p)}{1+(R_L+R_p)j\omega_0 C_p+j\omega_0 C_s R_L-j\omega_0^2 L_s C_p C_T(R_L+R_p)-\omega_0^2(L_s+R_L R_p)C_T} \quad (4.2)$$

The above equation must be separated into real and imaginary parts. The imaginary part is set to zero and subsequently solved for the capacitance C_T which makes the circuit resonant at midband frequency. After some manipulation, C_T may be derived as

$$C_T = \frac{L_s-R_L^2 C_p+\omega_0^2 L_s C_p^2(R_L+R_p)^2}{R_L^2+\omega_0^2[L_s^2+R_L^2 C_p(R_p^2 C_p-2L_s)]+\omega_0^4 L_s^2 C_p^2(R_L+R_p)^2} \quad (4.3)$$

where $C_T = C_L + C_s \approx C_L$ and $\omega_0 = 2\pi f_0$ is the midband frequency. In the actual circuit, the package capacitance may be taken into account by subtracting it from the C_T. Also, at resonance the input impedance is given by

$$R_{in} = \frac{R_L - \omega_0^2 L_s C_p (R_L + R_s)}{1 - J\omega_0^2 (L_s + R_L R_p C_p) C_T} \tag{4.4}$$

and is purely resistive. Fig. 4.2 and Fig. 4.3 show the input impedance of the equivalent circuit of Fig. 4.1 without and with the additional lumped capacitor C_L=4.7 pf. When adding shunt capacitors to reduce the characteristics impedance it also increases the package parasitics, therefore it is important that the 3 dB bandwidth of this resonant circuit with the additional lumped capacitor be larger than the desired circuit bandwidth. The above requirement sets forth the limit on the bond inductance so that the circuit is not bandlimited. Fig. 4.4 and 4.5 shows the ranges of realizable lumped capacitors as the function of frequency for four different series inductance. These figures may be used as the initial estimates to see if the scheme is feasible.

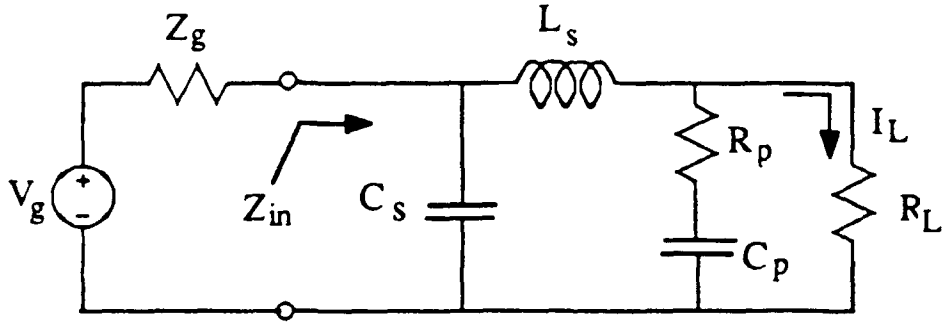

$R_L = 2\ \Omega$
$R_p = 0.5\ \Omega$
$C_p = 4.1$ pF
$L_s = 0.047$ nH
$C_s = 0.07$ pF

Fig. 4.1 The equivalent circuit of laser diode driven from a generator.

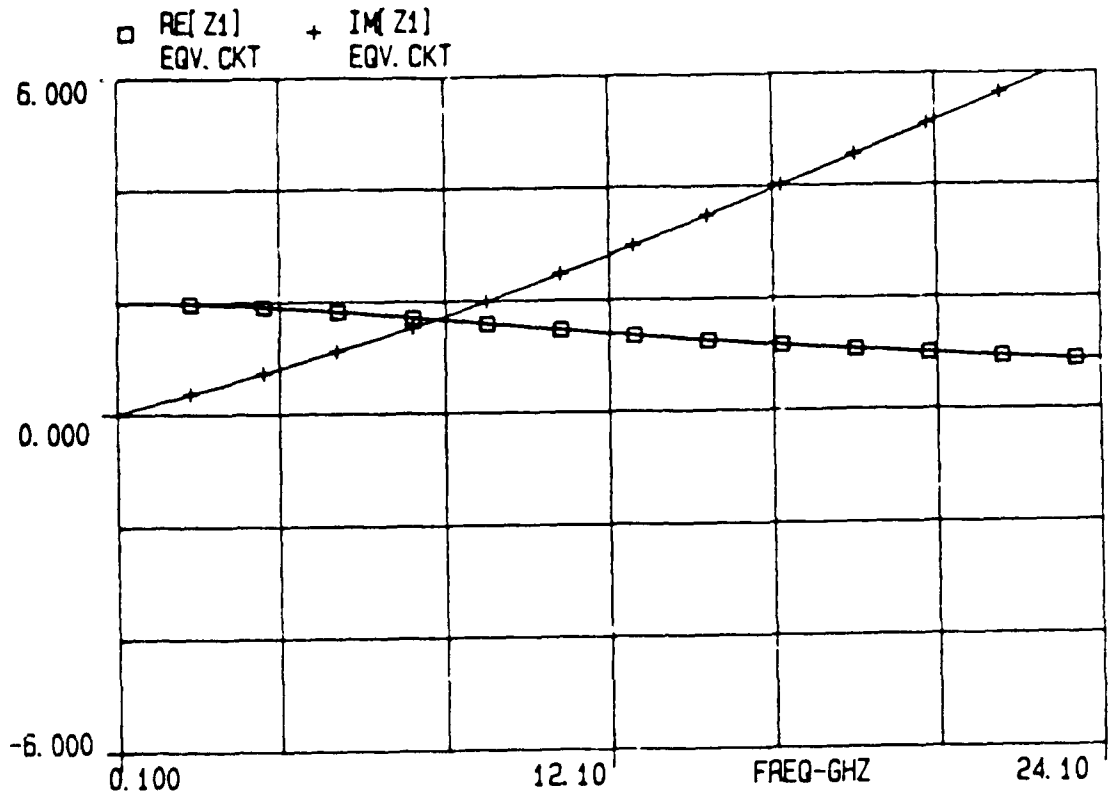

Fig. 4.2 Response of the equivalent circuit without the shunt capacitors.

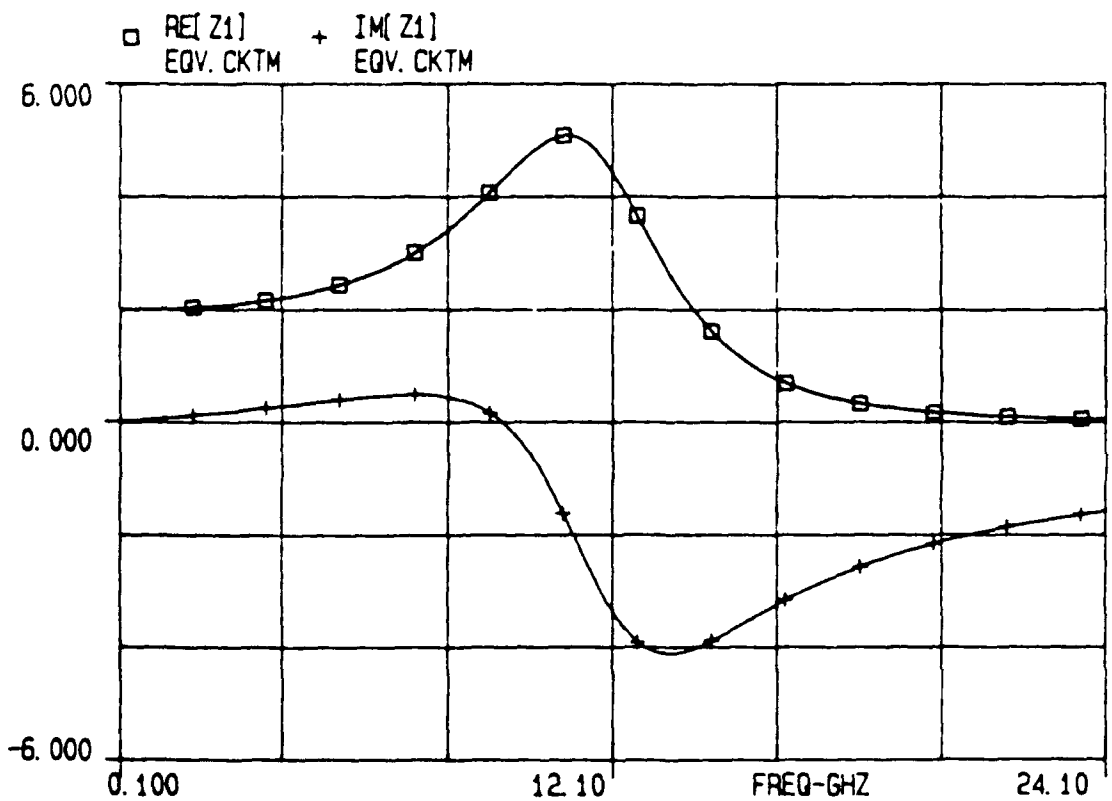

Fig. 4.3 Response of the equivalent circuit with the shunt capacitors.

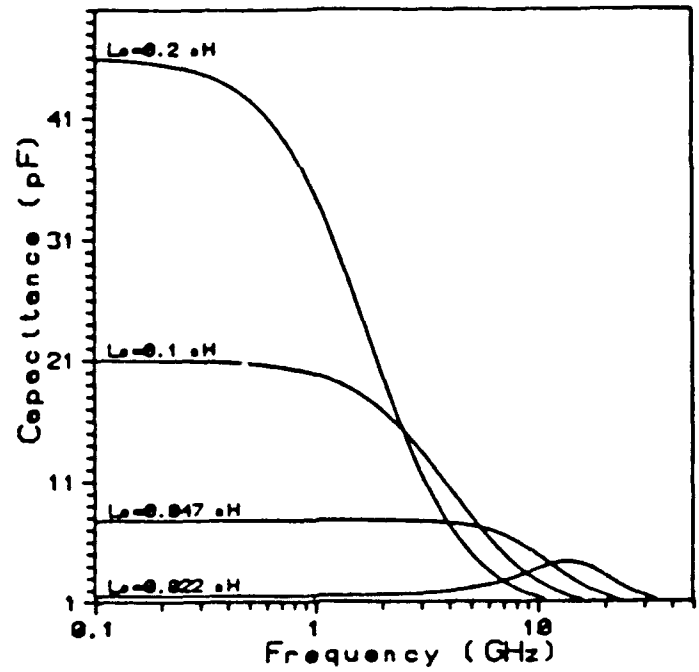

Fig. 4.4 Ranges of the shunt capacitance C_T for R_L=2 Ω and C_p= 2 pF.

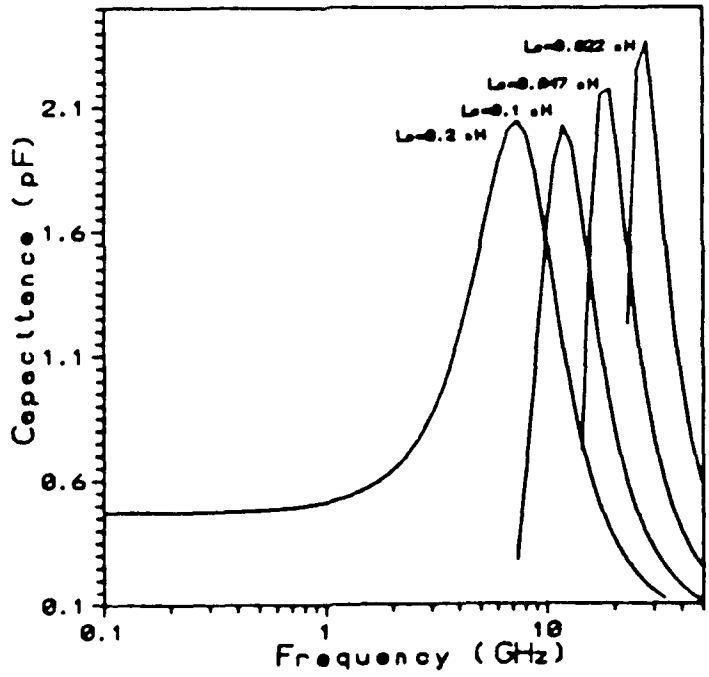

Fig. 4.5 Ranges of the shunt capacitance C_T for R_L=9 Ω and C_p= 2 pF.

4.3. Current Injection Response of the Laser Diode

Bandlimited criteria for a laser diode causes reduced current injection at higher frequencies and this in turn creates the rf 3 dB bandwidth. The rf modulation response is governed by the device's intrinsic characteristics and the package parasitics. The modulation response of a current driven device is written as

$$Y_{21}=\frac{\text{Current flowing into the intrinsic diode}}{\text{Voltage of the generator}} \tag{4.5}$$

Y_{21} gives the current injection ratio for the laser diode. Analysis of the laser equivalent circuit driven by a generator voltage V_g with internal impedance Z_g, from Fig. 4.1 one has

$$Y_{21}=\frac{I_L}{V_g}=$$

$$\frac{1+j\omega C_p R_p}{[1+j\omega(R_L C_T+R_p C_p)]\{(j\omega)^2 Z_g L_s C_T+j\omega L_s+Z_g\}+R_L(1+j\omega R_p C_p)(1+jwZ_g C_T)} \tag{4.6}$$

where Z_g is not known, but a good estimate is $Z_g \approx 2R_L$(4 ohms in our case). Equation 4.6 requires that the bond wire inductance L_s be small enough so that the bandwidth of the resonant circuit is larger than the required circuit bandwidth.

A simplified expression may be derived with closed form solution for the resonant frequency ω_0 and quality factor Q, if $C_T \approx 0$ and $R_P \approx 0$, as

$$\frac{I_L}{V_g}=\frac{1}{-\omega_0^2+j\omega_0\dfrac{L_s+Z_g R_L C_p}{L_s R_L C_p}+\dfrac{Z_g+R_L}{L_s R_L C_p}}. \tag{4.7}$$

The above circuit is a second order low pass filter with the resonant frequency ω_0

$$\omega_0 = \sqrt{\frac{Z_g+R_L}{L_s R_L C_p}} \tag{4.8}$$

and quality factor Q of

$$Q = \frac{\sqrt{L_s R_L C_p (Z_g+R_L)}}{L_s+Z_g R_L C_p} . \tag{4.9}$$

With or without the additional lumped capacitor, when the series inductance is small then the the dominant effect is RC low pass. As the frequency increases, the capacitor bypasses an increasing amount of the rf drive. Modulation response of the laser for different series inductances 0.022, 0.047, 0.2, and 0.8 nH and internal impedances 9 and 2 Ω, when driven from a generator with internal impedance of 50, 18 and 4 Ω as shown in Fig. 4.6, 4.7, and 4.8 respectively. These figures point to a very important fact: an increase in series inductance or the shunt capacitances decreases the bandwidth. A laser driven with a lower source impedance has higher current injection. Furthermore, when a low impedance laser is driven with a generator of higher impedance a larger injection current surge occurs at the resonance. These figures indicate that the best method to drive the laser is with a matching circuit which lowers the source impedance and increases the injection current. For very high-speed applications, adding additional lumped capacitor to decrease the characteristic impedance may not be feasible, especially if the bond inductance is large.

The values of inductance used in the above calculations are not unreasonable for a well packaged laser. To find typical wire length, one may use expression [59]

$$L = 5.03\text{x}10^{-3}\, l_w\left[\text{Ln}\left(\frac{4l_w}{D}\right) - 1\right] \text{nH/mil} \tag{4.10}$$

where l_w is wire length and D is the wire diameter. For example, an inductance of 0.047 nH corresponds to a bond wire of 4.2 mils long. Using mesh or ribbon bonding the inductance or the length may be reduced substantially.

As discussed in the next section, in the actual matching circuit the capacitor C_T, which is the parallel combination of C_s and C_L, is split in two and is then separated by a short length of transmission line. The calculation presented here does not take into account the additional phase shift introduced by the length of line. Therefore, these results are only for a quick check to ensure that the matching circuit is feasible. Generally speaking, after an approximate value for the capacitor C_L is obtained, a CAD program may be used to solve for an optimized matching circuit.

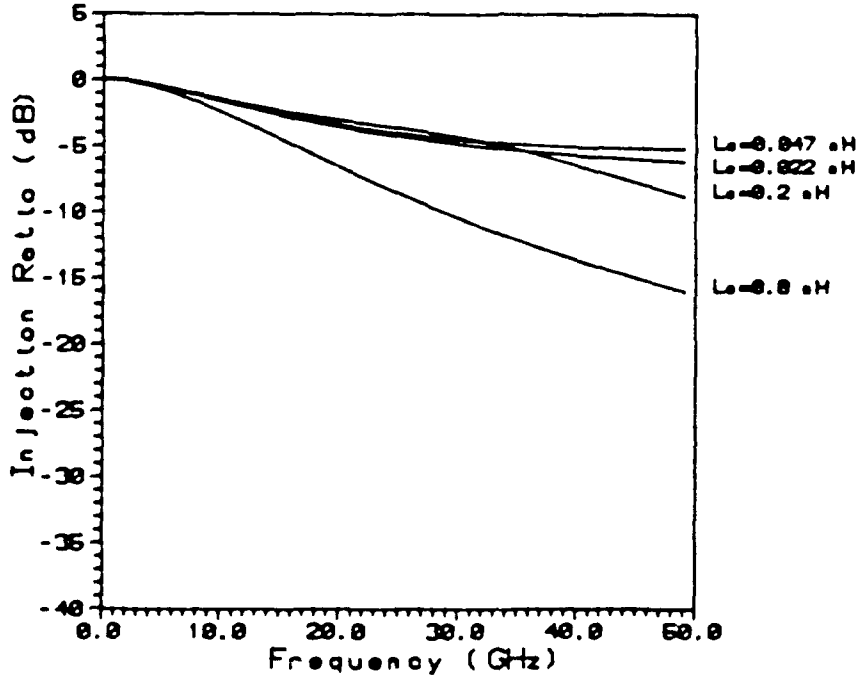

Fig. 4.6 Current injection for R_L=9 Ω, Z_g=50 Ω, C_p=2 pF, & C_T=0.1 pF.

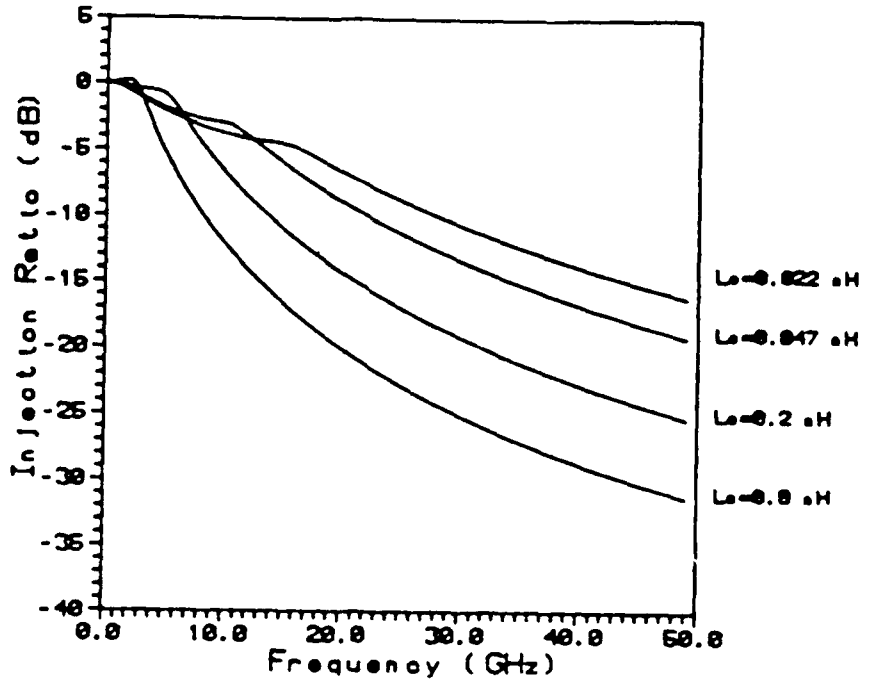

Fig. 4.7 Current injection for R_L=9 Ω, Z_g=18 Ω, C_p=2 pF, & C_T=4.7 pF.

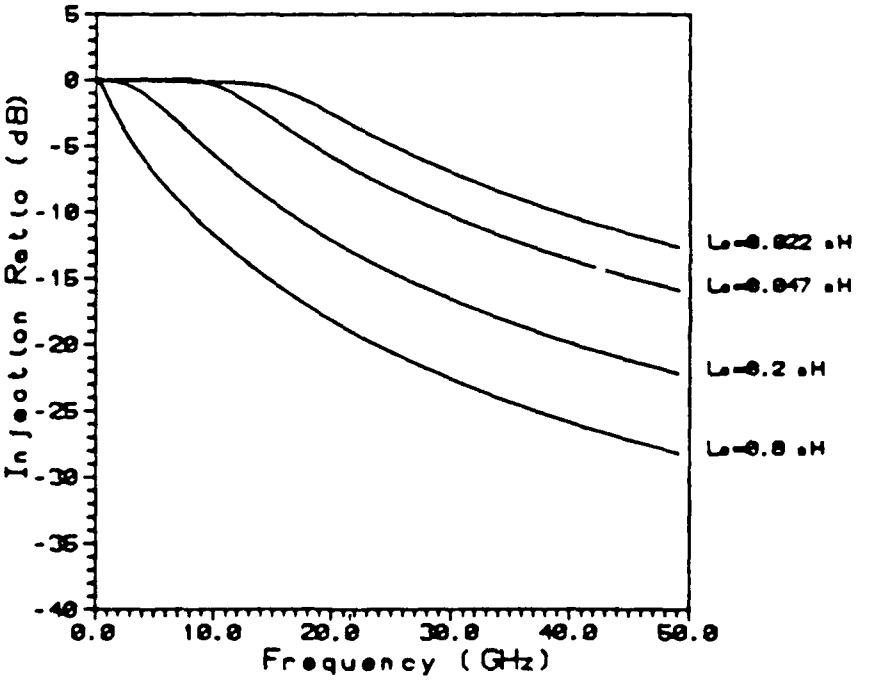

Fig. 4.8 Current injection for R_L=2 Ω, Z_g=4 Ω, C_p=4 pF, & C_T=4.7 pF.

4.4. Novel Wideband Matching Technique

In the matching circuit to be discussed, a novel method of reducing the microstrip line impedance is presented. A length of microstrip line with lumped shunt capacitors at either end reduces the line impedance to

$$Z_0 \approx \sqrt{\left(\frac{L_0}{C_{L_1} + C_{L_2} + C_d}\right)} \qquad (4.11)$$

where L_0 and C_d are the inductance and capacitance of this length of line, and C_{L_1} and C_{L_2} are the shunt capacitors attached to this line, as shown in Fig. 4.9. While this technique may be used to obtain 3.8 Ω lines in principle, we chose to use smaller shunt capacitors in the circuit discussed below.

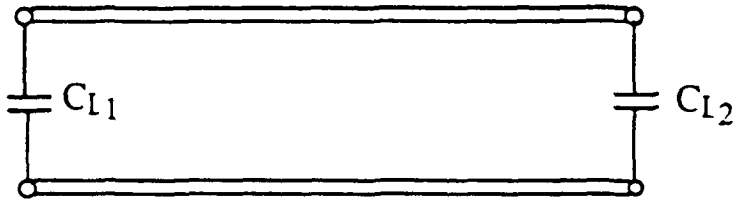

Fig. 4.9 Line length with two shunt capacitors.

The solution for this type of extreme matching from 50 Ω to 2 ohms is to first make a transformation from 50 Ω to the lowest characteristic

impedance allowed on a microstrip which corresponds to w/h of about 5[1] ($Z_0 \approx 17.5\ \Omega$). This is performed by the use of a standard step or tapered transformer with sufficient bandwidth [63, 64]. The transformation from 17.5 to 2 Ω may be completed by using an extra line length with the addition of the lumped capacitors, C_{L_1} and C_{L_2}, where $C_{L_1} + C_{L_2} \approx C_T \approx C_L$ and the exact ratio of C_{L_1} to C_{L_2} is computer optimized.

A third order Chebychev transformer was designed with impedance steps of 33, 17.5, and 9.2 Ω (100% fractional bandwidth). The transformer's lowest impedance section was replaced with the novel matching circuit, while the second section was restricted to the maximum w/h=5. The second circuit is a linear taper with maximum w/h of 5. The above transformers match 50 Ω to about 15 Ω and subsequently, the last transformer section is extended by about λ/16 together with the capacitors C_{L_1} and C_{L_2} to obtain additional phase shift [66, 67] and completes the matching from 50 Ω to 2 Ω [30, 68], as shown in Fig. 4.10 and 4.11.

When the additional line section and two lumped capacitors are attached to the equivalent circuit of Fig. 4.1, this circuit then transforms 2 Ω to about 15 Ω as shown in Fig. 4.12. The magnitude and phase responses of the novel matching circuits, with step and linear taper distributed sections, are shown in Fig. 4.13 and 4.14 respectively. The novel step and taper transformers both have nearly the same characteristics, which implies that the scheme is not configuration limited. The match is at center frequency of 10.5 GHz with a bandwidth of about 9 GHz. In this band the return and insertion loses are better than 10 and 1.5 dB respectively.

---

1 Wider microstrip line creates additional discontinuity when connected to a laser of typical size in 100's of microns, therefore it should be avoided.

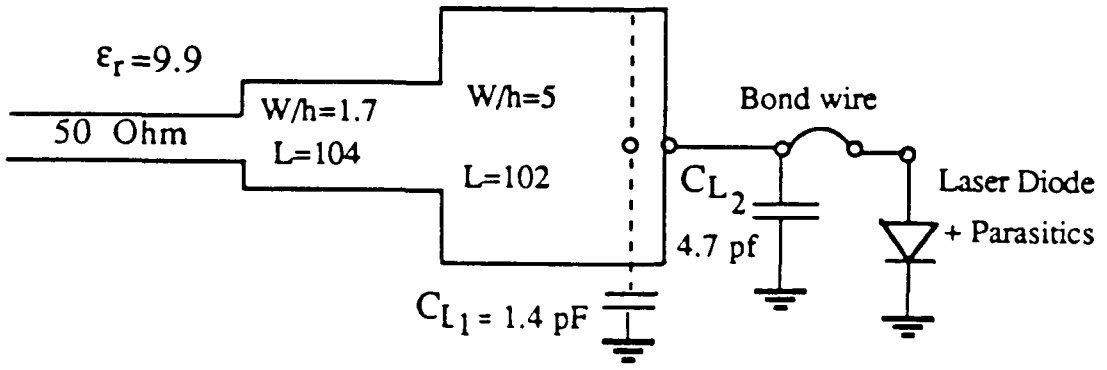

Figure 4.10 Layout of the novel step impedance matching circuit

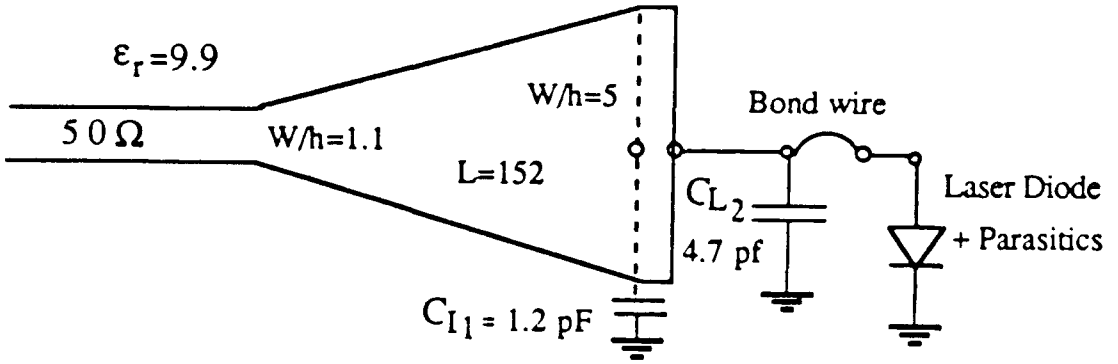

Figure 4.11 Layout of the novel taper impedance matching circuit

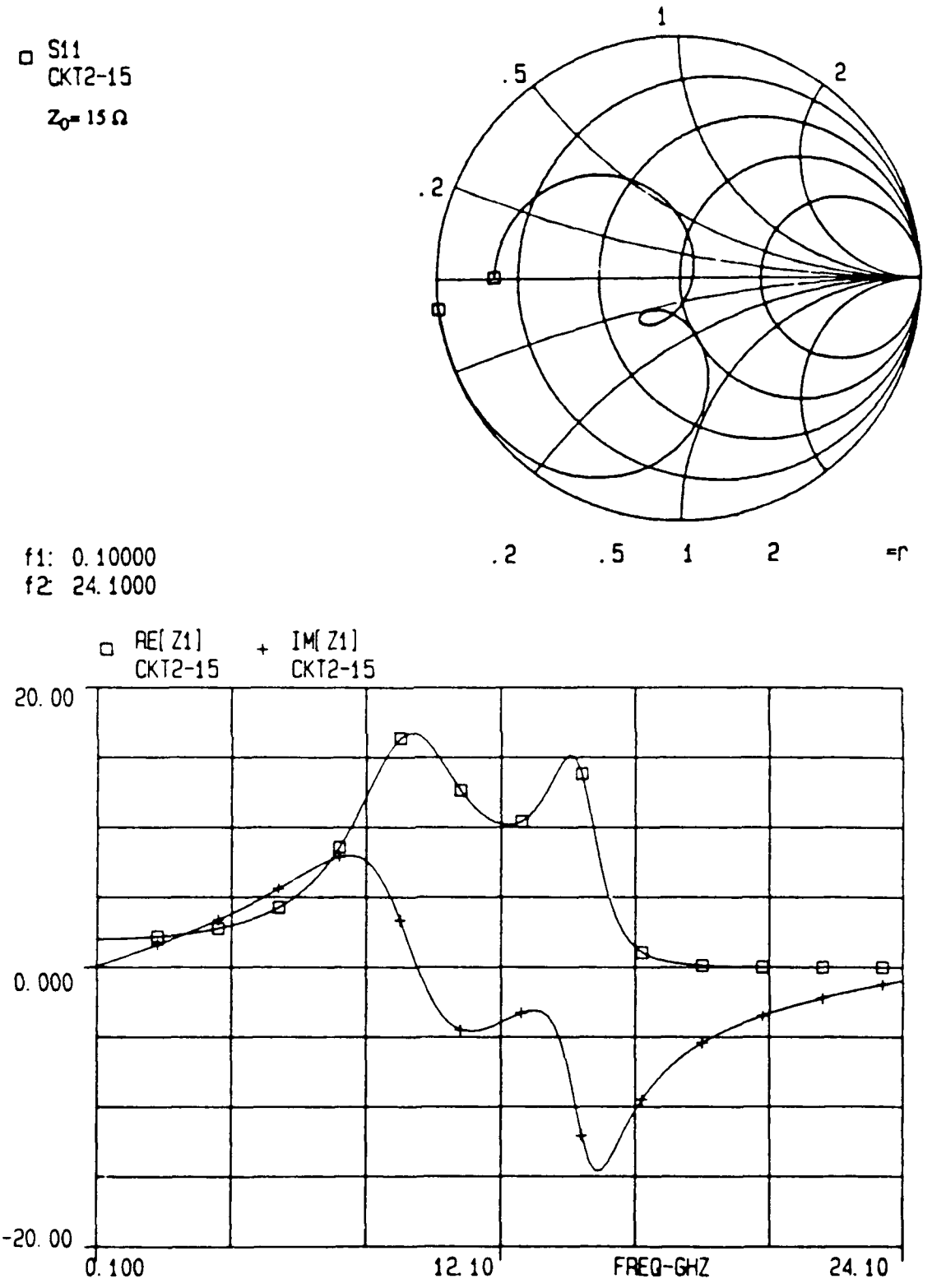

Fig. 4.12 Laser equivalent circuit response when cascaded with the novel transformer section for Z_0= 17.5 Ω, C_{L_1}=1.2 pf, and C_{L_2} =4.7 pf.

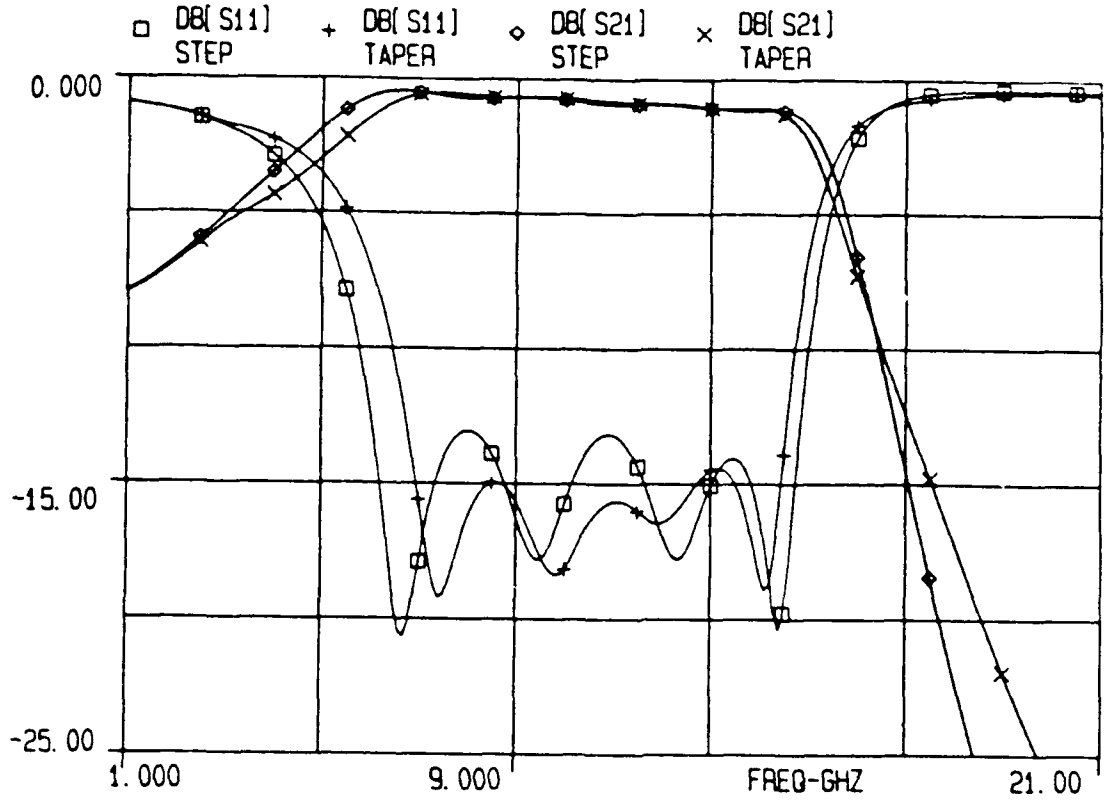

Fig. 4.13 Theoretical magnitude response for the step and taper circuits.

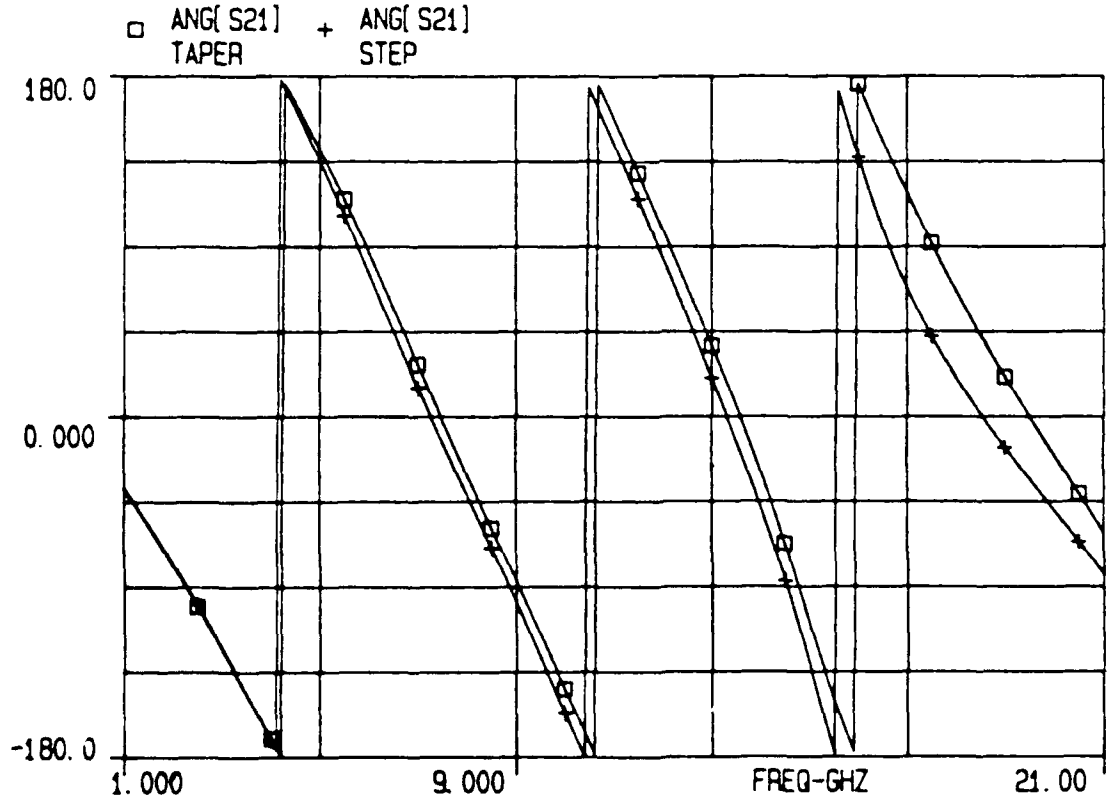

Fig. 4.14 Theoretical phase response for the step and taper circuits.

It is anticipated that the hybrid implementation may suffer from additional inductances due to the bond wires used to attach the capacitors to the line, although these were accounted for in the CAD optimization [60]. A monolithic implementation will not face these problems.

4.5. Experimental Setup and Measurements

A hybrid microwave circuit was fabricated on 10 mil Alumina and the additional lumped capacitor C_{L_1} was split in half and attached on each side of the microstrip to ground with a Via hole. The two capacitors were then mesh bonded to each side of the microstrip. The capacitor C_{L_2} was easily mounted at the end of the microstrip and served like a bridge to the laser.

Laser diodes purchased from Ortel Corp. did not arrive on time and therefor theoretical results discussed by the authors [8] were used to design and fabricate the matching circuits. Ortel lasers which were purchesed had a typical dc impedance of 7 to 10 Ω and diffusion capacitance of 2 pf instead of the 2 Ω, and 4.1 pf respectively, The de-embedded laser diode characteristics in Chapter III show this. Therefore, to test the matching circuit a 2 Ω chip resistor and a 4.1 pf chip capacitor were used instead. The lumped element were mounted on a shim and used as the terminating load for the matching circuit. The response of the lumped load was measured and de-embedded using TRL calibration, Fig. 4.15 shows the measured response (denoted by MEASURED), its computer optimized circuit model (DMODEL), and the response of the equivalent circuit of Fig. 4.1 (RCMODEL).

The terminating load had a self resonance at about 2 GHz because of chip resistor length which is about 0.8 mm long. The matching circuit was then terminated in this load and the presence of the load self resonance can also be seen in the circuit response. The measured response of the matching circuits connected to the load and the de-embedded response of the load were both used in Touchstone [60] to modify the original matching

circuit model. The response of the measured and modified matching circuits for step and taper are shown respectively in Fig 4.16 and 4.17. The measured and optimized response are well correlated even though the actual return loss is not low, but this is due to the load.

Finaliy, the equivalent circuit of Fig. 4.1 is connected to the modified circuits model for the step and taper transformers. The magnitude and phase responses of the matching circuits are measured based on the reflection measurements and computer modeling and are shown in Fig. 4.18 and Fig. 4.19 respectively. The measured results correspond very well to the theoretical results except at the upper part of band and this is in part to the unaccounted parasitics.

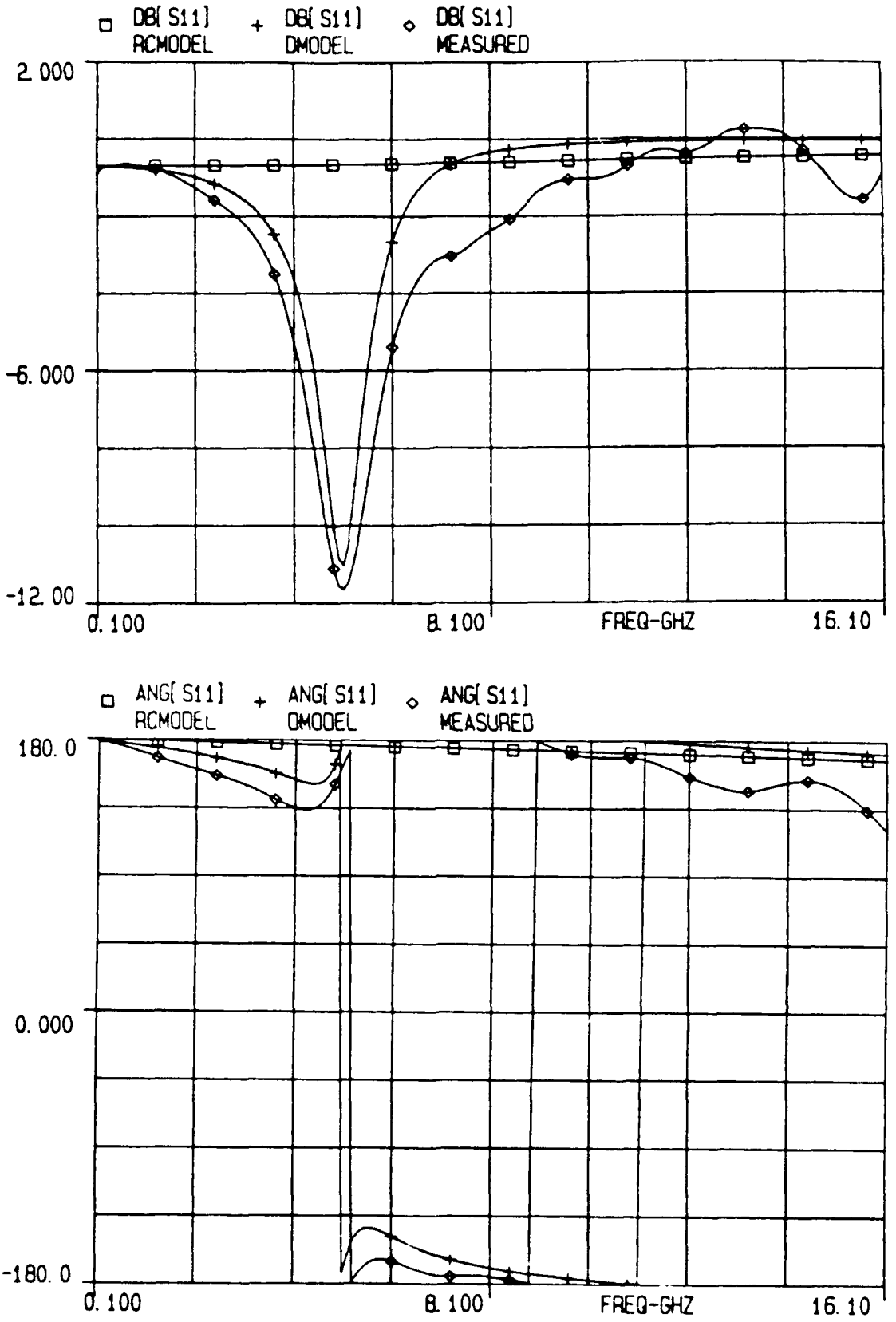

Fig. 4.15 De-embedded magnitude and phase response of the lumped load.

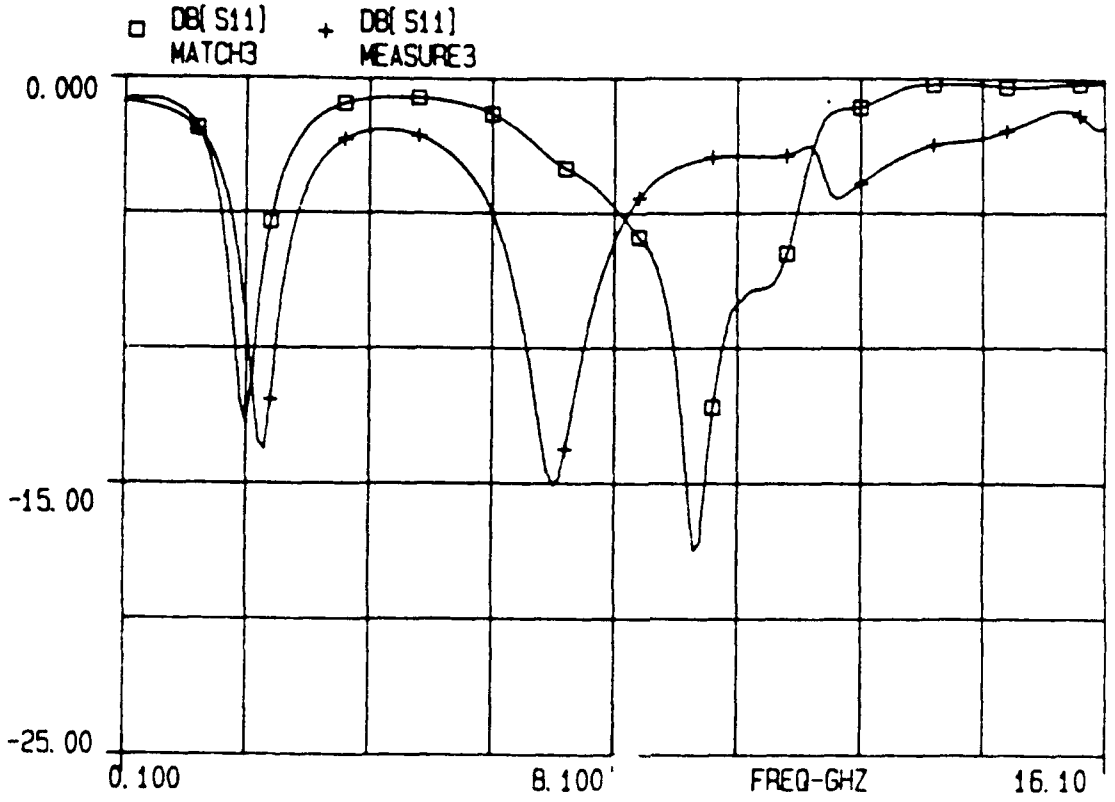

Fig. 4. 16 Response of the step matching with the lumped load

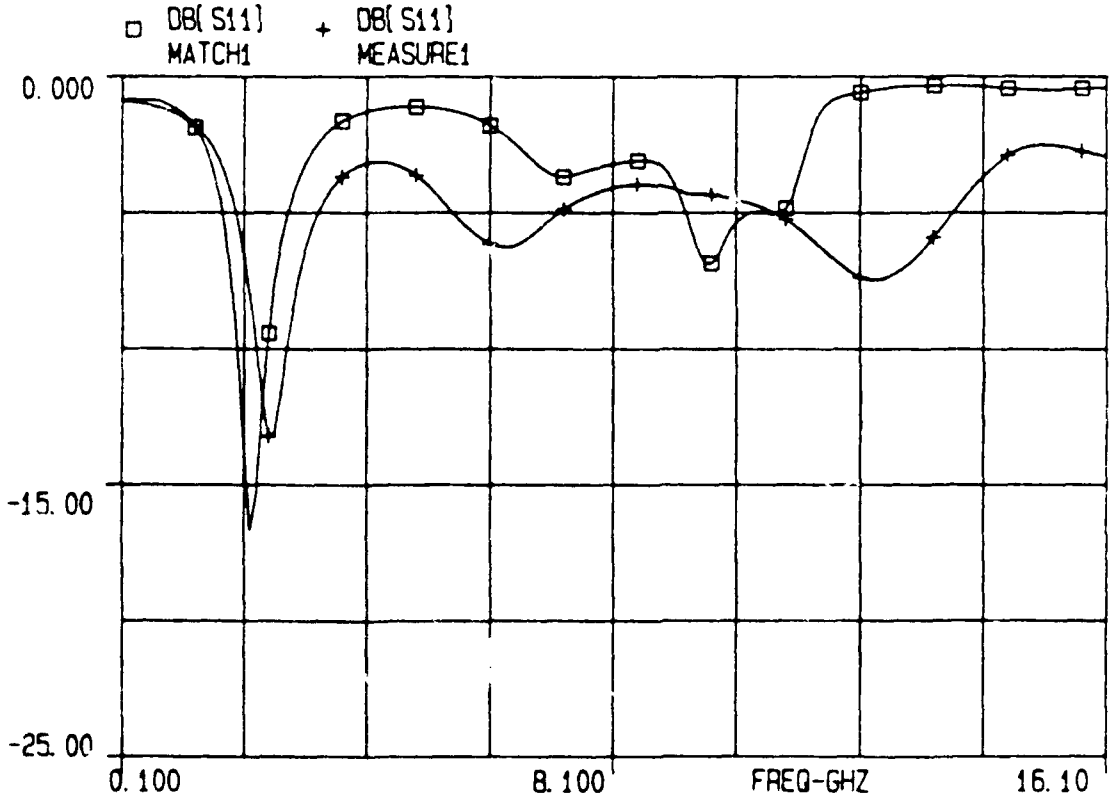

Fig. 4.17 Response of the taper matching circuit the lumped load

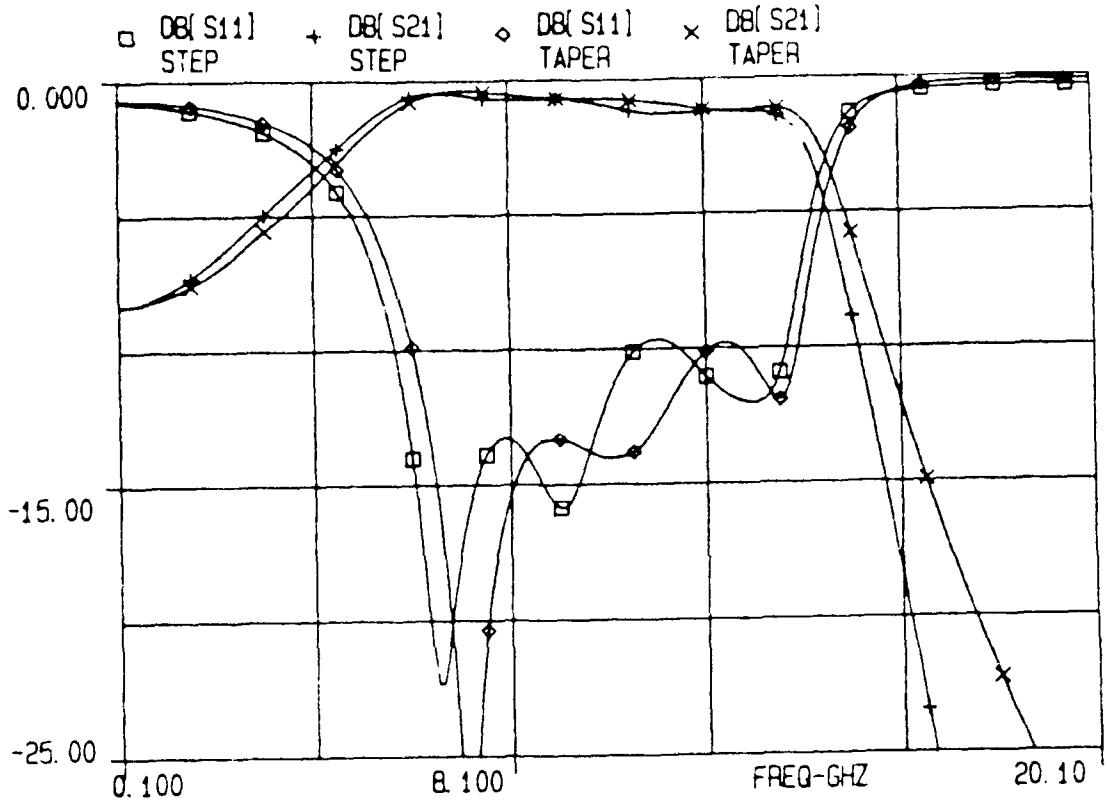

Fig. 4.18 Experimental magnitude response for the step and taper circuits.

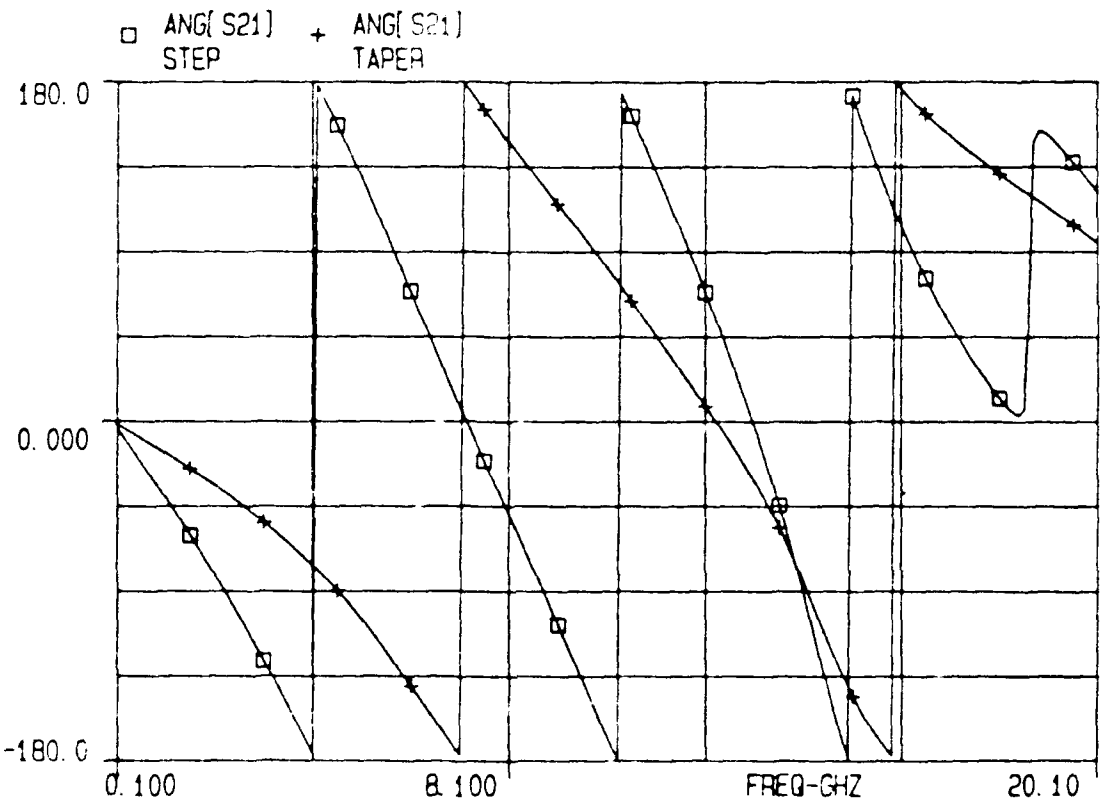

Fig. 4.19 Experimental phase response for the step and taper circuits

4.6. Summary

A novel impedance matching technique, which matches a 2 ohm laser diode and its parasitics to the 50 Ω line, has been demonstrated. This scheme transforms a 50 Ω line to the lowest allowable impedance on microstrip line which correspond to w/h≈ 5. The last transformer section is extended by about λ/16 and shunt capacitors are added on each side of the line to reduce line impedance further. Finally, the cascaded circuit is terminated to a the laser, which forms a resonant circuit that cancels the reactance associated with the device.

Hybrid microstrip circuits were fabricated for the step and taper transformer. The measured and theoretical results are similar. The matching circuits have a center frequency of 10.5 GHz, bandwidth of 9 GHz, reflection coefficient of better than -10 dB, and insertion loss of less than 1.5 dB.

The step and linear taper transformers have almost the same response, which suggests that the scheme is not configuration limited. This matching scheme may also be used to match other low impedances devices for example Impatt diodes, power FETs and Bipolar transistors. The scheme may also be realized with coplanar, making it very attractive for use with monolithic microwave integrated circuits (MMIC) use.

Chapter V

CHARACTERISTICS OF SEMICONDUCTOR LASER DIODE

A laser diode with AR coatings on one facet and a relaxation oscillation frequency of about 6 GHz was placed in an external cavities with fundamental resonances adjusted to be at 5 and 10 GHz. The modulation response of the laser diode showed enhancement of up to 34 dB over a 10% bandwidth with the external cavity compared to the output response without the cavity.

High frequency intensity modulation of laser diodes has been discused by several authors [2, 9, 28]. The maximum frequency of operation in these lasers is limited by the package parasitics and the relaxation oscillation frequency. Fig. 2.3 shows the effect of parasitics on the modulation response. In chapter III and IV the effect of parasitics was discussed in detail. However, for a well packaged laser the limiting factor would be the relaxation oscillation frequency and its 12 dB/octave or 40 dB/decade roll-off. Equation 2.2 indicates that the relaxation oscillation frequency may be increased by an increase in the optical gain coefficient a, photon density P, or by decreasing the photon lifetime τ_p. Reducing the laser cavity length or cooling the laser increases the relaxation oscillation frequency at the cost of increased threshold and inconvenience, respectively [7, 8].

It is preferred to devise a mechanism for increasing the optical density by a built-in structure and the material design to improve the laser modulation response. Some of the schemes that increase the optical gain coefficient are External Cavity Laser [14, 16], Coupled Cavity Laser [33], and Distributed Feedback Lasers (DFB) [32]. Semiconductor laser diodes, coupled to external cavities, have demonstrated that the modulation rate

may extend beyond the relaxation oscillation frequency f_r [13, 14]. This may provide a method of overcoming the f_r limitation.

The presence of the external cavity improves the laser performance through optical feedback. The main advantage is the periodic frequency enhancement at the frequency corresponding to the roundtrip time in the external cavity. Other improvements have also been seen, such as single longitudinal operation [69], frequency stability [70], and wavelength tunability [71]. Fig. 5.1 shows a typical external cavity laser mode profile, where the lasing wavelength λ_0 is 0.83 μm, laser cavity length l_D is 250 μm , and a 5 GHz external cavity is used. Frequency and mode spacing $\Delta\nu$ and $\Delta\lambda$ are respectively given by

$$\Delta\nu = \frac{c}{2\mu l_D} \tag{5.1}$$

$$\Delta\lambda = \frac{\lambda_0^2}{c}\Delta\nu \tag{5.2}$$

where c is speed of light in the vacuum and μ is material index. Fig. 5.1 also indicates that when the external cavity is long the range of wavelength tunability is small and mode hopping [71] is more probable. If a large range of tunability is desired, then the external cavity must be very short, 43.5 A° mode tuning has been reported for a 60 μm long external cavity [71]. However, due to the increased coherence length with an external cavity, mechanical and thermal tolerances and variation for optimal operation becomes very crucial. It has also been reported that external cavity may cause or even prevent the laser from exhibiting self pulsation [72]. The external cavity laser usually tends to oscillate in one mode which satisfies the lowest gain condition for the compounded cavity. However, because of physical changes, the laser frequency may jump to another external cavity mode that has a lower gain. Feedback induced pulsation are most troublesome when the external cavity is very short or the feedback is very strong [73]. If an external cavity laser is pulsing it may be stabilized by varying one or a combination of the following parameters: temperature, injection current, external cavity length, and strength of feedback.

The modulation speed beyond the usual f_r of the laser is enhanced through external cavity with three different techniques a.) fundamental rf mode-locking b.) subharmonic rf mode-locking c.) subharmonic cavity locking. These results were compared for the largest rf output. A generalized rate equation analysis of the of the semiconductor laser diode with and without external cavity was used to compare some of the measured characteristics to their theoretical values.

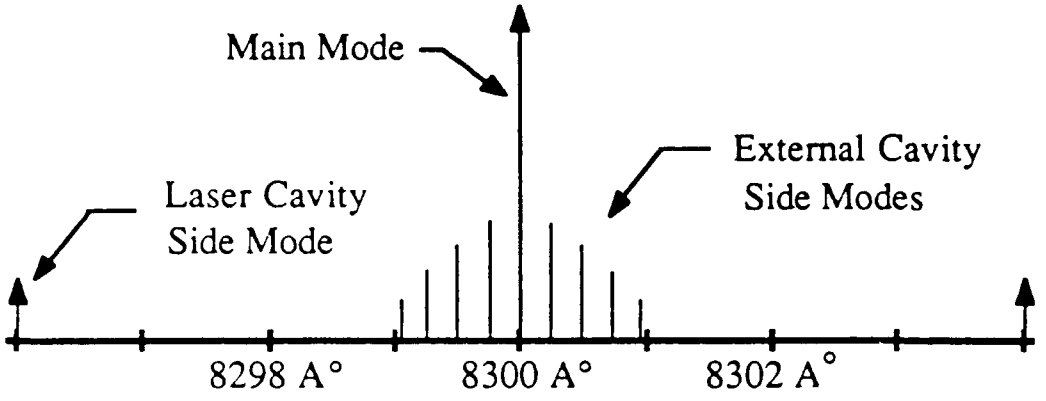

Fig. 5.1 External cavity laser, side modes.

5.1 Generalized Rate Equations

A set of rate equations is derived which can analyze the solitary laser, the external cavity laser or the effects of Fresnel reflection from the end of fiber. In an external cavity each of the Fabry-Perot sections has its own set of longitudinal modes which may nearly coincide periodically. The mode closest to the gain profile peak, with the overall loss at minimum, reaches threshold and starts lasing. The remaining side modes may be discriminated through the cavity mode mismatch or gain roll-off. It has been shown, both experimentally and theoretically [68], that the side-mode rejection, defined as the intensity ratio of the main mode to the most prominent side mode, can reach 20-35 dB. The lasers under investigation are BHDH, which normally lases in a single longitudinal mode. When the

external cavity is added further side mode discrimination occurs and such side mode does not significantly affect the laser characteristics. Therefore, single mode rate equations are formulated to study the laser.

To model the dynamical response of an external cavity laser, a generalized single cavity rate equation is modified by incorporating the feedback owing to the intercavity coupling [13]. An assumption made to simplify the analysis is the neglecting of the lateral variations of the optical field E. The main effect of the lateral carrier diffusion is to increase the relaxation oscillation damping [74]. Finally, to avoid complicated boundary-value problems [74], axial variation of E except for its standing-wave nature is neglected. The optical field E can be written as

$$E(z,t) = 1/2\ \psi(x)\phi(y)\left[E(t)e^{-j\omega 0t} + c.c.\right] \mathrm{Sin}(kz) \qquad (5.3)$$

where $\psi(x)$ and $\phi(y)$ are respectively the lateral and transverse field profile, ω_0 is the lasing frequency, k is the wave number, and z is the length along the laser waveguide. The wave-number is related to the cavity resonance frequency by

$$k = \frac{\mu\Omega}{c} = \frac{m\pi c}{L} \qquad (5.4)$$

μ is the active layer index, Ω is the cavity resonance frequency, c is the speed of light in the vacuum, L is the cavity section length, and m is an integer. The standing-wave assumption for a semiconductor laser diode, with facet reflectivities of 32%, is valid as long as the laser is above threshold [74]. It has been shown that no substantial error occurs even for a semiconductor laser diode with AR coating (~ 5%) as long as the gain-length products are larger than about 7 [74]. However, this assumption becomes invalid for reflectivities of < 2% [74]. In such a case, multiple reflection does not occur in the external cavity and a simple time domain analysis may be applied [17]. Another factor, which limits the spatial uniformity assumption, is when describing fast phenomena occurring on the time scale of the laser cavity transit time. In common semiconductor laser diodes which have a length of approximately 250 μm, the cavity

transit time is about 3 ps. Hence, this analysis is invalid for phenomena shorter than about 4.5 ps or at modulation frequencies higher than 75 GHz [74].

The electromagnetic field inside the laser cavity satisfies Maxwell's equations. Therefore, the starting point to obtain the field rate equation is the wave equation. The wave equation will be employed to obtain the photon rate equation for an uncoupled laser and then phenomenalogically a term accountable for intercavity coupling is then added. In the absence of coupling, the optical field in the cavity satisfies the wave equation [28]

$$\nabla^2 E - \frac{1}{c^2}\frac{\partial^2}{\partial t^2}(\varepsilon E) = 0 \tag{5.5}$$

where ε is the dielectric constant and it incorporates the contribution of the injected carriers. Substituting equation (5.3) in (5.4), assume that E(t) varies slowly. Multiply by $\psi(x)$ and $\phi(y)$ and integrate over the whole range of x and y, one has

$$\frac{2j\omega}{c^2}\left(<\varepsilon> + \frac{\omega}{2}\frac{\partial<\varepsilon>}{\partial\omega}\right)\frac{dE}{dt} + \left(\frac{\omega^2}{c^2}<\varepsilon> - k^2\right)E = 0 \tag{5.6}$$

where $<\varepsilon>$ is the spatially averaged dielectric constant and is given by

$$<\varepsilon> = \int_{-\infty}^{\infty}\int_{-\infty}^{\infty}\varepsilon(x,y)\psi(x)^2\phi(y)^2 dxdy\ . \tag{5.7}$$

The $<\varepsilon>$ is approximately equal to the effective dielectric constant of the waveguide mode and is given by

$$<\varepsilon> = \mu^2 + 2\Gamma\Delta\mu_p + j\mu\alpha/k_0 \tag{5.8}$$

where $k_0=\omega/c$, Γ is the confinement factor, μ is the refractive index at laser threshold, and $\Delta\mu_p$ is the carrier-induced index change. The mode absorption coefficient α, is the given by

$$\alpha = -\Gamma g + \alpha_{int} + \alpha_m \tag{5.9}$$

where g is the material gain, α_{int} is distributed losses, and α_m is the mirror losses given by Equation (2.4). It is observed that at the lasing frequency the output varies almost linearly with the injected carrier density n [28]. Therefore the gain g can be approximated by

$$g(n) = a(n - n_t) \tag{5.10}$$

were a is the gain coefficient and n_t is the carrier density required to achieve transparency (corresponding to the onset of population inversion). The gain g is also related to the net rate of stimulated emission by

$$G = \Gamma v_g g \tag{5.11}$$

where v_g is the mode group velocity and related to group velocity as

$$v_g = c/\mu_g \tag{5.12}$$

The group index μ_g is then defined as

$$\mu_g = \mu + \nu(\partial\mu/\partial\nu) \tag{5.13}$$

ν is the lasing frequency where $\omega=2\pi\nu$. Furthermore, $\Delta\mu_p$ may be related to the line width enhancement factor

$$\beta_c = -2k_0\left(\frac{\partial\mu/\partial n}{\partial g/\partial n}\right) = -2k_0\frac{\Delta\mu_p}{\Delta g} \tag{5.14}$$

and Δg is the change in gain due to the change in rate of stimulated emission given as.

$$\Delta g = \Delta G/\Gamma v_g \ . \tag{5.15}$$

where
$$\Delta G = G - \gamma \tag{5.16}$$

and γ is the photon decay rate and is given as:

$$\gamma = v_g(\alpha_{int} + \alpha_m) = \tau_p^{-1} \tag{5.17}$$

τ_p^{-1} is referred to as the photon decay time inside the laser cavity.

Further simplification is made by replacing the localized facet loss by an equivalent distributed loss and phenomenologically add it to α_{int}. Substituting the field equation (5.4) into the wave equation (5.5), using $(\omega_0^2-\Omega^2) \approx 2\omega_0(\omega_0-\Omega)$ and $<\varepsilon>\approx\mu^2$ on the left-hand side of equations (5.3) gives

$$\frac{dE}{dt} = \frac{j\mu}{\mu_g}(\omega_0 - \Omega)E(t) + \frac{j\omega}{\mu_g}(\Gamma\Delta\mu_p + j\alpha/2k_0)E(t) \qquad (5.19)$$

where μ_g is the group index and has been added to account for dispersive semiconductor material. The above equation is written in a more useful form through use of Equation (5.9), (5.13), and (5.14), simplifying one gets:

$$\frac{dE}{dt} = \frac{j\mu}{\mu_g}(\omega_0 - \Omega)E + \frac{v_g}{2}(\Gamma_j\beta_c\Delta g + j(-\Gamma g + \alpha_{int} + \alpha_m)) \qquad (5.20)$$

Further rearangment and the use of equations (5.15) and (5.16) gives:

$$\frac{dE}{dt} = \frac{j\mu}{\mu_g}(\omega - \Omega)E(t) + \frac{1}{2}(G - \gamma)(1 - j\beta_c)E(t) + \frac{1}{2}\kappa E_f(t) \qquad (5.21)$$

the last term has been added to account for the feedback from the external cavity. An expression, which characterizes wave amplitude of a solitary or an external cavity laser diode, has been derived. The feedback coupling rate κ is usually obtained from the concept of effective reflectivities and will be derived in the next section.

The carrier rate equation is derived next, and this is coupled with the field amplitude equation. Carrier diffusion has been neglected in this analysis, therefore it is only applicable to index-guided lasers. Let's define the number of carriers inside the active layer as

$$N = \int n\, dv = nV \qquad (5.22)$$

it is further assumed that the carrier density n is approximately constant in the active layer volume V, where $V=l_D wd$ for a laser of length l_D, width w, and thickness d. The carrier rate equation is then given as [23]

$$\frac{dN}{dt} = \frac{I}{q} - \gamma_e N - GP \tag{5.23}$$

where $I=wl_D J$, J is the current density flowing through the active layer, $P \propto |E|^2$ is referred to as the photon density or population, and γ_e is given as

$$\gamma_e = (A_{nr} + Bn + Cn^2) = \tau_e^{-1} \tag{5.24}$$

is the carrier recombination rate due to radiative and nonradiative recombination processes. τ_e is often referred to as the spontaneous carrier lifetime. The recombination rate A_{nr} is related to mechanisms such as trap or surface recombination. B accounts for the radiative recombination, while C is related to Auger recombination processes.

5.1.1. Effective Reflectivity Concept

An schematic drawing for an external cavity laser is shown in Fig. 5.2. Here r_1, r_2, and r_3 represent amplitude reflection coefficients, l_D and L are the laser diode and external cavity length, respectively. The laser facet facing the external cavity has a forward and reverse transmission denoted as t_2 and t_2'. Further on, the amplitude reflection facing the external mirror is refereed to as r_2'. The amplitude reflection coefficient r_1 and r_2 for each interface is given in terms of material indexes

$$r = \frac{\mu - 1}{\mu + 1} \ . \tag{5.25}$$

The phase shift incurred in the external cavity is denoted as $\omega_0 \tau$ where τ is the roundtrip time in the external cavity.

The effective reflectivity for external Fabry-Perot etalon may readily be derived from the EM theory [64]. Assume a wave E_i is incident

on the left facet of the laser with amplitude of unity. The total reflected wave E_r has a complex amplitude and is equal to total reflection coefficent, one has

$$E_r = r_2 + t_2 t'_2 r_3 e^{-j\omega_0 \tau} U(\tau) + t_2 t'_2 r_3^2 r'_2 e^{-j2\omega_0 \tau} U^2(\tau) + \qquad (5.26)$$

$$= r_2 + t_2 t'_2 r_3 e^{-j\omega_0 \tau} U(\tau) \sum_{n=0}^{\infty} r'_2{}^n r_3{}^n e^{-jn\omega_0 \tau} U^n(\tau) \qquad (5.27)$$

where $U^n(\tau)=U(n\tau)$ is time operator and $U(n\tau)E(t) = E(t-n\tau)$. The left hand side of equation (5.27) is a geometric series and is readily summed. This gives

$$E_r = r_2 + \frac{t_2 t'_2 r_3 e^{-j\omega_0 \tau} U(\tau)}{1 - r'_2 r_3 e^{-j\omega_0 \tau} U(\tau)} \qquad (5.28)$$

now, rewrite the above expression in terms of r_2 and r_3 only. The reflectivity $r_2=-r'_2$ and from conservation of energy for a lossless mirror, one has

$$r_2^2 + t_2 t'_2 = 1 \, . \qquad (5.29)$$

Replacing r'_2, t_2, and t'_2 in Equation (5.28) results in an expression for the effective reflectivity

$$r_{eff} = \frac{(\sqrt{R_2} + \sqrt{R_3} e^{-j\omega_0 \tau} U(\tau))}{(1 + \sqrt{R_2 R_3} e^{-j\omega_0 \tau} U(\tau))} \qquad (5.30)$$

where r_2 and r_3 are replaced, respectively by the fraction of intensity reflected $\sqrt{R_2}$ and $\sqrt{R_3}$.

The external cavity has effectively created a wavelength dependent $R(\lambda)$ mirror which modulates the losses in the external cavity as the function of the mirror spacing L. Let's return to the equation (5.9) mode

absorption and add the additional losses and rewrite this expression with the aid of equation (2.4), one then has

$$\alpha = -\Gamma g + \alpha_{int} - \frac{c}{\mu_g l_D} \ln(r_1 r_{eff}) \tag{5.31}$$

$$= -\Gamma g + \alpha_{int} - \frac{c}{2\mu_g l_D} \ln(R_1 R_2) - \frac{c}{\mu_g l_D} \ln\left(\frac{r_{eff}}{\sqrt{R_2}}\right) = \alpha_0 + \alpha_{ex} \tag{5.32}$$

where $\alpha_0 = -\Gamma g + \alpha_{int} - \frac{c}{2\mu_g l_D} \ln(R_1 R_2)$ is the cavity loss of the solitary laser and $\alpha_{ex} = \frac{c}{\mu_g l_D} \ln\left(\frac{r_{eff}}{\sqrt{R_2}}\right)$ is the additional loss caused by the external cavity.

For steady-state operating conditions the time operator $U(\tau)$ is neglected but, for small signal analysis or noise properties it must be included in the classical rate equation. Comparing equations (5.32) and (5.9) the mode absorption, one may then add α_{ex} to the classical single mode rate amplitude equation (5.19). Where the external cavity contribution would be $\frac{1}{2} E e^{j\omega_0 \tau}$ for steady state operation (CW).

Next the series expansion of α_{ex} will be explored for specific case of strong optical feedback for the purpose of small signal analysis. Applying Binomial expansion to the denominator of R_{eff}, one may write an expression reflected field ,E_f, which is $\frac{1}{2}\alpha_{ex}$ as

$$E_f = \frac{c}{2\mu_g l_D} \ln\left[\left(1+\sqrt{\frac{R_3}{R_2}} e^{-j\omega_0 \tau}\, U(\tau)\right) \sum_{n=0}^{\infty} (-U(n\tau))^n \, (R_2 R_3)^{n/2} \, e^{-jn\omega_0 \tau}\right] E(t)$$

(5.32)

expanding the above expression and keeping only the dominant terms, one gets

$$E_f = \frac{c}{2\mu_g l_D} \ln\left(1 + \sqrt{\frac{R_3}{R_2}}(1-R_2)\, e^{-j\omega_0\tau}\, U(\tau)\right) E(t) \qquad (5.33)$$

The case of a weak optical feedback has been addressed already [13, 16]. It has been stated, when $R_3<0.1$ it is a reasonable assumption to replace $\ln(1+a)\approx a$. For the case of strong feedback where $R_3\approx 1$ and $R_2\approx 0.05$ one may then approximate $\ln(1+a)\approx \ln(a)\angle a$, where a is complex. Fig. 5.3 shows the mirror loss (α_{ex}) and the effective reflectivity (R_{eff}) for a solitary laser with 0.31% facet reflectivity when a 10% Fresnel reflection occur as the function of the external reflector phase shift. Figs. 5.4 and 5.5 respectively give R_{eff} and α_{ex} as the function of the external cavity phase change for $r_1=0.33$, $r_3=0.95$ and r_2 as listed on the figures. Comparing Figs. 5.4 and 5.5 with Fig. 5.3 shows the validity of this assumption, since the laser losses does not change significantly when $r_2<10\%$ for external cavity phase variations. Equation (5.31) my then be written as

$$E_f = \kappa E(t-\tau) = \frac{c}{2\mu_g l_D} \ln\left(\sqrt{\frac{R_3}{R_2}}(1-R_2)\right) e^{-j\omega_0\tau}\, E(t-\tau)\ . \qquad (5.34)$$

In the above equation, the time operator shifts the time t by an amount of τ. Also, κ is definded as the feedback rate. The effect of feedback has been to change the laser loss and has already been taken into account. Now that the effect of the external cavity has been determined, the rate equation will be setup for a laser that is coupled to an external cavity in the following section.

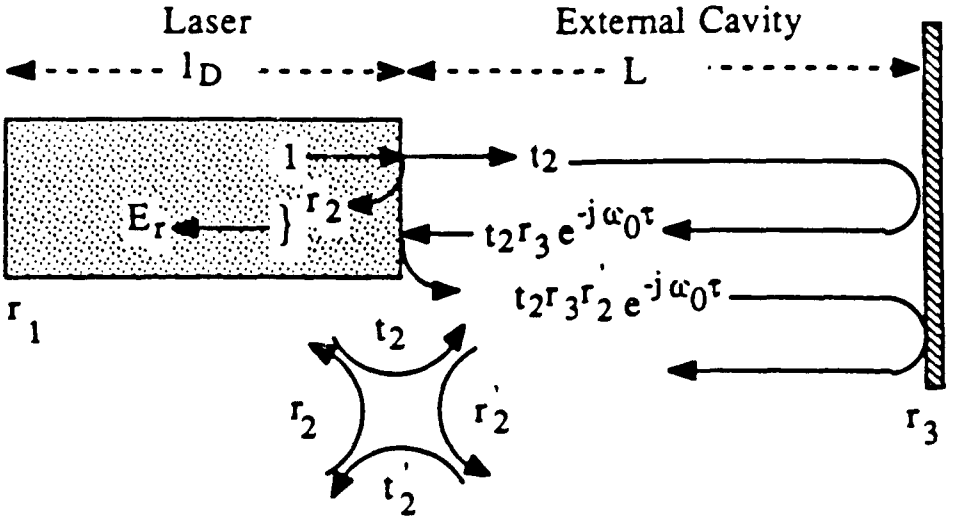

Fig. 5.2 Wave propagation in an external cavity laser.

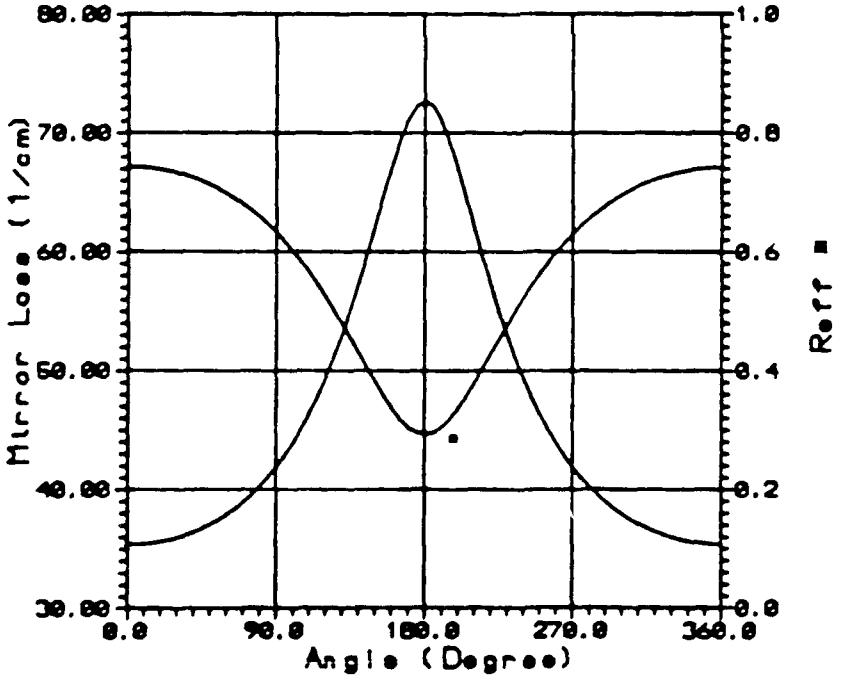

Fig. 5.3 Mirror loss and effective reflectivity, of a solitary laser when there is 10% Fresnel reflectance, as the function of the phase change.

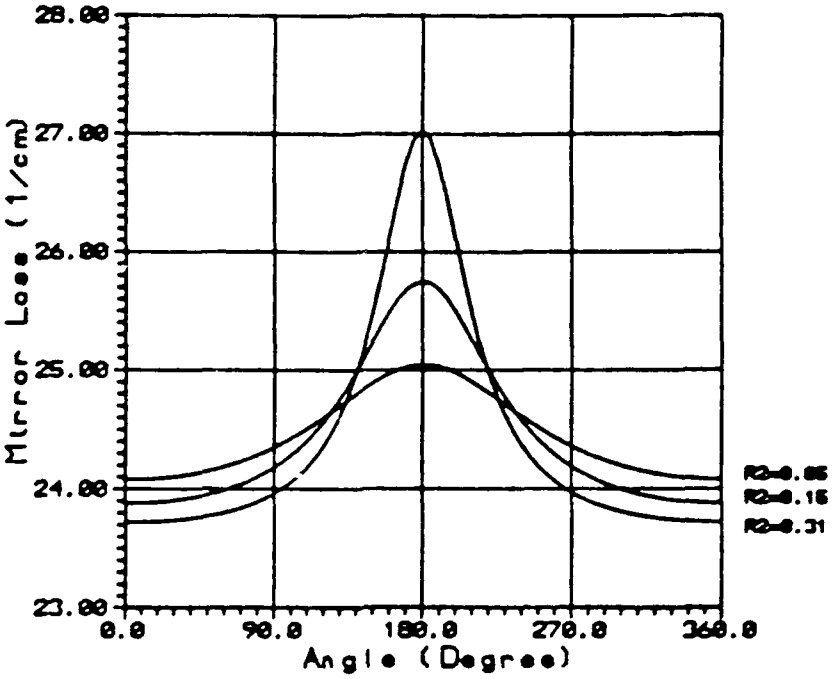

Fig. 5.4 Mirror loss as the function of the external cavity phase shift.

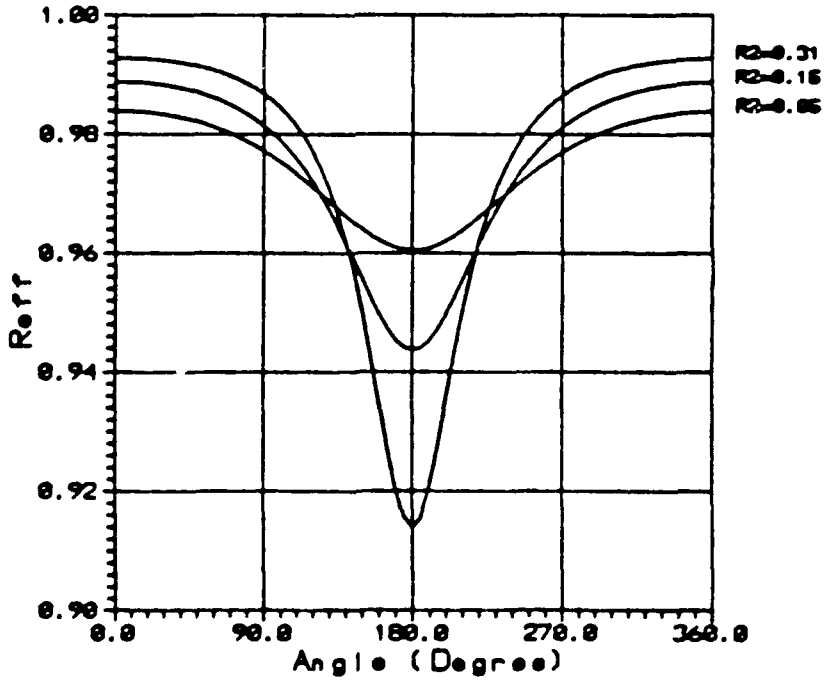

Fig. 5.5 R_{eff} as the function of the external cavity phase change.

5.1.2. Rate Equation Describing the External Cavity Laser

Let's return to the field amplitude equation (5.21) and rewrite it in the real and imaginary forms using

$$E = E_s \sqrt{P(t)}\, e^{-j(\omega_0 t+\phi(t))} \tag{5.36}$$

where E_s is the saturation amplitude, $P \propto E^2$ and is known as the photon number. Substituting equation (5.25) into the amplitude equation (5.21) and adding the feedback term, one gets

$$\frac{-1}{\sqrt{P(t)}} P'(t)+\sqrt{P(t)}(-j\phi'(t))$$

$$= 2\frac{j\mu}{\mu_g}(\omega_0-\Omega)\sqrt{P(t)}+(G-\gamma)(1-j\beta_c)\sqrt{P(t)}+ \kappa\sqrt{P(t-\tau)}e^{-j(\omega_0\tau+\Delta\phi(t))} \tag{5.37}$$

where $\Delta\phi(t)=\phi(t-\tau)-\phi(t)$ is the relative phase change between the incident and reflected wave, κ is feedback rate, P' and ϕ' represent time derivative. Separating into real and imaginary results in a set of equations describing the photon density and phase, such as

$$\frac{dP(t)}{dt} = (G(t)-\gamma)P(t) + 2\sqrt{P(t)P(t-\tau)}|\kappa|COS(\omega_0\tau+\Delta\phi(t)) + R_{sp}(N) \tag{5.38}$$

$$\frac{d\phi(t)}{dt} = \frac{\mu}{\mu_g}(\omega_0 -\Omega) + \frac{1}{2}\beta_c (G(t)-\gamma) + |\kappa|\sqrt{\frac{P(t-\tau)}{P(t)}}\, SIN(\omega_0\tau+\Delta\phi(t)) \tag{5.39}$$

$$\frac{dN(t)}{dt} = \frac{I}{q} - \gamma_e(N)N(t) - G(t)P(t) \tag{5.40}$$

$$G(t) = \Gamma v_g a(N(t) - N_0)/V \tag{5.41}$$

R_{sp} is added to equation (5.38) to take into account the rate at which spontaneously emitted photons are added to the intercavity photon population. R_{sp} is related to

$$R_{sp}(t) = \beta_{sp}\eta_{sp}\gamma_e(N)N(t) \tag{5.42}$$

where $\eta_{sp} = Bn/\gamma_e$ is the internal spontaneous quantum efficiency showing the fraction of carrier that emit photons through spontaneous recombination. The β_{sp} parameter is referred to as the spontaneous emission factor. Equation (5.41) gives the net rate of the stimulated emission in term of the carrier population and N. The set of equations (5.38) to (5.41) describes the characteristics of an external cavity laser, or a solitary laser if the feedback parameter is set to zero. Now that a general solution for an external cavity laser has been obtained the steady state solution will be examined next.

5.1.3. Steady-State Characteristics

The rate equations of the previous section are solved for the steady-state response of the semiconductor laser diode as the function of the injection current I. Steady-state solutions are obtained by setting all time derivatives equal to zero and are applicable for continuous-wave (CW) operation. Three steady state features of interest to characterize a laser diode are Light-Current (L-I), carrier population N, and lasing frequency ω_0 as the function of the device injection current.

A general CW solution for the external cavity laser will be derived and subsequently, by setting the feedback term to zero the solitary solution will be obtained. The photon magnitude equation (5.38) is solved by setting the time derivative to zero, solving for the photon density

$$P = \frac{R_{sp}(N_1)}{(\gamma - G) - 2|\kappa| \, COS(\omega_0 \tau)} \, . \qquad (5.43)$$

Substituting this equation in the carrier rate equation (5.40) and writing as a polynomial of N, one gets

$$N2\left[\frac{\Gamma v_g a \gamma_e(N)}{V}(\beta_{sp}\eta_{sp} - 1)\right]$$

$$+ N\left[\frac{\Gamma v_g a}{V}\left(\frac{I_1}{q} + \gamma_e(N)N_0(\beta_{sp}\eta_{sp} - 1)\right) - \gamma_e(N)\left(\gamma - 2|\kappa| \cos(\omega_0\tau)\right)\right]$$

$$- \frac{I}{q}(\gamma - 2|\kappa| \cos(\omega_0\tau)) = 0 \quad . \tag{5.44}$$

This equation gives the carrier density as the function of dc drive and it is assumed that $\gamma_e(N)$ does not change substantially from the previous current setting, when current steps are sufficiently small. The lasing frequency shift as the fuction of the injection drive. The frequency shift $\Delta\omega$ has not been determined and may be solved with the aid of photon phase equation (5.40)

$$\frac{\mu}{\mu_g}(\omega_0 - \Omega) + \frac{1}{2}\beta_c \frac{\Gamma v_g a}{V}(N - N_0) - \beta_{c2}\frac{\gamma}{} + |\kappa|\sin(\omega_0\tau) = 0 \tag{5.45}$$

The phase condition equation (5.45) may have multiple solutions corresponding to different external cavity modes but, the laser tends to oscillate in a mode with the lowest threshold and therefore the root with the lowest threshold is chosen [24].

The starting point for the recursive procedure was from carrier density at transparency $n_t = 1 \times 10^{18}\ cm^{-3}$. The corresponding current is obtained by setting $R_{sp}=0$ (ie. the laser is not lasing and there is no phase coherence) for the solitary laser in equation (5.38) gives P=0, and subsequently from the carrier rate equation (5.39), one has

$$I_t = q\gamma_e(N_t)n_t/V \tag{5.46}$$

where I_t is the current at laser transparency.

After solving equations (5.44) as the function of the injection current I and the use of equation (5.43) the photon population is obtained. The

power emitted from each facet of the laser is linearly related to the photon population and is given by

$$P_{out} = \frac{1}{2}(1 + K_f)h\nu_0 v_g(\alpha_{eff})P \qquad (5.47)$$

where h is the Plank constant, ν_0 is the lasing frequency, α_{eff} is the effective reflectivity, and K_f is the fraction of the reflected power. Intuitively, one may say $v_g\alpha_{eff}$ is the rate at which photons of energy hv escape through the two facets. In the next section, small signal analysis of the external and solitary laser will be discussed.

5.1.4. Small Signal Analysis of the Laser Diode

The modulation characteristics of semiconductor laser diodes for direct modulation of analog signal have been studied extensively by several authors [8, 75, 76]. In high speed lasers, the ultimate limiting phenomenon has been found to be associated with intrinsic photon resonance, which peaks at the relaxation oscillation frequency f_r. The light modulation depth sharply drops at a rate of 40 dB/dec for frequencies greater than the modulation frequency f_m. When a laser diode is directly intensity modulated (AM) with sinusoidal waveform the output light also produces variation in phase and frequency. The frequency variations are referred to as frequency chirping and are directly related to the linewidth enhancement factor β_c. Frequency chirping rises from the index changes that occurs when the optical gain changes in response to variations in the carrier population.

The set of rate equation (5.38) to (5.40) describes the behavior of either external cavity laser or a solitary laser. These expressions may in general be solved for large signal solution. However, a small signal analysis gives valuable information about the laser, such as the modulation response and the frequency chirping. For a laser diode biased at a DC current, When modulated sinusoidally the total injection current varies with the rf modulation. The total current I is given by

$$I(t) = I_b + \frac{I_m(t)}{I_b - I_{th}} \tag{5.48}$$

where the bias current I_b and the threshold current I_{th} are already either from experimental or the steady state analysis. The strength of the modulation depth is referred to as the modulation index m, given by

$$m = \frac{\Delta P_{max}}{P} = \frac{I_m(t)_{max}}{I_b - I_{th}} \tag{5.49}$$

ΔP is the variation in the photon number due to the injection current.

In the absence of rf drive, the laser operates continuously at the bias current I_b. The steady state values of photon number P_0, photon phase ϕ_0, and the carrier density N_0 are obtained in the previous section. The effect of the modulation current I_m is to introduce a deviation in these parameters P(t), ϕ(t), N(t), which is periodic with the modulation frequency ω_m. In small signal analysis, it is assumed that the modulation index m<<1. Small signal analysis is a procedure that linearizes the laser rate equation around the bias point I_b. The following set of equations are used to linearize the rate equation

$$I_m(t) = I_m e^{j\omega t} \tag{5.50}$$

$$P(t) = P_0 + p\, e^{j\omega t} \tag{5.51}$$

$$\phi(t) = \phi_0 + \phi\, e^{j\omega t} \tag{5.52}$$

$$N(t) = N_0 + N\, e^{j\omega t} \quad . \tag{5.53}$$

Before substituting the above equation in the rate equation, the quantities under the radical in the photon magnitude and phase equations (5.38) and (5.39) are respectively expanded using Binomial expansion, one has

$$\frac{dP(t)}{dt} = (G(t)-\gamma)P(t) + 2|\kappa|\left(P(t) - \frac{1}{2}\Delta P(t)\right)\cos(\omega_0\tau+\Delta\phi(t)) + R_{sp}(N) \tag{5.54}$$

$$\frac{d\phi(t)}{dt} = \frac{\mu}{\mu_g}(\omega_0 - \Omega) + \frac{1}{2}\beta_c\,(G(t)-\gamma) + |\kappa|\left(1 - \frac{\Delta P(t-\tau)}{2P(t)}\right)\sin(\omega_0\tau+\Delta\phi(t)) \tag{5.55}$$

where $\Delta P(t)$ is given by

$$\Delta P(t) = P(t) - P(t-\tau) \tag{5.56}$$

which is the photon population change in on external cavity cavity roundtrip time τ and it is usually adequate to describe the changes due to the external feedback.

Linearizing the photon population, photon phase, and carrier density equations (5.54), (5.55), and (5.40) with the aid of equation (5.50) to (5.53). Assuming that $\Delta\phi(t)$ is small and replacing $j\omega t$ by st, one has a set of rate equations in Laplace domain

$$sP(s)\,e^{st} = (P_0 + Pe^{st})\left[\frac{\Gamma v_g a}{V}(N_0 + Ne^{st} - N_t) - \gamma\right] + \beta_{sp}\eta_{sp}(N_0 + Ne^{st})\gamma_e$$

$$+ 2|\kappa|\left[P_0 + Pe^{st} - \frac{1}{2}\Delta P(s)\right]\{\cos(\omega_0\tau) - \Delta\phi(s)\sin(\omega_0\tau)\} \tag{5.57}$$

$$s\phi(s)\,e^{st} = \frac{1}{2}\beta_c\left[\frac{\Gamma v_g a}{V}(N_0 + Ne^{st} - N_t) - \gamma\right]$$

$$- |\kappa|\left[1 - \frac{\Delta P(s)}{P_0 + Pe^{st}}\right]\{\Delta\phi(s)\cos(\omega_0\tau) + \sin(\omega_0\tau)\} \tag{5.58}$$

$$sN(s)\,e^{st} = \frac{I_b}{q} + \frac{I_m(t)\,e^{st}}{q(I_b - I_{th})}(P_0 + Pe^{st}) - \left[A_{nr} + B\frac{N_0 + Ne^{st}}{V}\right](N_0 + Ne^{st})$$

$$- \frac{\Gamma v_g a}{V} \left[N_0 + Ne^{st} - N_t \right] \left\{ P_0 + Pe^{st} \right\} \qquad (5.59)$$

In the above equation all terms that are not multiplied by the complex exponential factor have already been solved for in the steady state solution and it equals to a net zero, so they are dropped. Further on, all higher order terms such as e^{2st} are neglected for a small signal solution. The quantities $\Delta P(s)$ and $\Delta\phi(s)$ are related to their time domain expression through the Laplace time shift operator, given as

$$\Delta P(s) = (1 - e^{-s\tau})P(s) \qquad (5.60)$$

$$\Delta\phi(s) = (1 - e^{-s\tau})\phi(s) \ . \qquad (5.61)$$

Substituting $\Delta P(s)$ and $\Delta\phi(s)$ in the equations (5.57) to (5.59) results in a set of linear equation in the Laplace domain. This set of equations may be written as a 3x3 matrix,

$$\left(s - (G_0-\gamma) + |\kappa|COS(\omega_0\tau)(1-e^{-s\tau})\right)P(s) + \left(2|\kappa|P_0SIN(\omega_0\tau)(1 - e^{-s\tau})\right)\phi(s)$$

$$- \left(P_0\frac{\Gamma v_g a}{V} + \beta_{sp}\eta_{sp}\gamma_{e0}\right)N(s) = 0 \qquad (5.62)$$

$$\left(- |\kappa|\frac{1}{2P_0}SIN(\omega_0\tau)(1 - e^{-s\tau})\right)P(s) + \left(s + |\kappa|COS(\omega_0\tau)(1 - e^{-s\tau})\right)\phi(s)$$

$$- \left(\beta_c \frac{\Gamma v_g a}{2V}\right)N(s) = 0 \qquad (5.63)$$

$$(G_0)P(s) + (\ 0\ )\phi(s) + \left(s + \gamma_{e0} + \frac{B}{V} + \frac{\Gamma v_g a}{V} P_0\right)N(s) = \frac{I_m}{q(I_b-I_{th})} \qquad (5.64)$$

The criteria for a stable operation is that the determinant D(s) of equations (5.61) to (5.62) has all its' roots in the left half s-plane. One may write the determinant as

$$D(s) = s^3 +$$

$$\left[2|\kappa|COS(\omega_0\tau)(1 - e^{-s\tau}) + \left(\gamma_{e0} + \frac{B}{V} + \frac{\Gamma v_g a}{V} P_0\right) - (G_0-\gamma)\right] s^2$$

$$- \left[\left(1 + (G_0-\gamma) - |\kappa|COS(\omega_0\tau)(1 - e^{-s\tau})\right)\left(|\kappa|COS(\omega_0\tau)(1 - e^{-s\tau})\right)\right.$$

$$+ (G_0-\gamma)\left(\gamma_{e0} + \frac{B}{V} + \frac{\Gamma v_g a}{V} P_0\right) + G_0\left(P_0\frac{\Gamma v_g a}{V} + \beta_{sp}\eta_{sp}\gamma_{e0}\right)$$

$$\left. - |\kappa|^2 SIN^2(\omega_0\tau)(1 - e^{-s\tau})^2\right] s$$

$$- \left[\left\{\left((G_0-\gamma) - |\kappa|COS(\omega_0\tau)(1 - e^{-s\tau})\right)\left(\gamma_{e0} + \frac{B}{V} + \frac{\Gamma v_g a}{V} P_0\right)\right.\right.$$

$$\left.\left. + G_0\left(P_0\frac{\Gamma v_g a}{V} + \beta_{sp}\eta_{sp}\gamma_{e0}\right)\right\}\left(|\kappa|COS(\omega_0\tau)(1 - e^{-s\tau})\right)\right.$$

$$- G_0|\kappa|\beta_c \frac{\Gamma v_g a}{V} P_0 SIN(\omega_0\tau)(1 - e^{-s\tau})$$

$$\left. - \left(\gamma_{e0} + \frac{B}{V} + \frac{\Gamma v_g a}{V} P_0\right)|\kappa|^2 SIN^2(\omega_0\tau)(1 - e^{-s\tau})^2\right] \qquad (5.65)$$

The final quantities of interest are the modulation bandwidth (f_r) and the frequency chirping. Since the determinant of equation (5.62) to (5.64) has already been solved, one may use Cramer's rule to solve for P(s), ϕ(s), and N(s), the solution are as the follows:

$$P(s)D(s) = \frac{I_m}{q(I_b-I_{th})}\left[s\left(P_0\frac{\Gamma v_g a}{V} + \beta_{sp}\eta_{sp}\gamma_{e0}\right)\right.$$

$$+ |\kappa|\left(P_0\frac{\Gamma v_g a}{V} + \beta_{sp}\eta_{sp}\gamma_{e0}\right) COS(\omega_0\tau)(1 - e^{-s\tau})$$

$$\left. - |\kappa|\beta_c P_0 \frac{\Gamma v_g a}{V} SIN(\omega_0\tau)(1 - e^{-s\tau})\right] \qquad (5.66)$$

$$\phi(s)D(s) = \left[\left((G_0-\gamma) - |\kappa|COS(\omega_0\tau)(1 - e^{-s\tau})\right)\beta_c \frac{\Gamma v_g a}{2V}\right.$$

$$\left. + |\kappa|^2 SIN^2(\omega_0\tau)\,(1 - e^{-s\tau})^2\right] \frac{I_m}{q(I_b-I_{th})} \qquad (5.67)$$

$$N(s)D(s) = \left[\left(s-(G_0-\gamma) +|\kappa|COS(\omega_0\tau)(1 - e^{-s\tau})\right)\left(s + |\kappa|SIN(\omega_0\tau)(1 - e^{-s\tau})\right)\right.$$

$$\left. + |\kappa|^2SIN^2(\omega_0\tau)(1 - e^{-s\tau})^2\right] \frac{I_m}{q(I_b-I_{th})} \qquad (5.67)$$

A similar expression, but less complicated, may be derived for the solitary laser such as the following

$$P(s) = \frac{\frac{I_m}{q(I_b-I_{th})}\left(P_0\frac{\Gamma v_g a}{V}+\beta_{sp}\eta_{sp}\gamma_{e0}\right)}{s^2+s\left(\gamma_{e0}+\frac{B}{v}+P_0\frac{\Gamma v_g a}{V}-(G_0-\gamma)\right)+(G_0-\gamma)(\gamma_{e0}+\frac{B}{V}+P_0\frac{\Gamma v_g a}{V})-G_0(P_0\frac{\Gamma v_g a}{V}+\beta_{sp}\eta_{sp})} \qquad (5.67)$$

where the carrier density N(s) has the same denominator D(s) and is given by

$$N(s)D(s) = \frac{I_m}{q(I_b-I_{th})}\,(s - (G_0-\gamma)) \quad . \qquad (5.68)$$

Two quantities of practical interest are the normalized power response and the frequency chirping respectively denoted as $H(j\omega)$ and $\delta(v)$. One has

$$H(j\omega) = \left|\frac{P(j\omega)}{P(0)}\right| \qquad (5.69)$$

and the frequency chirping per milliampere of modulation current is defined as

$$\delta\phi(f)= \left|\frac{\phi'}{2\pi I_m}\right| . \qquad (5.70)$$

The frequency response for the external cavity laser or the solitary has already been solved. One may just replace s by jω and take the normalized amplitude. The frequency chirping for the external cavity laser is obtained by substituting P(s), f(s), N(s) into the phase rate equation (5.55) ϕ' according to equation (5.70) the chirping magnitude is given. For the solitary laser, a simple expression is derived and is included here, therefore one has

$$\phi' = \beta_c \frac{\Gamma v_g a}{4\pi I_m V} |N(s)| \qquad (5.71)$$

where N(s) is substituted from equation (5.68).

Analytic solution, describing the modulation behavior of either external or solitary semiconductor laser diode, has been derived. Several authors [13, 18] have also discussed a similar analytic solution for the external cavity laser under weak optical feedback. However, these authors neglected the external cavity harmonics and the effect of gain variation G with the change in the population density N. Further more, the contribution of the spontaneous emission was also neglected by them.

5.2 Results of Laser Modulation Enhancement

The results of a study on direct modulation of a laser diode beyond its relaxation oscillation frequency f_r is presented here, using optical feedback by means of an external cavity. The experiments were performed on a laser diode (Ortel SL1000) with $f_r \approx 6$ GHz, and the external cavity lengths were set for the fundamental resonance at 5 and 10 GHz. The results show that the bandwidth of the modulation peaks in this configuration are wide enough to have signatures impressed on the modulation signal.

5.2.1 Experimental Setup

The measurement system used for this experiment is shown in Fig. 5.6. It is composed of a Double Channel Buried Heterojunction (DCBH) single mode GaAlAs laser diode (Ortel SL 1000) with anti-reflection (AR~ 5%) coating on one facet, mounted on an open heat sink. The laser was inserted in our custom 30 GHz fixture, with optical access to both facets of the laser diode. The laser diode is biased by a constant current source to 1.6 times the I_{th} (threshold current) and is rf modulated through a bias-Tee (HP 11612A). A lens (UKA LP-01) and a gold coated plane mirror was positioned at the AR (anti-reflection) coated facet of the laser diode which forms an external cavity as shown in Fig. 5 6. At the other facet of the diode, a collimating lens (UKA LP-01) focuses light onto an Ortel PD 025C high-speed GaAs PIN photodiode with 3 dB bandwidth of 12 GHz. The cavity is tuned using a translation stage with a resolution of 0.1 micron and further tuning is done by varying the current, which also serves to prevent self-pulsation. Fine resolution is required because the reflected light from the external cavity must be in phase with the light emitted. Also, delayed light from the external cavity must be in the same temporal position as the light in the laser cavity for constructive interference. Thus:

$$L = m\mu l_D \qquad (5\text{-}72)$$

where L is the external air filled cavity length, m is an integer, μ is material index (for GaAs it is 3.4), and l_D is the laser diode length.

When the light is fed back from the external cavity into the active region of the laser and is in phase with that reflected light from the AR coated facet, the maximum dc output occurs. However, significant rf enhancement only occur when there is phase mismatch between the two cavities. At $\pm \pi/2$ phase diference, the external cavity behaves as it is a solitary laser. For phasees larger than $\pm\pi/2$ the threshold current increases which has destructive effect on the overall rf enhancement.

In setting the external cavity, the first step is to adjust the external mirror tilt such that the light is coupled back to laser facet which is 1.25x0.15 μm. When the light reflected from the external cavity shines on the back facet of the laser, then the light emerging from the front facet will become brighter. Additional adjustment is made by varying the external cavity length with a submicron resolution micropositioner. The micropositioner was varied until the relative intensity noise (RIN) level increases dramatically as scanned with a spectrum analyzer. Since only at discrete frequencies satisfying equation (5.72) minimum stable gain occurs, it is necessary to vary the bias current so the enhancement peak is positioned at such frequencies. The external cavity resonance frequency was confirmed by examining the RIN noise on a spectrum analyzer, which shows resonance peaks at the multiples of cavity roundtrip $m(c/2L_{ex})$, where c is speed of light. The relative intensity noise spectrum is shown in the Fig. 5.7 for a 10 GHz external cavity. In the next section, the steady state response of the laser will be investigated.

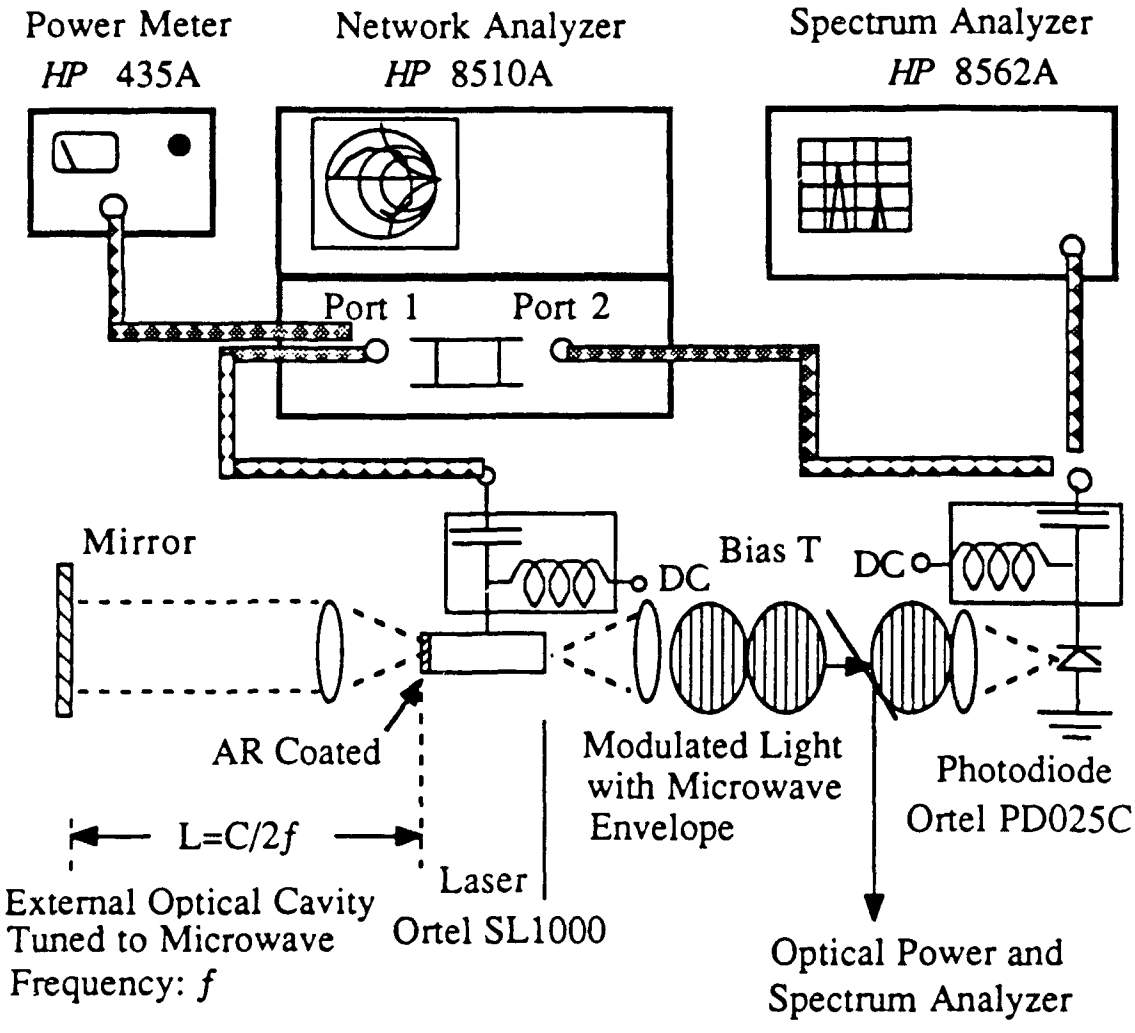

Fig. 5.6 Measurement system used in this Experiment.

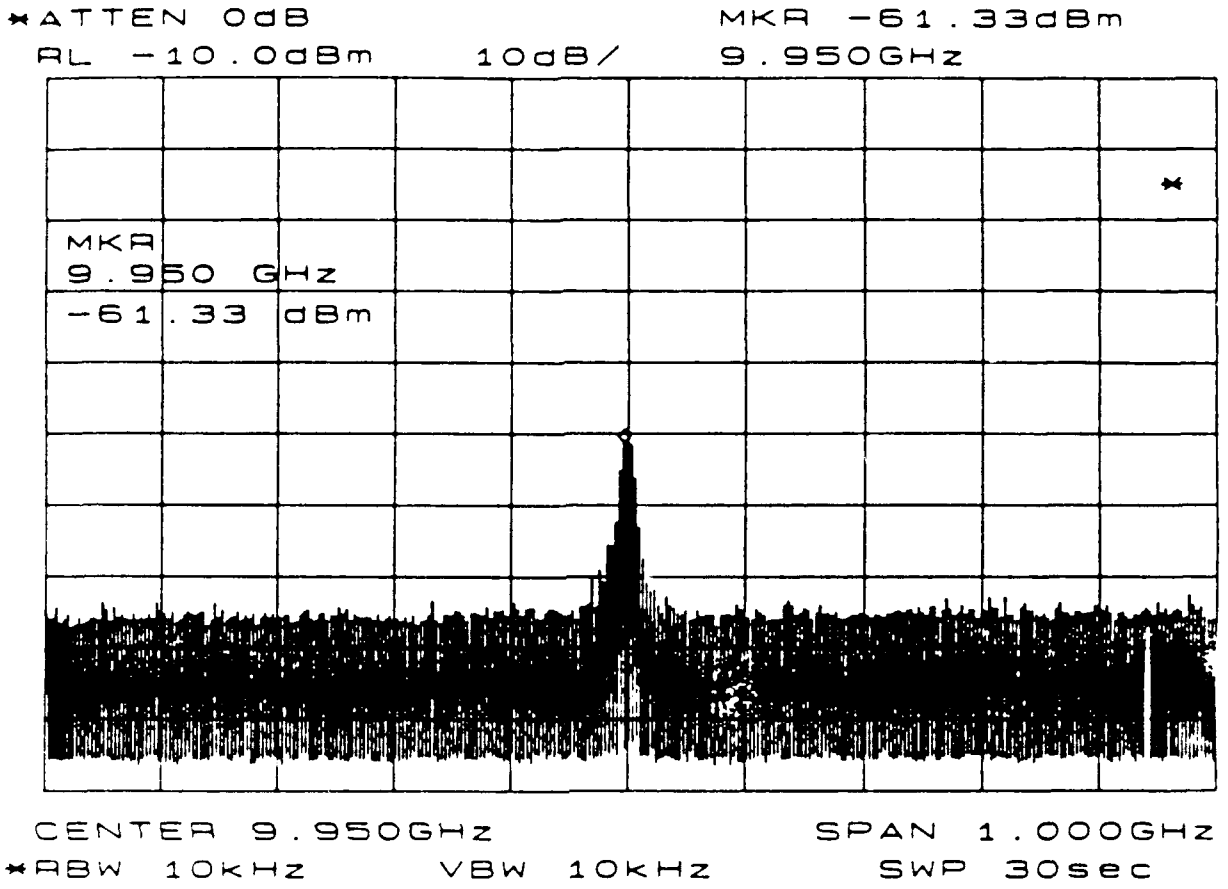

Fig. 5.7 Typical RIN noise spectrum of the external cavity laser.

5.2.2. Steady State Results

For a steady state solution, the equations of section 5.13 are solved for the carrier density N and the emitted power P as functions of the drive current. The program listed in appendix B solves the laser rate equations of either a solitary or an external cavity laser diode. The typical parameters for the 0.83 μm buried-heterostructure (Ortel SL1000) laser [8, 24, 28, 29] are listed in Table 5.1.

The results, both experimentally and theoretically, indicate that when a laser is coupled to an external cavity, significant reduction in threshold and increased output photon density is possible. Figs. 5.8 and 5.9 show respectively the theoretical and experimental LI (Light-Current) curves, which indicates the threshold is reduced with external cavity. The theoretical results were simulated for 100% coupling and a phase lag of 72°. The threshold current for the theoretical graph is lower than the experimental curve in part because the leakage current was not taken into account. Also, Fig. 5.10 shows the carrier density reduction with feedback for the same quantities.

To understand the behavior of a semiconductor laser diode coupled to an external cavity, the phase of external cavity and its fraction of reflected light was varied in the rate equations. The results are for an external cavity phase shift of 0° to 120°. From 120° to 180°, no significant changes occur. The results in the lower quadrants are the same as the upper quadrants, and therefore are not shown. The fraction of reflected light is varied from 0 to 1 in steps of 0.25 and from the simulation, the threshold current I_{th}, normalized carrier density n/n_0, and output power P, are shown in Figs. 5.11, 5.12, and 5.13 respectively. On these figures, the corresponding value for a solitary laser (S.L.) with facet reflectivities of 0.31 is also shown. When the coupling is in phase, a very large increase in the optical power is possible but sustained operation is not possible due to the facet damage.

Finally, the laser was biased to 1.6 I_{th} and then using a 0.25 meter long spectrometer which has a resolution of about 2 A°, the laser mode profile was scanned and showed a single mode spectrum, Fig. 5.14.

Parameter	Symbol	Value
Cavity Length	l_D	250 μm
Active Region Width	w	1.25 μm
Active Layer Thickness	d	0.15 μm
Confinement Factor	Γ	0.4
Effective Mode Index	μ	3.4
Group Refractive Index	μ_g	3.7
Line Width Enhancement Factor	β_c	5
Internal Loss	α_{int}	20 cm^{-1}
Carrier Density at Transparency	n_0	1×10^{18} cm^{-3}
Gain Constant	a	3×10^{-16} cm^2
Nonradiative Recombination Rate	A_{nr}	1×10^{8} s^{-1}
Radiative Recombination Rate	B	1×10^{-10} $cm^3/_s$
Auger Recombination Rate	C	1×10^{-10} $cm^6/_s$
Front Facet Reflectivity	R_1	0.31
Back Facet Reflectivity (AR Coated)	R_2	0.05
External Mirror Reflectivity	R_3	0.95

Table 5.1 Typical parameter value for Ortel SL 1000 laser diode.

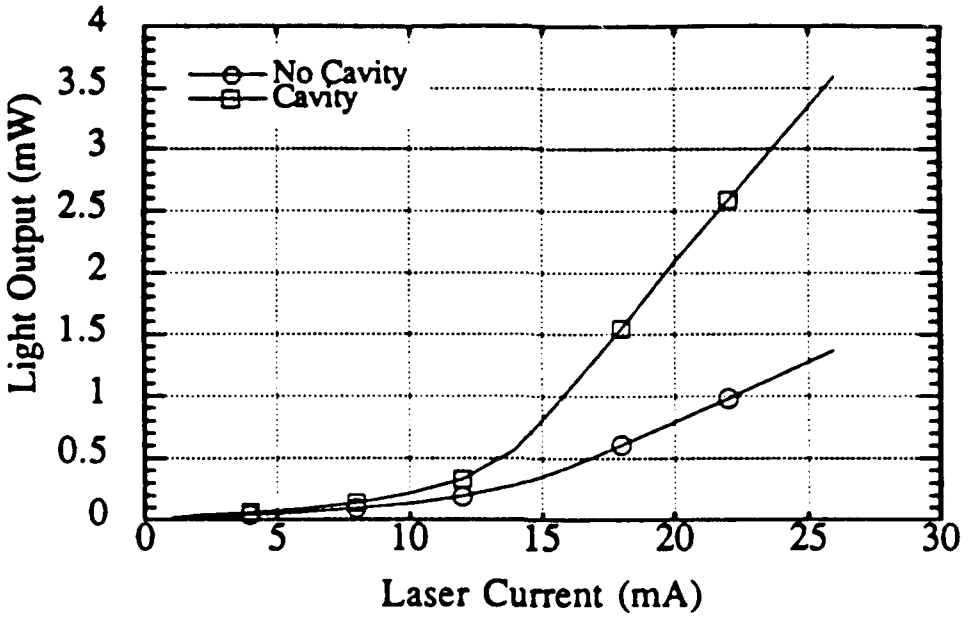

Fig. 5.8 Experimental LI curves with and without feedback.

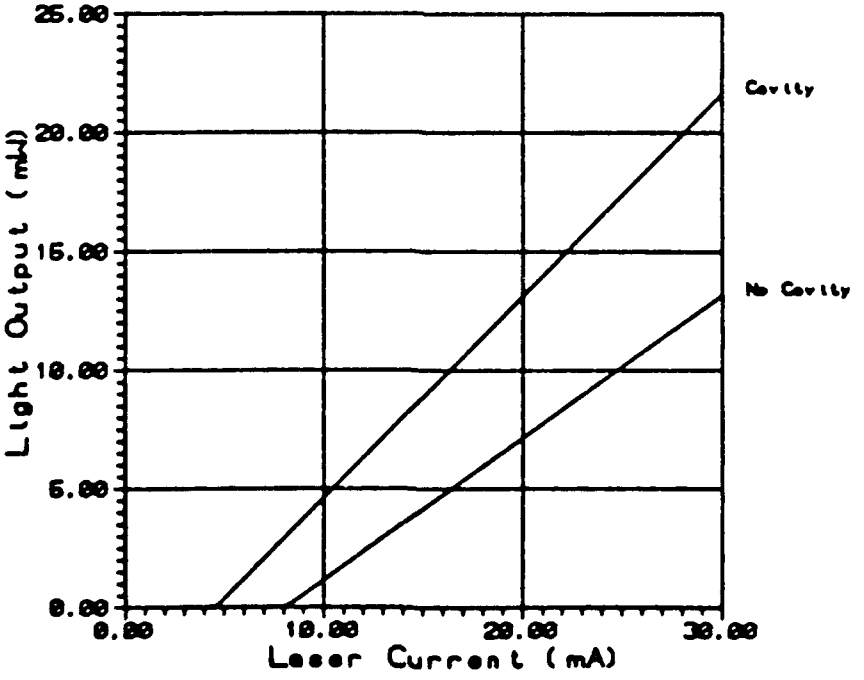

Fig. 5.9 Theoretical LI curves with and without feedback.

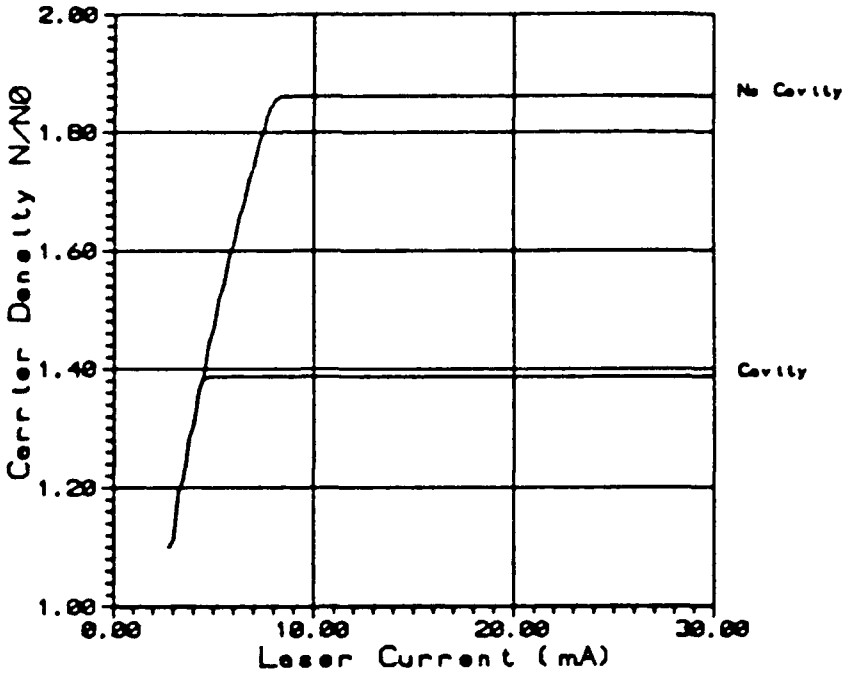

Fig. 5.10 Carrier density as the function of the current.

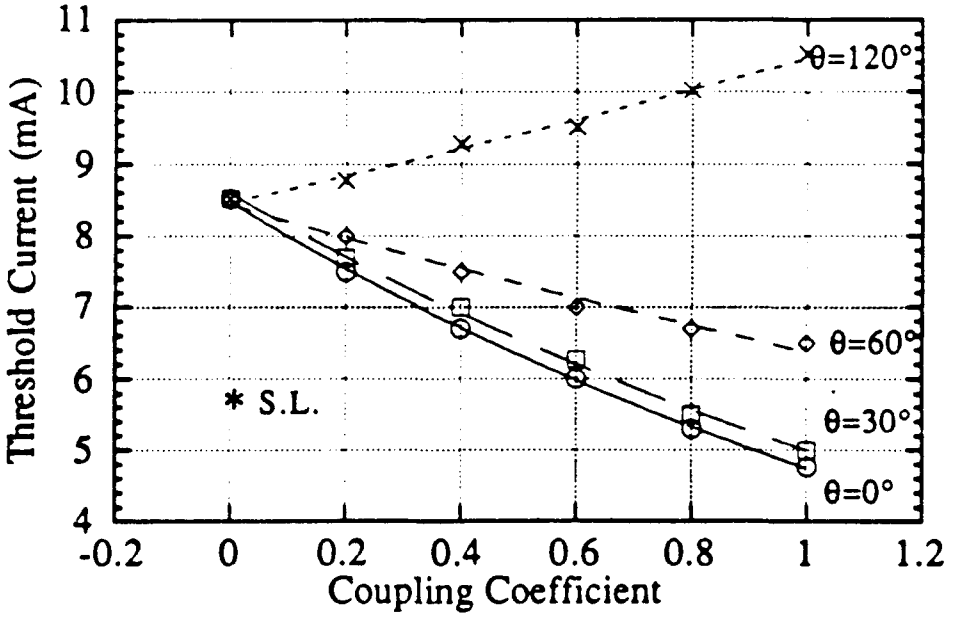

5.11 Threshold current as the function of the external cavity parameter.

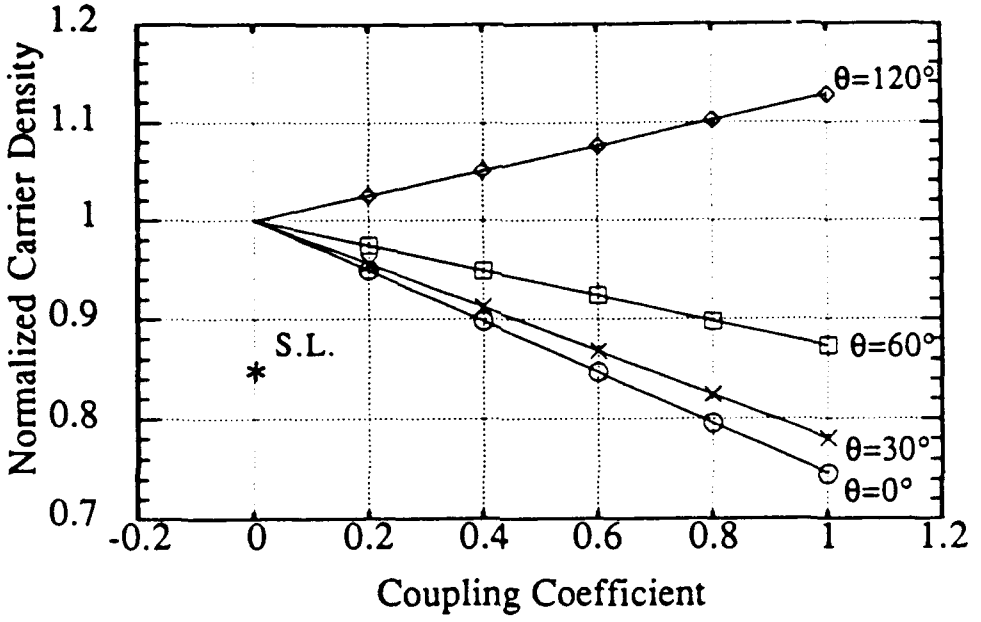

Fig. 5.12 Carrier density normalized at threshold.

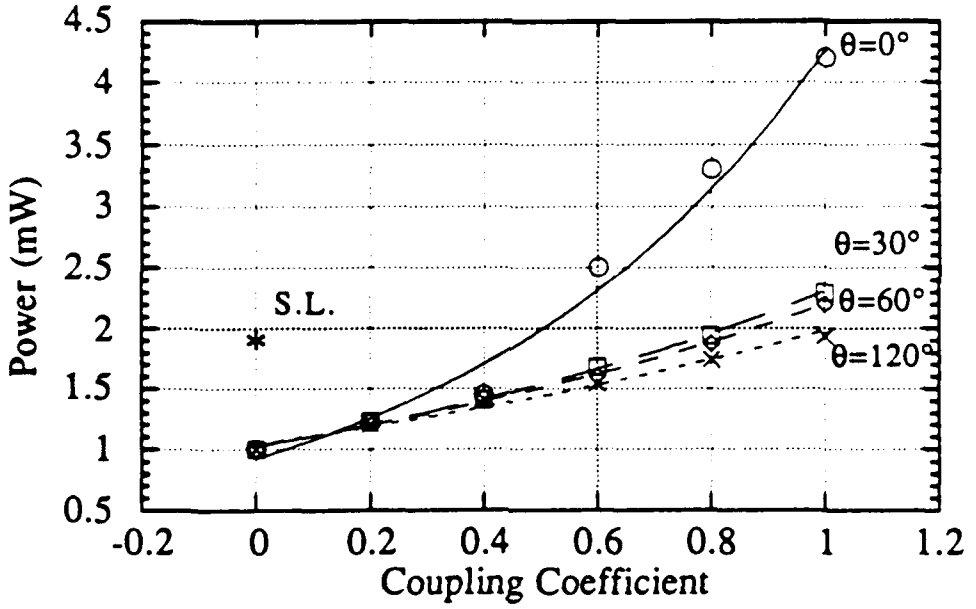

Fig. 5.13 Output power as the function of the external cavity parameter.

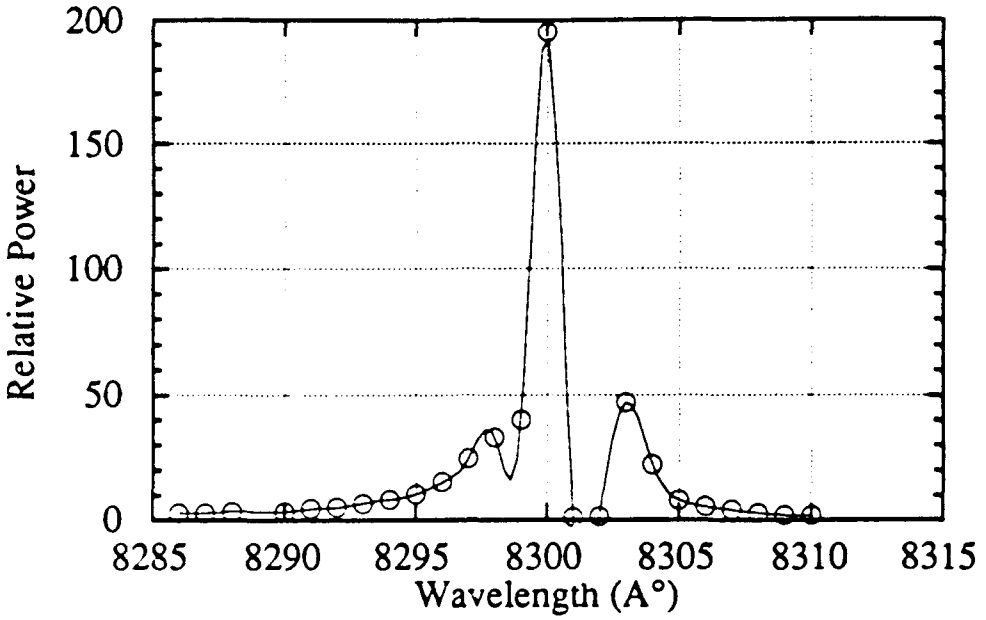

Fig. 5.14 The lasing spectrum.

5.2.3. Small Signal Modulation Results

The effect of the optical feedback on modulation enhancement of the laser diode was next investigated with superimposed rf modulation. In the experiments reported here, the laser diode was biased at 1.6 I_{th} (threshold current), where the threshold current is about 10 mA. Due to its' physical dimensions, the external cavity could only be tuned from 2 to 12 GHz, therefore the laser was tuned to two external cavity resonances, one at 5 GHz and another at 10 GHz.

The laser was driven from the Network Analyzer (8510 A), where the forward transmission S_{21} gives the modulation characteristics of the laser diode. The output power level from the network analyzer was calibrated with the HP 435A power meter so that the modulation depth may be determined eventually. The laser diode was modulated at two different

power levels respectively at -20 dBm and -30 dBm. To find the actual modulation depth, either a two-port Scattering parameter describing the laser chip submount is needed or a very high resolution spectrometer which resolves the microwave sidebands. For example, to determine the 5 GHz microwave profile, the instrument resolution should be at least 500 MHz, from Eq. 5.2 this correspond to a wavelength resolution of 0.011 A° at lasing wavelength of 0.83 μm. Conventional optical spectrum analyzer do have resolution of 0.011 A°, and they are not suitable for this application because of their large intermode spacing.

The experiments in this chapter were all carried with the modified 50 Ω package, which has the largest cutoff frequency. Fig. 3.14 readily gives the two-port S-parameters of the laser submount. One may also add the contribution of the microstrip package loss, but this is negligible as shown in Fig. 3.7. Using Fig. 3.14 and Fig. 3.19, the rf current flowing through the laser junction may be determined, then from equation 5.49 the modulation depth is calculated. Table 5.2 shows the modulation index and some of the intermittent quantities when the modulation frequencies are at 5 and 10 GHz respectively for input power levels of -10, -20 and -30 dBm.

The measured responses are shown in Figs. 5.15 and 5.16 for the 5 GHz cavity when the input power is respectively at -20 and -30 dBm. Similarly, Figs. 5.17 and 5.18 show the responses for the 10 GHz cavity. The response without the external cavity is also overlaid in these figures. For the 5 GHz cavity, the rf enhancement peak is even higher than the laser response at the low frequency range. However, in the 10 GHz cavity the response improves, but not to the same level, in part due to the detector response. The detector is an Ortel PD025C and has a 3 dB bandwidth in the X-band region (10 to 12 GHz).

To further understand the external cavity effect, various simulations were carried out by varying the cavity phase shift and the strength of the external coupling. Figs. 5.19 and 5.20 respectively show results of the 5 and 10 GHz cavity for a phase shift of 0, to -0.5π in step of 0.1π for 100% coupling. Similarly Figs. 5.21 and 5.22 respectively show the laser response at a phase shift of -0.4π for the fraction of the reflected power of

0, 0.25, 0.5, 0.75, and 1. As Fig. 5.8 shows the experimental LI curves and the threshold is reduced with the external cavity, therefore the phase difference must be less than $\pm\pi/2$. Also, when the phase differences are from 0 to $\pi/2$, anti-symmetric modulation enhancement develops, therefore theoretical results presented here are only for phases in the forth quadrant.

Theoretical results are similar to the experimental results, and they explain the mystery of a small dip in Figs.5.15 and 5.16. Unfortunately the 10 GHz graphs, Figs. 5.17 and 5.18 do not show the dip because the network analyzer 8510A was not calibrated just before the measurement. The theoretical results predict a very sharp dip where as the experimental observations show only a small dip. This is due to the finite scanning resolution of 8510A and 2% smoothing of the data. Prior to the theoretical proof, the nature of the dip was believed to be caused by a measurment glitch. The dip at the modulation enhancement region arises from the cavity reflected wave destructively interfering with the standing wave in the laser.

Case	rf power at the junction (dBm)	rf current at the junction (mA)	Modulation index (%)
5 GHz, -10 dBm	-17	1.49	35
5 GHz, -20 dBm	-27	0.47	11
5 GHz, -30 dBm	-37	0.15	3.5
10 GHz, -10 dBm	-19.8	1.08	25
10 GHz, -20 dBm	-29.8	0.34	8
10 GHz, -30 dBm	-39.8	0.11	2.6

Table 5.2 Modulation index.

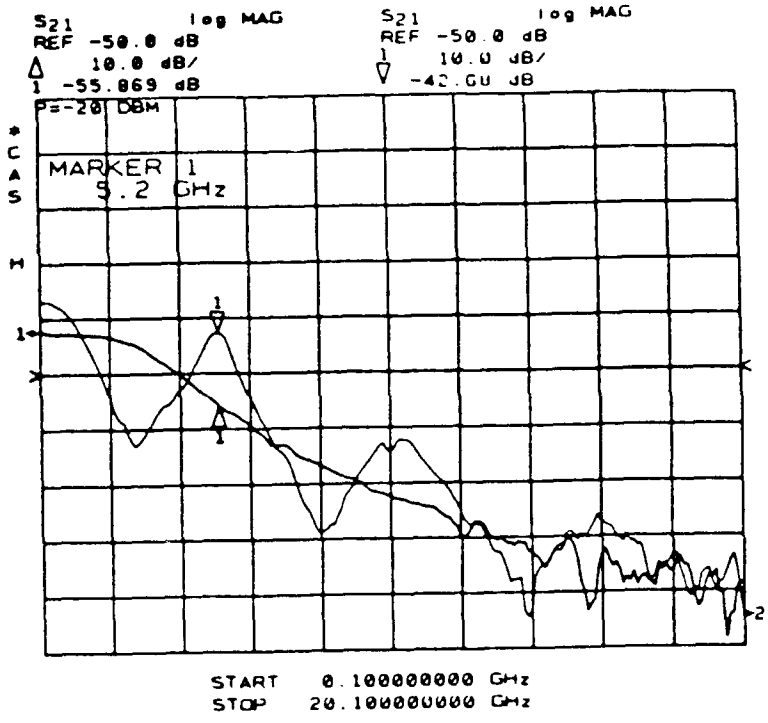

Fig. 5.15 Experimental laser response for 5 GHz cavity at -20 dBm.

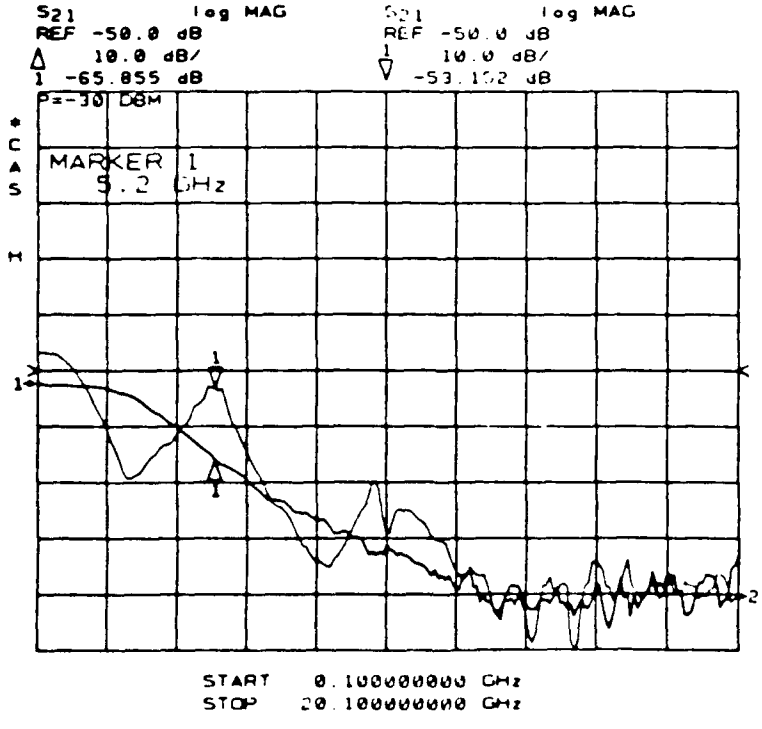

Fig. 5.16 Experimental laser response for 5 GHz cavity at -30 dBm.

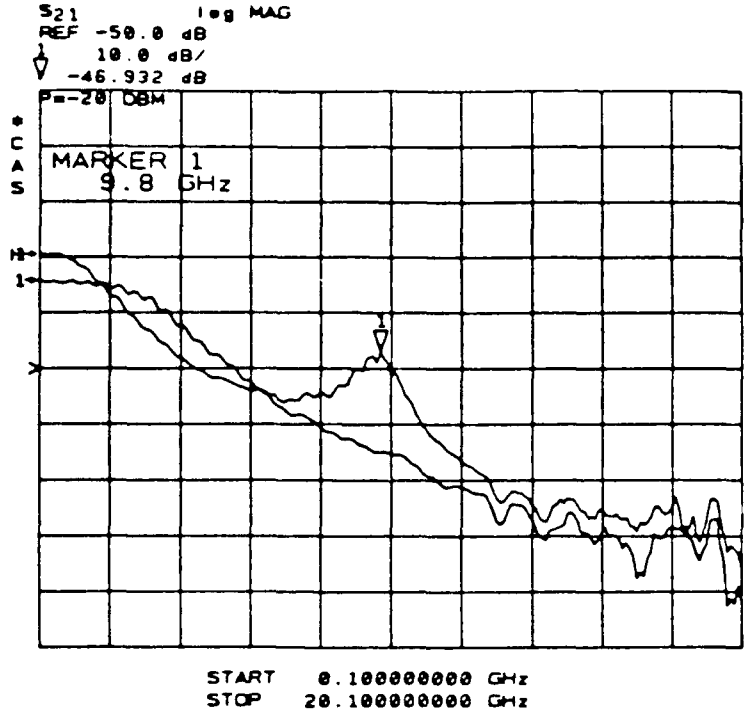

Fig. 5.17 Experimental laser response for 10 GHz cavity at -20 dBm.

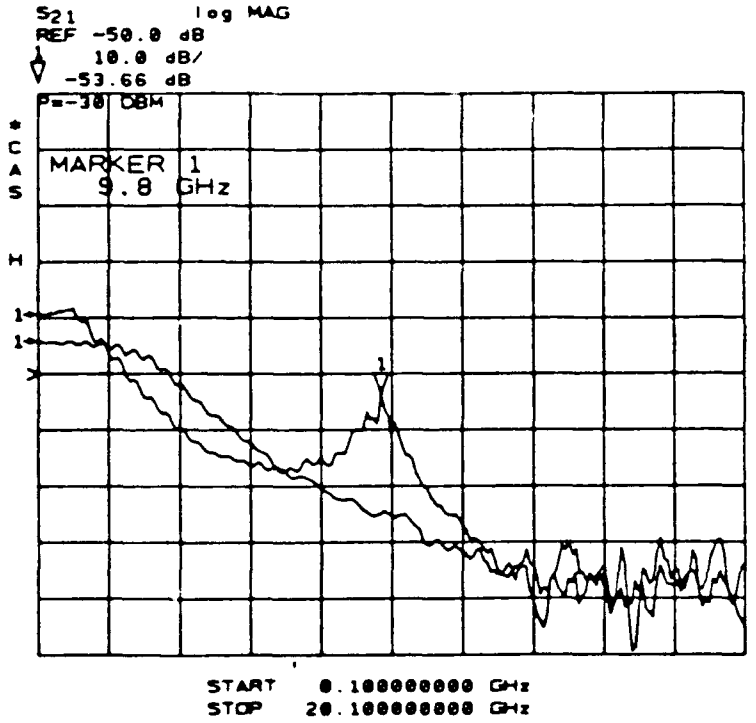

Fig. 5.18 Experimental laser response for 10 GHz cavity at -30 dBm.

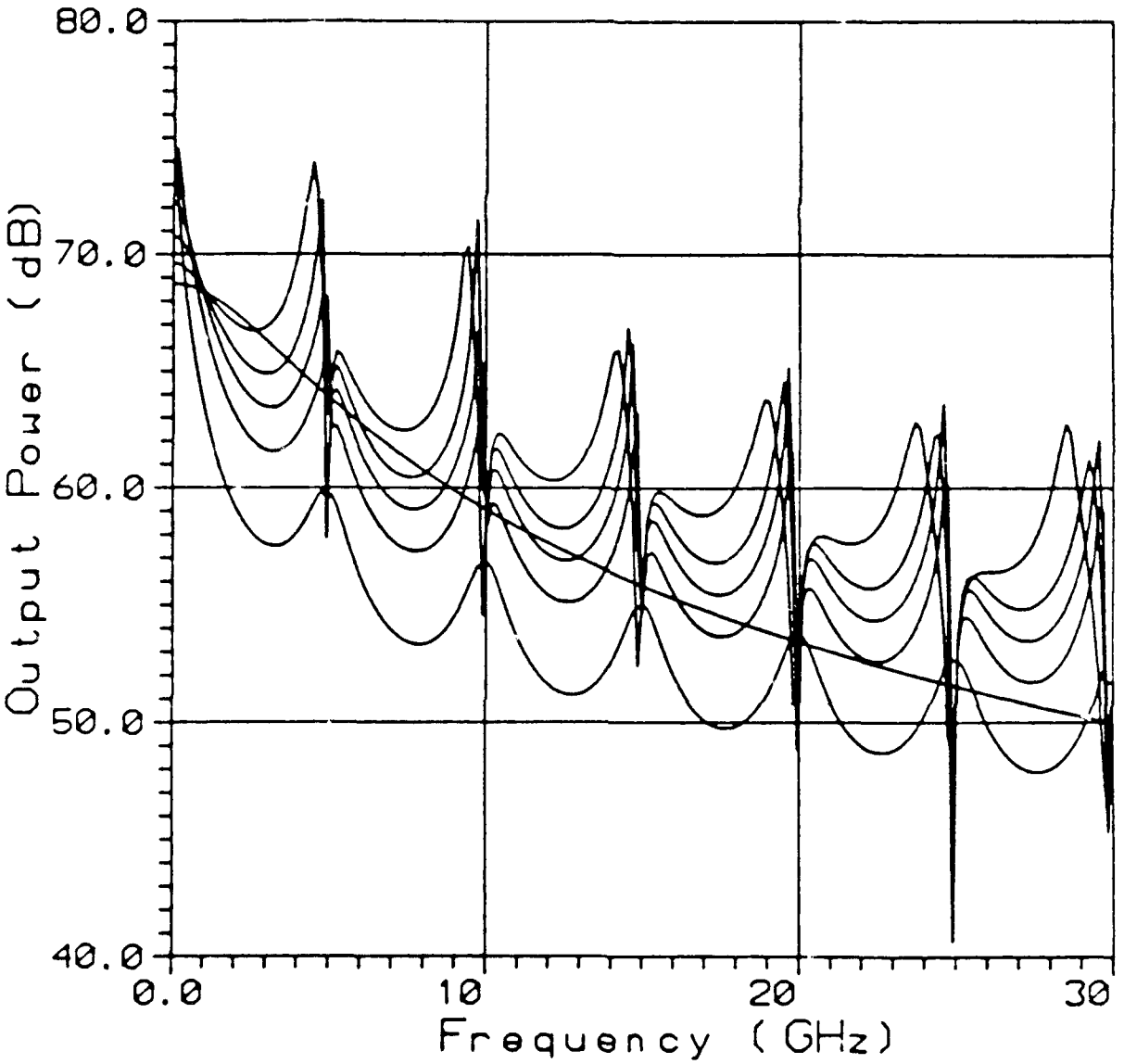

Fig. 5.19 Theoretical response of the 5 GHz cavity with various phases.

At 0 phase shift, the output is lowest with a small bump, at - 0.5 π the output is similar to the solitary response, and for other phases varying in step of 0.1π the response successively shifts to the left.

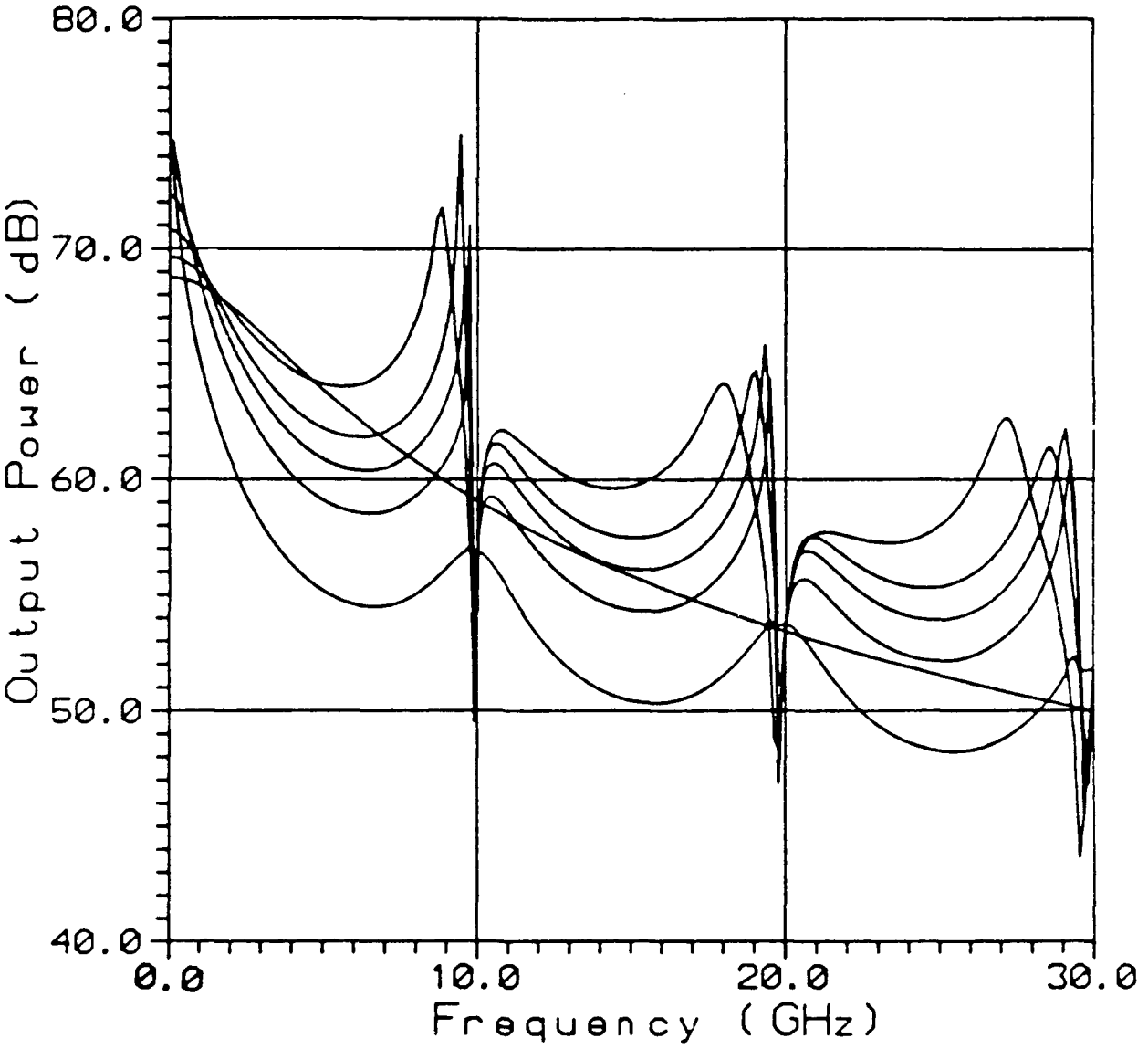

Fig. 5.20 Theoretical response of the 10 GHz cavity with various phases.

At 0 phase shift, the output is lowest with a small bump, at - 0.5 π the output is similar to the solitary response, and for other phases varying in step of 0.1π the response successively shifts to the left.

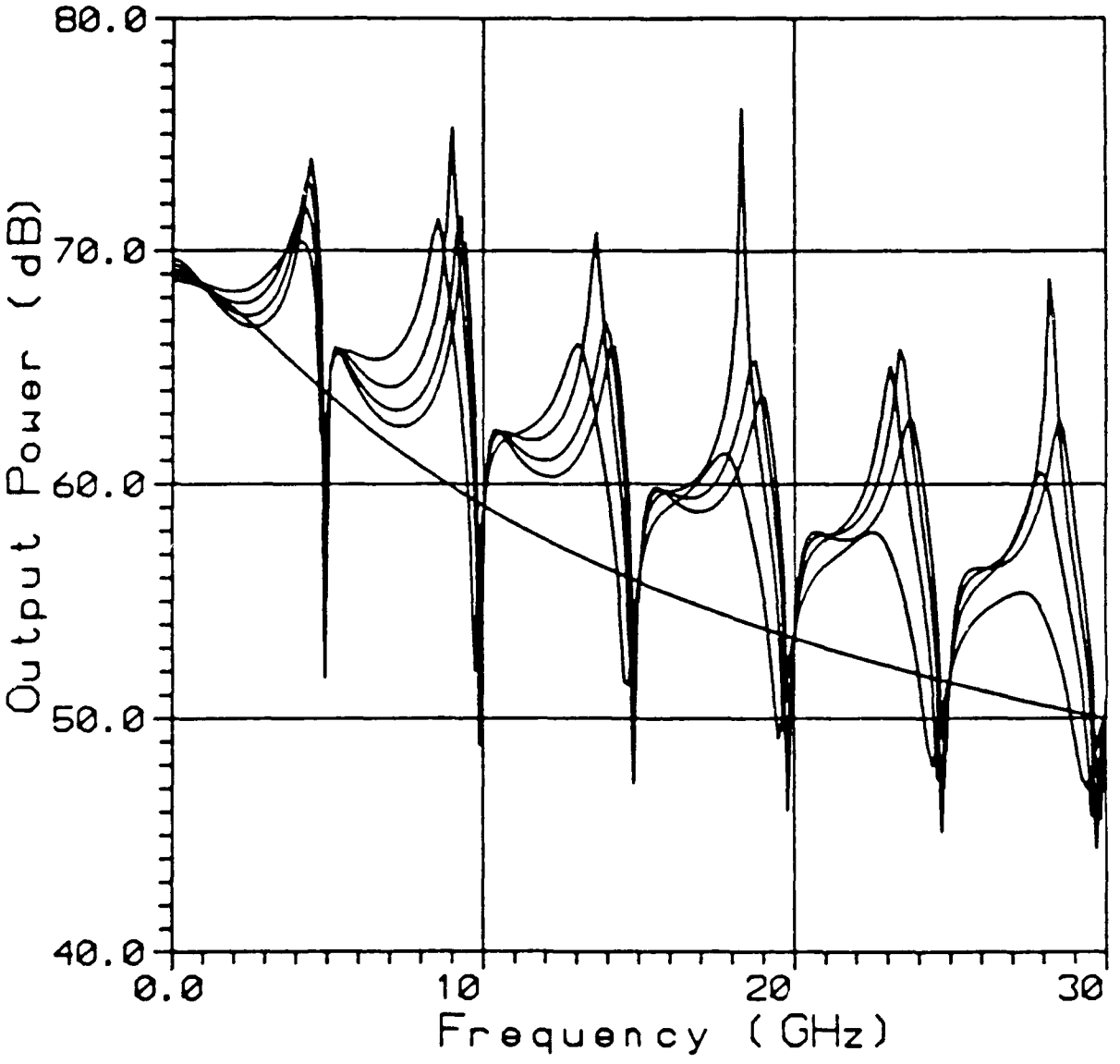

Fig. 5.21 Theoretical response of the 5 GHz cavity for various coupling.

At 0 coupling, the output is similar to the solitary response, and for other coupling 1, 0.75, 0.5, and 0.25 the response successively shifts to the left.

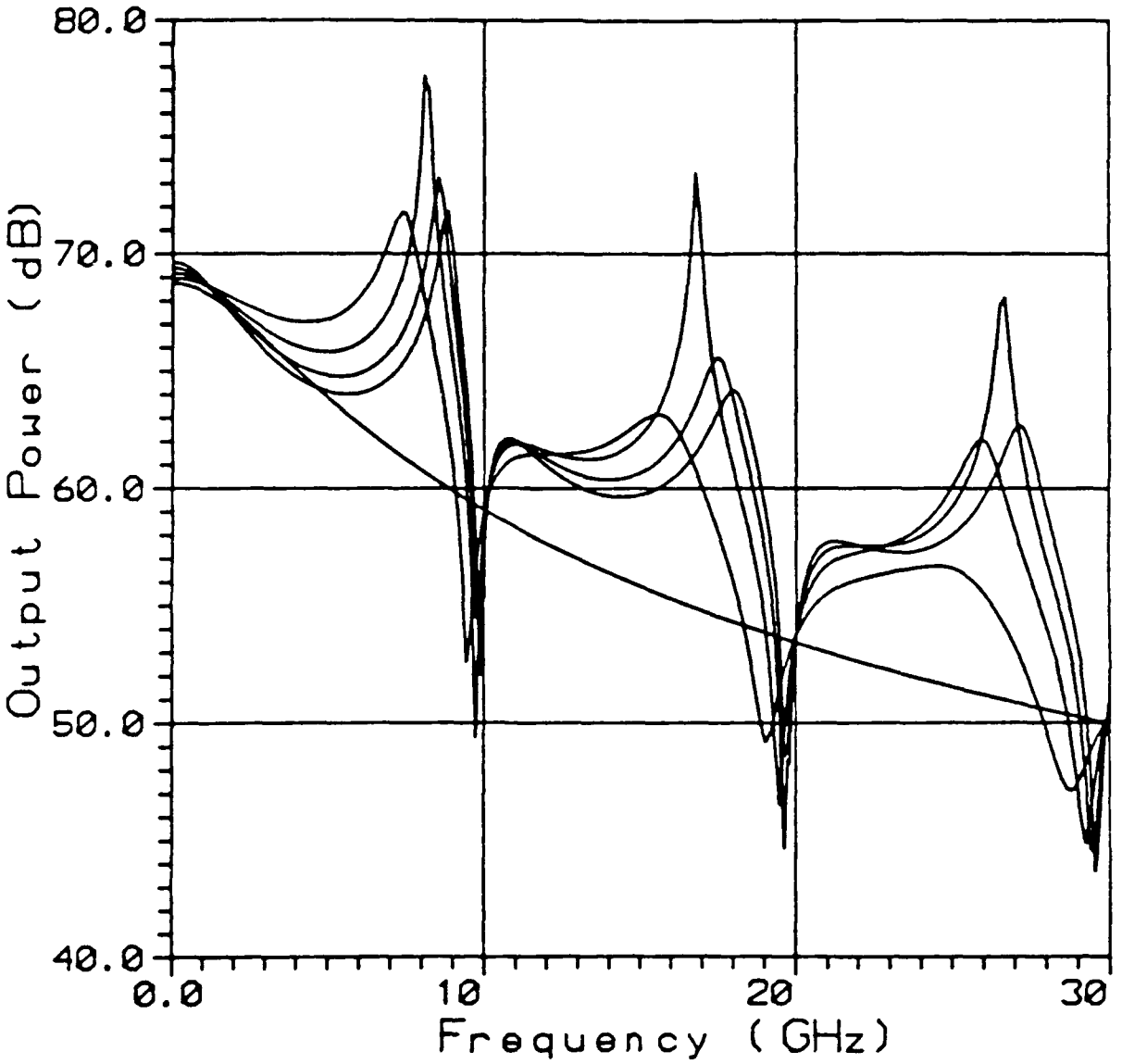

Fig. 5.22 Theoretical response of the 10 GHz cavity with various phases.

At 0 coupling, the output is similar to the solitary response, and for other coupling 1, 0.75, 0.5, and 0.25 the response successively shifts to the left.

These figures indicate that the rf enhancement is dependent on the cavity phase shift, the strength of the external coupling, and also indicated that the best rf response may not occur at the strongest coupling. Furthermore, the harmonic enhancement may even be at a higher level than the fundamental response. Finally, as the effective coupling becomes weaker or the pumping rate decreases, the frequency deviation from the cavity resonance increases and the peak shifts to a lower frequency.

The theoretical results, supported with the experiment, all indicate that millimeterwave generation of light with a semiconductor laser diode coupled to an external cavity is possible. To demonstrate this point, theoretically 24 GHz fundamental external cavity result is shown in Fig. 5.23 with effective rf enhancement of about 45 dB, compared to the low frequency level.

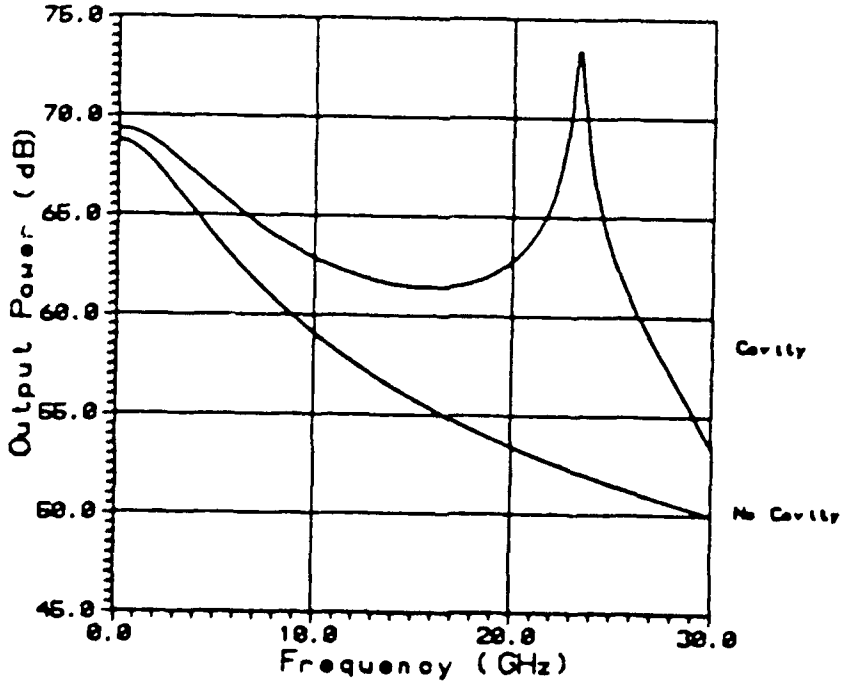

Fig. 5.23 A 24 GHz external cavity response.

5.2.3. Large Signal Measurements Results

A spectrum analyzer HP 8562A is used to compare the modulated light output at 5 and 10 GHz as the function of the input power. The external cavity was initially setup for approximately 5 GHz and the laser was also driven at 5 GHz. A typical output spectrum for an input power of -30 dBm with and without the external cavity is shown respectively in Figs. 5.24 and 5.25. Other similar spectrum peak signal levels are tabulated as the function of the input drive power and the individual graphs are not shown. The fundamental and second harmonic output with and without feedback show gain increases of up to 25 and 34 dB respectively for the fundamental at 5 and second harmonic 10 GHz signal as seen in Fig. 5.25. The laser in the 5 GHz cavity was then driven at twice the frequency which is 10 GHz and the detected 10 GHz signal with and without optical feedback shows an increase in gain of up to 17 dB as shown in Fig. 5.27. The second harmonic output at 20 GHz is not shown since, it was indistinguishable from the noise floor except at a very large modulation depth.

The external cavity fundamental resonance was then adjusted to approximately 10 GHz and the laser is driven at a fundamental frequency of 10 GHz for a wide range of input power. The results with and without feedback show fundamental enhancement of up to 25 dB, as shown in Fig. 5.28. Again, the second harmonic is not shown since it was not detectable. In each of these cases, considerable improvement in the modulated output light occurs due to the presence of the external cavity. The level of enhancement is reduced for a very large input power, for example for input power level of -10 dBm, which corresponds to a modulation depth of approximately 25% to 35% as shown in Table 5.2 when rf mismatch is taken into account. However, for input power less than -20 dBm which corresponds to a modulation depth of 5% to 10%, no significant reduction in the level of enhancement due to large signal effect is observable. One may conclude that small signal analysis of a semiconductor laser diode adequately describes the behavior even at a modulation depth in the 5% to 10% range.

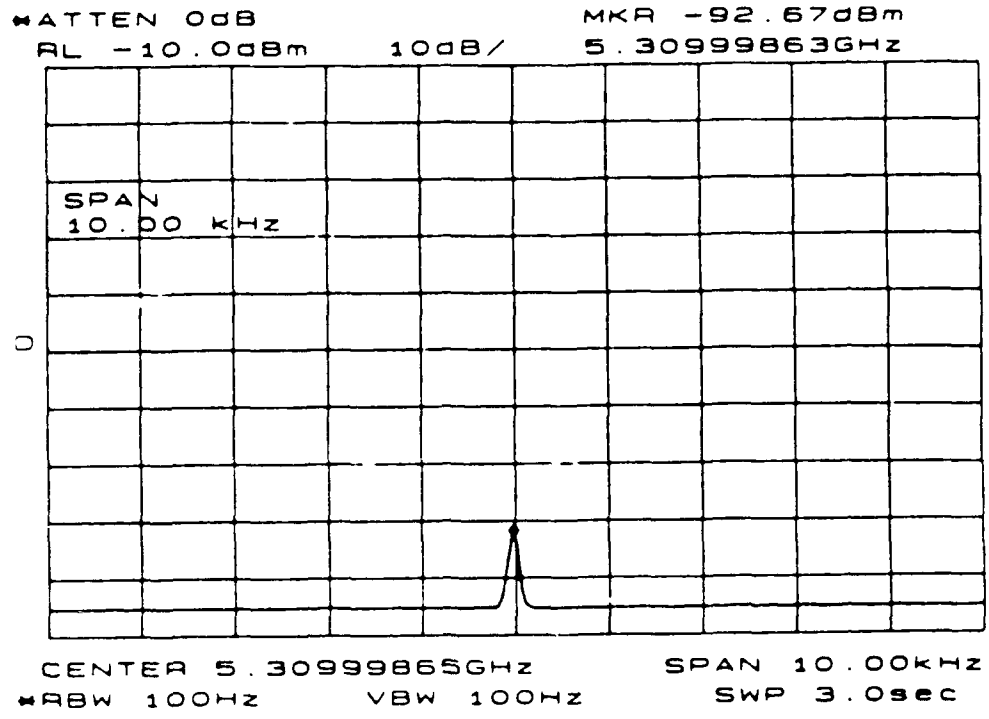

Fig. 5.24 Typical output spectrum of the 5 GHz cavity with no cavity.

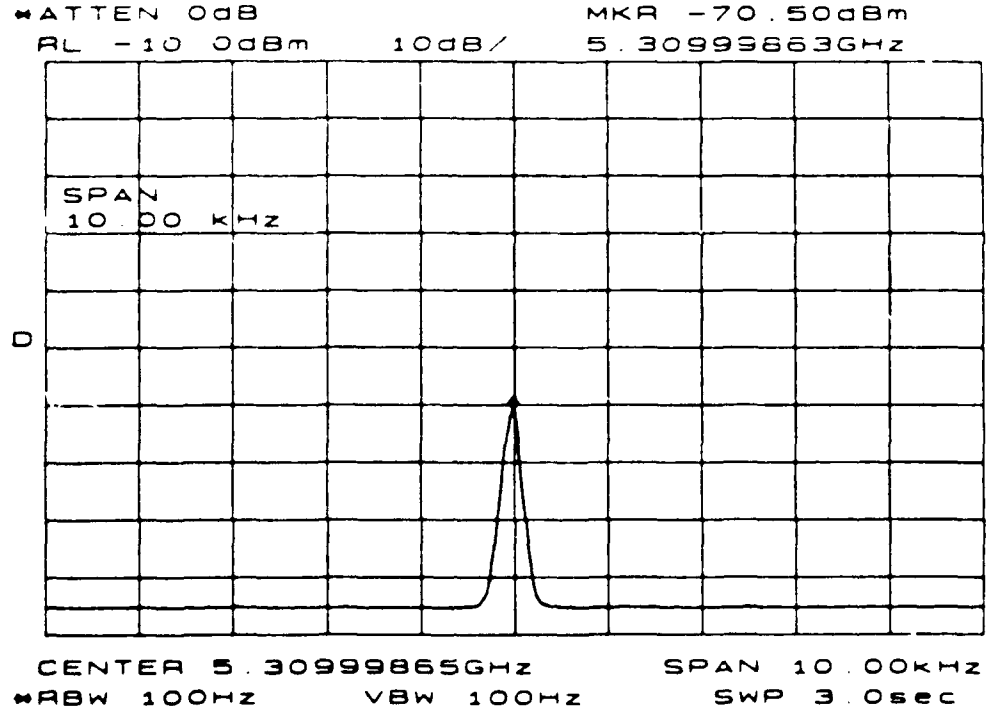

Fig. 5.25 Typical output spectrum of the 5 GHz cavity with the cavity.

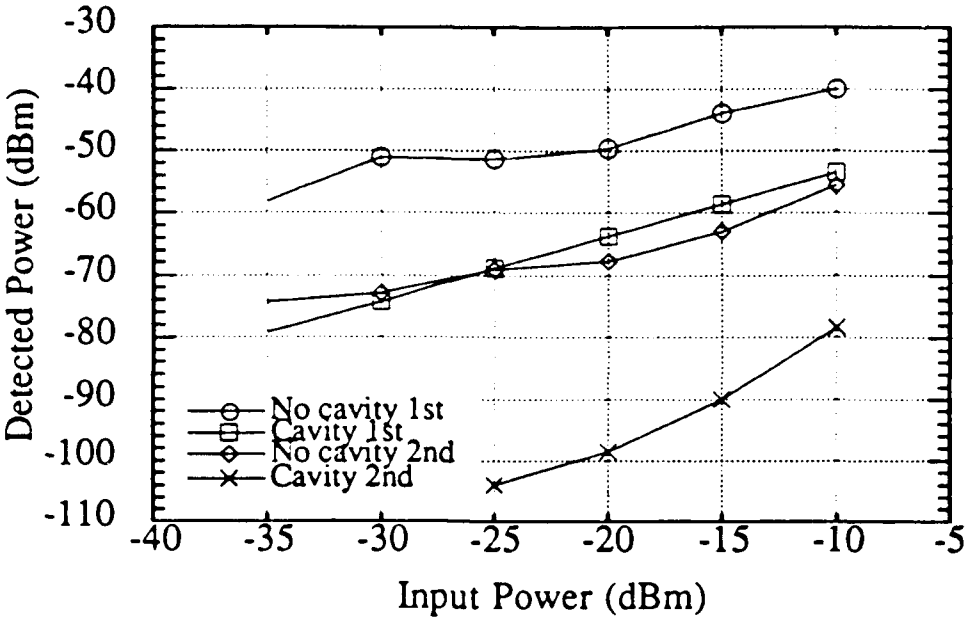

Fig. 5.26 Fundamental and second harmonic for the 5 GHz cavity

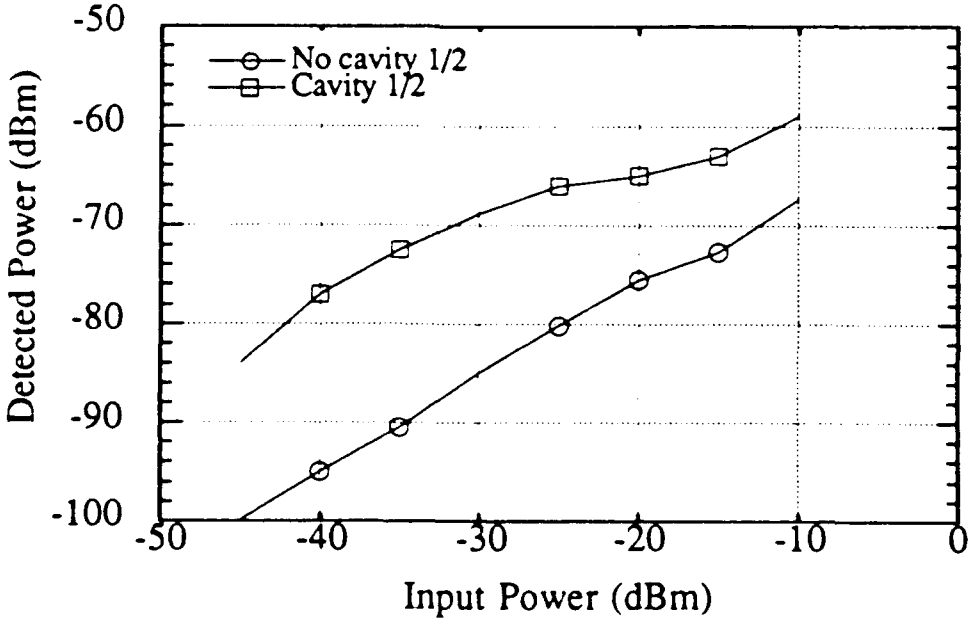

Fig. 5.27 Fundamental signal at 10 GHz for a 5 GHz cavity.

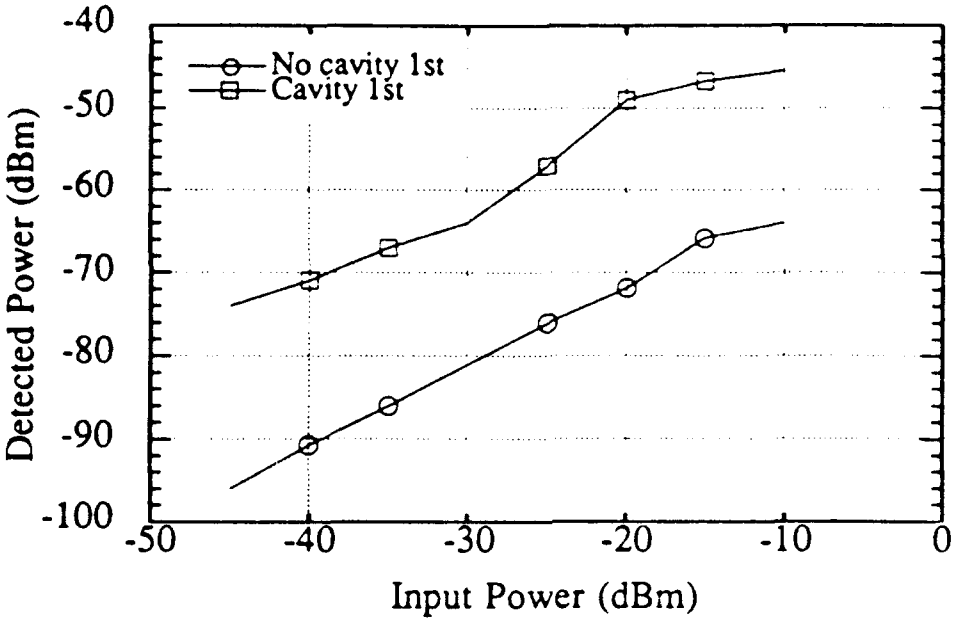

Fig. 5.28 Fundamental signal at 10 GHz for a 10 GHz cavity.

The detected rf spectrum with the external cavity shows no self-pulsation at the -30 dB input power level, however at a power level of -10 dB and larger, which corresponds to a modulation depth greater than 30%, self-pulsation may be present. It was reported when the laser diode driven at modulation depth greater than 90%, self pulsation may occur, therefore the presence of an external cavity increases the potential for self-pulsation. In summary, generation of a 10 GHz output, an external cavity set to 10 GHz gives the best results, and followed by the 5 GHz cavity, and least gain was observed when the cavity was at 5 GHz and the modulation drive was at 10 GHz.

5.3. Summary

A theory based on Maxwell's equations has been developed to characterize a semiconductor laser diode coupled to an external cavity. Experimental results agree closely with the theoretical predictions. Several authors have discussed similar theories [13, 16, 73] but these are only applicable for the case of a weak optical feedback (<5% reflection). The theory presented here predicts a dip at modulation enhancement peak similar to experimental observations. Previous experimental results [13, 14, 21] do not indicate such behavior, which may indicate poor scanning resolution.

Theoretical results show that the best rf improvement occurs for phases in the 4th quadrant. This is similar to the results reported by Lang and Kobayashi [13] . Furthermore, these authors heuristically indicate that the external cavity must be a multiple in the length of the laser cavity, and it has also been demonstrated theoretically in this dissertation.

Experimental results from intensity modulation of a laser diode optically coupled to an external cavity, are presented. The optical feedback increases light modulation depth. Enhancement of up to 25 and 34 dB in the detected fundamental and second harmonics respectively were observed without pulsation being present. The modulation peak had a fractional bandwidth of about 10%. Theoretically, the enhancement of up to 45 dB has been demonstrated, but the fractional bandwidth is about 5%.

The question of whether the fundamental frequency of the external cavity should be at millimeterwave or sub-millimeterwave frequency should be resolved by other factors such as: fabrication difficulty and the rf coupling. For a 60 GHz system, the laser diode may be placed in a 60 GHz cavity. However, the diode cavity and diode parasitics may pose a significant problem for an adequate rf drive. Alternatively, the laser may be modulated at 30 GHz in an external cavity of 30 GHz and the second harmonic, which is at the system frequency, may be used.

Chapter VI

CONCLUSIONS AND SUGGESTIONS

The large aperture phased array radar system for commercial and military applications are composed of transceiver modules, all of which are phase synchronized to a master oscillator. Optical signal distributing of this synchronization signal in a phased array system or in other high speed applications is attractive. This thesis has documented techniques to achieve high frequency direct modulation of semiconductor laser diodes. The major problems of concern in high speed modulation of semiconductor laser diode are the parasitics, matching, and the relaxation oscillation frequency. These limitations are discussed and techniques to overcome them are presented

In chapter II, a review of the elements of high-speed lightwave system is made. The two primary elements of these systems are the semiconductor laser diode and photodetector. Currently, the semiconductor laser diode is limiting the maximum operation of the high-speed lightwave system. PIN and Schottky photodiode have demonstrated 3 dB bandwidth of 67 GHz [50] and 100 GHz [48] respectively. In contrast, reliable operation of a semiconductor laser diode has only been demonstrated up to a modulation rate of 20 GHz and therefore, attention here has been given to schemes that enhance the maximum modulation rate of the laser.

In chapter III, a de-embedding technique for extracting Scattering parameters of a laser diode on chip is discussed. This is a necessary step to predict the effect of the parasitics on the modulation characteristics of the semiconductor laser diode. The laser S-parameters are measured in a custom fixture that was calibrated using TRL technique and subsequently

de-embedded . From the physical dimensions and parameters of the laser chip submount, a mixed lumped and distributed elements equivalent circuit is modeled. The extracted model implemented on Touchstone CAD program, which optimizes the circuit parameter to the de-embedded measured Scattering parameters. The optimized two-port model was then used to predict the rf current flowing through the laser junction. Also, the two-port circuit model indicates substantial improvement after the laser chip submount was modified when compared to the original manufacturer's package. In the modified package, the laser was bonded with a wire bond of about 18 mils, where as in the manufacture package it is effectively greater than 80 mils. Further reduction in the bond wire length would have been possible if the laser diode chip was not mounted on a separate submount and instead bonded directly to the microstrip package.

In chapter IV, wide band matching circuits using lumped and distributed elements were fabricated and tested. The matching circuits consist of step and linear taper microstrip transformer with additional lumped shunt capacitors to reduce the characteristic impedance to about 2 Ω without the need for very wide microstrip lines. The matching circuits had a center frequency of 10.5 GHz, bandwidth of 9 GHz, reflection coefficient of less than -10 dB, and an insertion loss of less than 1.5 dB. The step and liner transformers both have similar responses, which suggest that the scheme is not configuration limited. This matching technique may also match other low impedance devices such as Impatt diodes, power FETs, and bipolar transistor.

In chapter V, theoretical and experimental results of a Double Channel Buried Heterostructure (DCBH) semiconductor laser diode coupled to an external cavity is presented. The theoretical and experimental results are in good agreement. Furthermore, the theoretical results have indicated the presence of a dip in the modulation enhancement region. The experimental results have also shown a similar dipping but not as dramatic. The dips become more pronounced when the quality factor of the cavity is high. This type of behavior has not been reported previously. The experimental and theoretical results all indicate that at frequencies well

past the solitary laser relaxation oscillation frequency, f_r, the response may be enhanced to a level even higher than the low frequency response. Such observations open the door for millimeterwave light modulation with a semiconductor laser diode, assuming the parasitic limitation can be overcome. These results indicate that the resonant peak is slightly lower than the actual external cavity resonant frequency. Further more, the results show that resonant peak shifts to a lower frequency and away from the external cavity resonance for reduced coupling. This process also occurs when the phase lag is increased from 0 to - 0.5π, where at $\pm 0.5\pi$ phase shift the laser with the external cavity behaves as a solitary laser. At zero phase shift, no enhancement occurs and the peak is positioned at the external cavity resonance with no frequency deviation. However, for rf enhancement to occur with an external cavity there must be a either a phase lag or lead. It was shown when the phase difference is from 0 to $-\pi/2$ the best symmetrical signal enhancement and reduction of threshold current occurs.

Theoretically, the signal enhancement of 34 and 38 dB respectively has been demonstrated respectively for the fundamental and second harmonic of the external cavity respectively at 5 and 10 GHz. Experimentally, the enhancement has been about 25 and 20 dB respectively for first and second harmonic of the cavity. Also, modulation of light at 24 GHz was demonstrated theoretically with a 45 dB of rf enhancement and bringing the level even higher than the low frequency response. Finally, the large signal result indicates that small signal analysis of the external cavity is adequate even for modulation depths in the 5 to 10% regime. These results also indicate when the laser coupled to an external cavity the second harmonic (rf) enhances by as much as 34 dB.

6.1 Recommendation for Future Work

Experimental and theoretical results documented in this thesis demonstrate that modulation of a 5 GHz bandwidth semiconductor laser diode beyond its' relaxation oscillation frequency is possible even at the

millimeterwave frequencies. For these experiments, lasers were the commercially available Double Channel Buried Heterostructure (DCBH) mounted on an open heat sink. The length of the bond wire in the original manufacture package was about 80 mils, which correspond to an inductance of about 2 nH [59]. In the specially designed package the length of the bond wire was reduced to about 18 mils with the corresponding inductance of 0.3 nH. Although, this represents significant improvement, it may not be adequate. For example, for a laser with a diffusion capacitance of 2 pF, the series resonance is at about 6.5 GHz and there is no hope for implementation of a wide-band matching technique [30, 68]. Thus, proper packaging of high-speed lasers is a major prerequisite for further improvements.

In the experimental setup, light from the back facet of the laser was collimated with a compound laser diode lens and due to the physical size, the external cavity could only be tuned to a maximum frequency of 12 GHz ($L \approx 1.25$ cm). For higher frequencies, a Gradient Rod Index Lens (GRIN) may be be used [77, 78] or alternatively, an integrated reflector may be more practical. Other devices similar to the external cavity laser include the Coupled Cavity Lasers [28, 33, 79, 80]. However these devices have not been studied in regard to their high-speed modulation capabilities. Several authors have treated the second cavity as an intensity reflector without taking into account the time delay in the second cavity; the time delay in the external cavity was responsible for the periodic enhancement in the work presented here.

For millimeterwave applications, an integrated reflector positioned at the system frequency is the best choice. Further improvement may be obtained by integrating the matching circuit with the laser thus eliminating the additional packaging parasitics. Alternatively, the modulation drive could be at a subharmonic of the system frequency with the external cavity resonance set at the system frequency.

BIBLIOGRAPHY

[1] A. M. Levine, "Fiber Optics for Radar and Data System", Proc., SPIE Vol 150, Laser and Fiber Optics communication, Bellingham, MA, 1978.

[2] K. B. Bhasin, and D. J. Connolly, " Advances in Gallium Arsenide Monolithic Microwave Integrated-Circuit Technology for Space Communication Systems ", IEEE Trans. on Microwave Theory Tech., Vol MTT-34, No 10, pp. 994-1001, October 1986.

[3] A. J. Seeds, J. R. Forrest, "Initial Observation of Optical Injection Locking of an X-Band IMPATT Oscillator", Electron. Lett., Vol. 14, No. 25, pp. 25-26, 1978.

[4] A. Daryoush, P. R. Herczfeld, Z. Turski, P. K. Wahi, "Comparison of Indirect Optical Injection-Locking Techniques of Multiple X-Band Oscillators", IEEE Trans. Microwave Theory Tech., Vol. MTT-34, No. 12, pp. 1363-1370, 1986.

[5] J. F. Singleton, A.J. Seeds, and S.P. Brunt, "Optical Control of W-Band Impatt Oscillators", IEEE Proc., Vol.-133, No. 6, pp. 349-352, 1986.

[6] A Haq Al-Ani, Alexader L. Cullen and John R. Forrest, "A Phase-Locking Method for Beam Steering in Active Array Antennas", IEEE Trans. on Microwave Theory Tech., Vol MTT-22, No. 6, pp. 698-703, June 1974.

[7] K. Y. Lau, C. Harder, and A. Yariv, "Longitudinal Mode Spectrum of Semiconductor Lasers Under High-Speed Modulation", IEEE J. of Quantum Electron., Vol.-QE-20, No. 1, pp.71-79, 1984.

[8] K. Y. Lau and A. Yariv, "Ultra-High Speed Semiconductor Lasers," IEEE J. Quantum Electronics, Vol. QE-21, 1985, PP. 121-137.

[9] R. S. Tucker and I. P. Kaminow, "High-Frequency Characteristics of Directly Modulated InGaAsP Ridge Waveguide and Buried Heterostructure Lasers", IEEE J. of Lightwave Tech., LT-2, No. 4, 1984, pp. 385-393.

[10] C. B. Su and V. A. Lanzisera, "Ultra-High-Speed Modulation of 1.3-um InGaAsP Diode Lasers", IEEE J. Quantum Electron., Vol. QE-22, No. 9, pp. 1568-1578, 1986.

[11] K. Uomi, T. Mishima and N. Chinnone, "Ultrahigh Relaxation Oscillation Frequency of Highly P-doped GaAs/GaAlAs Multiple Quantum Well Lasers", Appl. Phys. Lett., Vol. 51, No. 2, pp. 78-80, 1987.

[12] K.Y. Lau, Bar-Caim, I. Ury, C Harder, and A. Yariv, "Direct Amplitude Modulation of Short-Cavity GaAs Lasers Up To X-Band Frequencies", Appl. Phys. Lett. 43 (1), pp. 1-3, 1983.

[13] R. Lang and K. Kobayashi, "External Optical Feedback Effects on Semiconductor Injection Laser Properties", IEEE J. of Quantum Electron., Vol. QE-16, No-3, pp. 347-355, 1980.

[14] K. Y. Lau, "Direct Modulation and Active Mode Locking of Ultrahigh Speed GaAlAs Lasers at Frequencies up to 18 GHz", Appl. Phys. Lett., Vol. 46, No. 4, pp. 326-328, 1985.

[15] K.Vahala, J. Paslaski, and A. Yariv, "Observation of Modulation Speed Enhancement, Frequency Modulation Suppression, and Phase Noise Reduction By Detuned Loading In a Coupled-Cavity Semiconductor Laser", Appl. Phys. Lett. 46 (11), pp. 1025-1027, 1985.

[16] G. P. Agrawal, "Generalized Rate Equations and Modulation Characteristics of External-Cavity Semiconductor Lasers", J. of Appl. Phys. 56 (11), pp. 3110-3115, 1984.

[17] L. Glasser, "A Linearized Theory for the Diode Laser in an External Cavity", IEEE J. of Quantum Electron., Vol. QE-16, No. 5, pp. 525-531, 1980.

[18] B. Tromborg, J. Osmundsen and H. Olesen, "Stability Analysis for a Semiconductor Laser in an External Cavity", IEEE J. of Quantum Electron., Vol. QE-20, No. 9, pp. 1023-1032, 1984.

[19] D. Hjelme and A. Mickelson, "On the Theory of External Cavity Operated Single-Mode Semiconductor Lasers", IEEE J. of Quantum Electron., Vol. QE-23, No. 6, pp. 1000-1004, 1987.

[20] V. M. Contarino, A. S. Daryoush, and P. R. Herczfeld, "Large-Signal Modulation of Semiconductor Lasers With Optical Feedback For Millimeter Wave Applications", IEEE MTT-S Digest, Q-29, pp. 653-656, 1987.

[21] R. S. Tucker, U. Koren, G. Raybon, C. A. Burrus, B. I. Miller, T. L. Koch, G. Eisenstein, and A. Shahar, "40-GHz Active Mode-Locking in A Monolithic Long-Cavity Laser", Int. Laser Conference, Boston, 1988.

[22] D. Botez and G. J. Herskoowitz, "Component of Optical Communication Systems", Proc. of IEEE, Vol. 68, No. 6, pp. 689-730, 1980.

[23] J. I. Yamada, S. Machida, T. Mukai, H. Tsuchiya, and T. Kimura, "Long-Span Single-Mode Fiber Transmission Characteristics in Long Wavelength Region", IEEE J. Quantum Electron., QE-16, pp. 1086-1092, 1980.

[24] A. Yariv, Optical Electronics, New York, Holt Rinehart and Winston, 1985.

[25] W. T. Tsang and A. Y. Cho, "Growth of GaAs/GaAlAs by Molecular Beam Epitaxy Over Perefentially Etched Channels", Appl. Phys. Lett., Vol. 30, No. 6, pp. 293-296, 1977.

[26] J. Hayashi, M. B. Panish, and P.W. Foy, "A Low-Threshold Room-Temperature Injection Laser", IEEE J. Quantum Electron., Vol. 5, pp. 211-212, 1969.

[27] H. Kressel and H. Nelson, "Close Confinement Gallium Arsenide p-n Junction Laser with Reduced Optical Loss at Room Temperature", RCA Rev., Vol 30, pp. 106-113, 1969.

[28] G. P. Agrawal and N .K. Dutta, Long-Wavelength Semiconductor Lasers, New York, Van Nostrand Reinhold, 1986.

[29] F. Stern, " Calculated Spectral Dependence of Gain in Excited GaAs", J. of Appl. Phys., Vol. 47, No. 12, pp. 5382-5385, 1976.

[30] A. Ghiasi, A. Gopinath, "Novel Wide-Bandwidth Matching Techniques for Laser Diodes", IEEE Trans. Microwave Theory Tech., Vol 38, No. 5, pp. 673-676, 1990.

[31] K. Kishino, S. Auki, and Y. Suematsu, "Wavelength Variation of 1.6 μm Wavelength Buried Heterostructure GaInAsP/InP Laser Due to Direct Modulation", IEEE J. Quantum Electron., No. 18, pp. 343-351, 1982,

[32] K. Aiki, M Nakamura, J. Umeda, A. Yariv, A. Katzir, and H. W. Yen, "GaAs-GaAlAs Distributed Feedback Laser with Separate Optical and Carrier Confinement", Appl. Phys. Lett., Vol 27, No. 3, pp 145-146, 1975.

[33] G. P. Agrawal, "Coupled-Cavity Semiconductor Lasers Under Current Modulation: Small-Signal Analysis", IEEE J. of Quantum Electron, Vol. QE-21, No. 3, pp. 255-263, 1985.

[34] K. Sato, "Intensity Noise of Semiconductor Laser Diodes in Fiber Optic Analog Video Transmission", IEEE J. of Quantum Electron, Vol. QE-19, No. 9, pp. 1380-1391, 1983.

[35] D. E. McCumber, "Intensity Fluctuations in the Output of cw Laser Oscillators", Physical Review, Vol.-141, No. 1, pp. 306-322, 1966.

[36] J. W. M. Biesterbos and A. J. Den Boff, "High-Frequency Noise in the Output of DH (AlGa)As Injection Lasers with Different Structures and Waveguiding Mechanisms", IEEE J. Quantum Electron., QE-17, pp. 701-706, 1981.

[37] T. Paoli, "Noise Characteristics of Stripe-Geometry Double-Heterostructure Junction Lasers Operating Continuously-I. Intensity Noise at Room Temperature", IEEE J. of Quantum Electron., Vol. QE-11, NO. 6, pp. 276-283, 1975.

[38] R. Schimpe, B. Stegmuller, and W. Harth, "FM Noise of Index-Guided GaAlAs Diode Lasers", Electronics Letters, Vol.-20, NO. 5, pp. 206-208, 1984.

[39] G. P. Agrawal, N.A. Olsson and N.K. Dutta, "Effect of Fiber-Far-End Reflections on Intensity and Phase Noise in InGaAsP Semiconductor Lasers", Appl. Phys. Lett. 45 (6), pp. 597-599, 1984.

[40] K. Y. Lau and H. Blauvelt, "Effect of Low-Frequency Intensity Noise on High-Frequency Direct Modulation of Semiconductor Injection Lasers", Appl. Phys. Lett. 52 (9), pp. 694-695, 1988.

[41] K. Y. Lau, "Microwave Phase Stability of Directly Modulated Semiconductor Injection Lasers", Appl. Phys. Lett. 52 (17), pp. 1377-1378, 1988.

[42] G. Acket, D. Lenstra, A. Den Boef, and B. Verbeek, "The Influence of Feedback Intensity on Longitudinal Mode Properties and Optical Noise in Index-Guided semiconductor Lasers", IEEE J. of Quantum Electron., Vol. QE-20, NO. 10, PP. 1163-1169, 1984.

[43] C. Henry, "Theory of the Phase Noise and Power Spectrum of a Single Mode Injection Laser", IEEE J. of Quantum Electron., Vol. QE-19, NO. 9, pp. 111391-1397, 1983.

[44] J. Gowar, Optical Communication Systems, London, Printice Hall International, 1984.

[45] Y. M. Pang, C. Y. Chen, P. A. Garbinski, "1.5 GHz Operation of an AlxGa1-xAs/GaAs Modulation-Doped Photoconductive Detector", Electron. Lett., Vol. 19, No. 18, pp.716-717, 1983.

[46] R. N. Simons and K. B. Bhasin, "Analysis of Optically Controlled Microwave/Millimeter-Wave Device Structures", IEEE Trans. Microwave Theory Tech., Vol. MTT-34, No. 12, pp. 1349-1355, 1986.

[47] R. Darling and J. Uyemura, "Optical Gain and Large-Signal Characteristics of Illuminated GaAs MESFET's", IEEE J. of Quantum Electron., Vol. QE-24, No. 7, pp. 1160-1171, 1987.

[48] S. Y. Wang and D.M. Bloom, "100 GHz Bandwidth GaAs Schottky Photodiode", Electron Lett., Vol. 19, No. 14, pp. 554-555, 1983.

[49] N. Bar-Chaim, K.Y. Lau, I. Ury, and A. Yariv, "High-Speed GaAlAs/GaAs p-i-n Photodiode On a Semi-Insulating GaAs Substrate", Appl. Phys. Lett. 43 (3), pp. 261-262, 1983.

[50] R. S. Tucker, A.J. Taylor, C.A. Burrus, G. Eisenstein, and J.M. Wiesenfeld, "Coaxially Mounted 67 GHz Bandwidth InGaAs Pin photodiode", Electronics Letters, Vol.-22, NO. 17, pp. 917-918, 1986.

[51] G. Keiser, Optical Fiber Communications, New York, McGraw-Hill, 1983.

[52] J. C. Campell, W. S. Holden, J. T. Freguson, A. G. Dentai, and Y. K. Jhee, "Improved Frequency Response of InP/InGaAsP/InGaAs Avalanche Photodiodes with Separate Absorption, Grading, and Multiplication Region" Electron. Lett., Vol. 21, No. 20, pp. 886-887, 1985.

[53] G. Engen, "Calibration of an Arbitrary Six-Port Junction for Measurement of Active and Passive Circuit Parameters", IEEE Trans. Instrum. Meas., Vol-22, No. 4, pp. 295-299, 1973.

[54] R. Pollard and R. Lane, "The Calibration of a Universal Test Fixture", IEEE MTT Digest, pp. 498-500, 1983.

[55] N. Franzen and R. Speciale, "A New Procedure for System Calibration and Error Removal in Automated S-Parameter Measurements", Proc. 5th European Microwave Conf., Hamburg, pp. 69-73, 1975.

[56] E. F. Da Silva and M.K. Mc Phun, "Calibration of Microwave Network Analyzer for Computer-Corrected S Parameter Measurements", Electron, Lett., Vol.-9, NO. 6, pp. 126-128, 1973.

[57] R. Bauer and P. Penfield, "De-Embedding and Unterminating" IEEE Trans. on Microwave Theory and Tech., MTT Vol.-22, NO. 3, pp. 282-288, 1974.

[58] G. Engen, "An Improved Circuit for Implementing the Six-Port Technique of Microwave Measurements", IEEE Trans. on Microwave Theory and Tech., MTT Vol.-25, NO. 12, pp. 1080-1083, 1977.

[59] K. C. Gupta, R. Garg, and R. Chadha, "Computer Aided Design of Microwave Circuits", Dedham, Artech House, 1981.

[60] Touchstone CAD Package for Microwave Circuits, EEsof Co., 5795 Lindero Canyon Rd., Westlake Village, CA.

[61] W. E. Stephens T.R. Joseph, " A 1.3-μm Microwave Fiber-Optic Link Using A Direct-Modulated Laser Transmitter", IEEE J. Lightwave Technology, Vol LT-3, No. 2, pp 308-315,1985.

[62] T. T. Ha, Solid-State Microwave Amplifier Design, New York, Wiley Interscience, 1981.

[63] W. A. Davis, Microwave Semiconductor Circuit Design, New York, Van Nostrand Reinhold, 1984.

[64] R. E. Collin, Foundations for Microwave Engineering, New York, McGraw-Hill, 1966.

[65] T. C. Edwards, Foundations for Microstrip Circuit Design, New York, John Wiley & Son, 1981.

[66] G. L. Matthaei, L. Young, and E.M.T. Jones, Microwave Filters, Impedance-Matching Networks, and Coupling Structures, New York, McGraw-Hill, 1964.

[67] R. Levy, "Synthesis of Mixed Lumped and Distributed Impedance-Transforming Filters", IEEE Trans. on Microwave Theory and Tech., MTT Vol-20, No 3, pp. 223-233, 1972.

[68] A. Ghiasi, A. Gopinath, "Novel Low Loss, High Bandwidth Impedance Matching Technique for Laser Diodes", SPIE Vol. 1102, Orlando, pp. 2-5, 1989.

[69] M. J. Adams and J. Buus, "Two-Segment Cavity Theory for Mode Selection in Semiconductor Lasers", IEEE J. of Quantum Electron., Vol. QE-20, No. 2, pp. 99-103, 1984.

[70] J. Osmundsen and N. Gade, "Influence of Optical Feedback on Laser Frequency Spectrum and Threshold Conditions", IEEE J. of Quantum Electron., Vol. QE-19, No. 3, pp. 465-469, 1983.

[71] K.R. Preston, K.C. Woollard, and K.H. Cameron, "External Cavity Controlled Single Longitudinal Mode Laser Transmitter Module", Electronics Letters, Vol. 17, No. 24, pp. 232, 1981.

[72] K. Lau, L. Figueroa, and A. Yariv, "Generation and Quenching of Intensity Pulsations in Semiconductor Lasers Coupled to External Cavities", IEEE J. of Quantum Electron., Vol. QE-16, No. 12, pp. 1329-1336, 1980.

[73] C. Henry and R. Kazarinov, "Instability of Semiconductor Lasers Due to Optical Feedback from Distant Reflectors", IEEE J. of Quantum Electron., Vol. QE-22, No. 2, pp. 294-301, 1986.

[74] K. Y. Lau, A. Yariv, "High-Frequency Current Modulation of Semiconductor Injection Lasers", Semiconductor and Semimetals, Vol. 22, Part B, pp. 69-152, 1985.

[75] R. S. Tucker, "Large-Signal Circuit Model for Simulation of Injection-Laser Modulation Dynamics.", IEE Proc, Vol. 128, No. 5, pp. 180-184, 1981.

[76] T. Ikegami and Y. Suematsu "Large-Signal Characteristics of Directly Modulated Semiconductor Injection Lasers", Electron. and Comm. in Japan, Vol. 53-B, No. 9, pp. 69-75, 1970.

[77] S. Akiba, G.E. Williams, H. A. Haus, "High Rate Pulse Generation From InGaAsP Laser in SELFOC Lens External Resonator", Electron. Lett., Vol. 17, No. 15, pp. 527-529, 1981.

[78] K. Y. Liou, C. A. Burrus, R. A. Linke, I. P. Kaminow, S. W. Granlund, C. B. Swan, and P. Besomi, "Single-Longtitudinal-Mode Stabilized graded index Rod External Coupled-Cavity Laser", Appl. phys.Lett., Vol. 45, No. 7, pp. 729-731, 1984.

[79] D. Marcuse and T-P Lee, "Rate Equation of a Coupled-Cavity Laser", IEEE J. Quantum Electron., Vol. QE-20, No. 2, pp.166-176, 1984.

[80] L. A. Coldren, T. L. Koch, "Analysis and Design of Coupled-Cavity Lasers", IEEE J. Quantum Electron., Vol. QE-20, No. 6, pp. 671-682, 1984.

☆U.S. GOVERNMENT PRINTING OFFICE